**TITLE**

# CSF1R inhibitor levels determine sex-specific phenotype of resilient microglia and neurofunctional rescue leading to extended survival in tauopathy mice

**AUTHORS**

Noah R. Johnson[1,2†], Peng Yuan[1,3†], Erika Castillo[1], T. Peter Lopez[1], Weizhou Yue[1], Annalise Bond[1], Brianna M. Rivera[1], Miranda C. Sullivan[1], Masakazu Hirouchi[1,4], Kurt Giles[1,5], Atsushi Aoyagi[1,4], and Carlo Condello[1,5†*]

[1] Institute for Neurodegenerative Diseases, UCSF Weill Institute for Neurosciences, University of California, San Francisco, CA 94158, USA.

[2] University of Colorado Alzheimer's and Cognition Center, Linda Crnic Institute for Down Syndrome, Department of Neurology, University of Colorado Anschutz Medical Campus, Aurora, CO 80045, USA.

[3] Department of Rehabilitation Medicine, Huashan Hospital, State Key Laboratory of Medical Neurobiology, Institute for Translational Brain Research, MOE Frontiers Center for Brain Science, Fudan University, Shanghai 200032, China.

[4] Daiichi Sankyo Co., Ltd., Tokyo, 140-8710, Japan.

[5] Department of Neurology, UCSF Weill Institute for Neurosciences, University of California, San Francisco, CA 94158, USA.

[†]N.J., P.Y. and C.C. contributed equally to this work. *Correspondence to: carlo.condello@ucsf.edu

## ABSTRACT

Microglia are central to pathogenesis in many neurological conditions. Drugs targeting colony-stimulating factor-1 receptor (CSF1R) to block microglial proliferation in preclinical disease models have shown mixed outcomes, thus the therapeutic potential of this approach remains unclear. Here, CSF1R inhibitors were evaluated in tauopathy mice using multiple dosing schemes, drug analogs, and longitudinal measurements in the brain and plasma. A sex-independent reduction in pathogenic tau was seen in several models and non-microglial gene expression patterns reverted toward a normal wild type signature. Surprisingly, despite greater drug exposure in male mice, functional rescue and extended survival was only observed in female mice. A dose-dependent upregulation of immediate early genes was observed in male mice only, indicating excitotoxicity that may have precluded functional benefits. Drug-resilient microglia in male mice exhibited morphological and gene expression patterns consistent with increased neuroinflammatory signaling, suggesting a mechanistic basis for sex-specific excitotoxicity. These data argue that complete microglial ablation is neither required nor desirable for neuroprotection and that therapeutics targeting microglia must consider sex-dependent effects on functional outcomes.

## INTRODUCTION

Microglia, the resident innate immune cells of the central nervous system (CNS), are important for neurodevelopment and homeostasis, and are a fundamental component to pathogenesis in many neurological conditions. We now appreciate that microglia are heterogeneous cells, are influenced by the periphery, have sex-dependent biology, and can be helpful or harmful depending on the disease stage or specific pathology[1-4]. Gene mutations affecting the expression and sequence of microglial genes (e.g. *TREM2*, *CD33*, and *MS4A*) increase risk for Alzheimer's disease (AD), and implicate microglia in several disease pathways including toxic protein aggregation (Aβ and tau) and neuroinflammation[5,6]. Thus, for the first time, there is unequivocal evidence in humans that certain microglial functions are robustly involved in the pathogenesis of neurodegenerative disease. However, the precise mechanisms governing microglia function in disease are still not well understood.

In tauopathy (a family of neurodegenerative disorders characterized by tau inclusions in neural cells), there is growing evidence that microglia play an early and constant role in tau

aggregation and neuronal loss. Disease-activated microglia can secrete pro-inflammatory cytokines that regulate neuronal kinases and phosphotases causing tau hyperphosphorylation, aggregation and consequent neurodegeneration[7-9]. Genome-wide transcriptomic studies have identified innate immune pathways that implicate early and robust involvement of microglia in human tauopathy[10,11] and related mouse models[12,13]. Deletion of microglia-specific genes or genetic ablation of microglial cells in rodents have been useful approaches to dissect microglia-mediated mechanisms in disease models, but pharmacologic tools to more dynamically manipulate microglial function have been limited. Recently developed small-molecule drugs targeting colony-stimulating factor-1 receptor (CSF1R), a receptor kinase critical for survival and proliferation of CNS microglia, peripheral tissue macrophages and blood myeloid cells[14], are approved for clinical use in various oncology indications[15], and have now been adopted by the neuroscience community to study microglia biology. In the past few years, there have been numerous studies using CSF1R inhibitors in models of neurological disease, but only a few studies in models of primary tauopathy[16-19]. While important first steps, these studies only explored single, static time points of treatment, or used only one sex. Given the dynamic nature and complexity of microglial activation, the timing of CSF1R inhibition in tauopathy and its translational relevance is still an open question.

Thus, the goal of our study was to define a therapeutic window that not only reduced pathological markers, but also led to functional improvement. Moreover, we questioned whether complete or continuous microglial ablation using CSF1R inhibitors was necessary given the important and diverse roles these cells play in brain health and disease. Here, we systematically test CSF1R inhibition using multiple drug analogs at several time points in transgenic mice developing spontaneous tauopathy, and in an inoculation model of induced tauopathy. We demonstrate a reduction of tau pathology in multiple dosing schemes without complete microglial ablation; drug exposure levels correlated with the extent of tau-prion[20] and microglial reduction. Surprisingly, we observed suppressed plasma biomarkers of neurodegeneration, rescue of aberrant behavior, and extended survival in female mice only. These data reveal a previously unrecognized sex-dependent therapeutic benefit of pharmacological CSF1R inhibition. Transcriptome analyses showed that treated tauopathy mice exhibited a restored gene expression profile similar to wild type mice; however, we observed a specific module of sex- and drug concentration-dependent gene expression that might explain the lack of functional rescue in male mice. Interestingly, residual microglia had a morphology similar to wild type microglia and their gene expression pattern indicated a unique, homeostatic-like signature

that was not responsive to tauopathy nor CSF1R inhibition. These data highlight yet another context for microglial heterogeneity with implications for novel microglial biology, and argue that tempering microglial activation with drugs, rather than cellular ablation, is a better therapeutic strategy with clinical relevance.

## RESULTS

### CSF1R inhibition reduces pathogenic tau in the brains of Tg2541 mice

Building on previous findings[16-19], we first evaluated the effect of CSF1R inhibition on the levels of pathogenic tau in the brains of transgenic mice expressing human tau, using a cell-based tau-prion bioassay, enzyme-linked immunosorbent assay (ELISA), and immunohistochemical (IHC) analysis. To deplete microglia, Tg2541 mice were dosed with one of two potent, orally bioavailable, and brain-penetrant CSF1R inhibitors: PLX3397 (pexidartinib), which binds receptor tyrosine kinases CSF1R, and to lesser extent, KIT and FLT3[21], and PLX5622, which selectively binds CSF1R[22]. Three different treatment paradigms were evaluated: acute (2−4 months old), chronic (2−7 months old), and terminal (2 months old until death) (Fig. 1a−c). Transgenic B6-Tg(Thy1-MAPT*P301S)2541 mice[23], referred to here as Tg2541 mice, express the 0N4R isoform of human tau with the familial frontotemporal lobar degeneration (FTLD)-linked P301S mutation[24], which increases its aggregation propensity and prion-like characteristics[25,26]. We previously demonstrated that the levels of pathogenic tau in hindbrain regions of Tg2541 mice were greater than in forebrain regions[27]. This observation is consistent with the neuropathological staging of human FTLD and specifically of progressive supranuclear palsy (PSP) where tau deposition begins and predominates in subcortical and brainstem nuclei[28]. Therefore, the forebrain and hindbrain regions were examined separately in this study (Fig. 1d).

We confirmed that CSF1R inhibition effectively reduced microglial markers Iba1 and P2YR12 by an average of ~60% in both the forebrains and hindbrains of Tg2541 mice compared to vehicle treatment, and that they had similar effects in the brains of C57BL/6J wild type mice (Supplementary Fig. 1a−p). Principal component analysis of all Iba1 and P2YR12 data combined showed that sex did not have a significant effect on the extent of microglial depletion by CSF1R inhibitors (Supplementary Fig. 1q and Supplementary Data File 1), and therefore male and female mice were grouped together for analysis unless otherwise noted.

We next employed a reproducible and rapid cell-based bioassay[27,29,30] to measure the activity of

replication-competent tau-prions in brain homogenates from Tg2541 mice. To ensure an appropriate dynamic range in this bioassay, we optimized for dilution factor and assay duration using aged Tg2541 mouse brain samples, which showed greater than 100-fold higher signal than wild type mouse brain samples (Supplementary Fig. 2). Following acute, chronic, or terminal treatment with PLX3397 or PLX5622, tau-prion activity in the forebrains of Tg2541 mice was significantly decreased compared to vehicle-treated mice (Fig. 1e−g). Hyperphosphorylation and aggregation of tau occurs first in hindbrain regions of Tg2541 mice, especially in the brainstem and spinal cord, leading to motor deficits caused by severe paraparesis[23]. This is consistent with our previous report of early and aggressive tau-prion activity in hindbrain regions of Tg2541 mice[27]; as such, we found that acute CSF1R inhibition was insufficient to reduce tau-prion activity in the hindbrain (Fig. 1e). However, chronic or terminal treatment with PLX3397 did significantly reduce tau-prion activity in hindbrain regions (Fig. 1f,g) and the spinal cords of Tg2541 mice (Supplementary Fig. 3). To examine other markers of pathogenic tau, we measured the levels of tau phosphorylated at Ser396 (pS396) by ELISA, and tau phosphorylated at Ser202/Thr205 (pS202/T205) by IHC. Acute, chronic, or terminal PLX3397 treatment robustly reduced pS396 tau in both forebrain and hindbrain regions of Tg2541 mice (Fig. 1h−j), and also reduced pS202/T205 tau in forebrain regions (Fig. 1k−m) and in the spinal cord (Supplementary Fig. 3d). Since the various measures of tau pathology represent different steps of tau pathogenesis (hyperphosphorylation vs. oligomerization vs. filament formation), they may be differentially impacted by CSF1R inhibition with different treatment regimens. Thus, to consider all tau measurements and both brain regions together, we performed principal component analysis which revealed that pathogenic tau was reduced by both CSF1R inhibitors, and that there was no significant effect of sex on drug efficacy (Fig. 1n and Supplementary Data File 1).

Having verified the benefits of microglial depletion at an early disease stage, we next wondered whether initiating CSF1R inhibition at a more advanced stage of disease would have similar effects, simulating an interventional drug treatment. Thus, we dosed Tg2541 mice with PLX3397 in a delayed treatment paradigm (4−7 months old). Similar to terminal treatment, interventional treatment also significantly reduced tau-prion activity in both the forebrain and hindbrain (Supplementary Fig. 4a,b). Although pS396 tau levels were unchanged after interventional treatment, levels of tau phosphorylated at Thr231 (pT231) were reduced in the forebrain (Supplementary Fig. 4c,d). Considering the potential off-target effects of continuous, long-term microglial depletion on brain function, we also wondered whether periodic CSF1R inhibition

might provide a safer, yet similarly efficacious therapy. Thus, we also tested PLX3397 dosed intermittently by repeating dosing cycles of three weeks on followed by three weeks off. The intermittent dosing interval was selected based on prior studies showing that there is rapid microglial repopulation of the brain, and that morphological and transcriptional changes in the microglia return to baseline levels within 21 days of removing PLX[31]. Intermittent treatment produced similar reductions in the levels of microglial markers in both brain regions as for continuous treatment (Supplementary Fig. 1r–t), but tau-prion activity and pT231 levels were reduced only in the forebrain (Supplementary Fig. 4e–h). Taken together, these data suggest that intermittent/interventional dosing is sufficient to reduce pathogenic tau in the forebrain of Tg2541 mice, likely due to slower disease kinetics; however, continuous CSF1R inhibition is necessary for the extended reduction of pathogenic tau in the hindbrain.

Tau has been shown to propagate throughout the brain in a prion-like fashion along interconnected neural networks[32,33]. To test the hypothesis that microglial depletion may reduce the propagation of tau-prions[20] in the brains of Tg2541 mice, we inoculated fibrils of the microtubule-binding repeat domain of tau, referred to as K18 fibrils[34], into the hippocampus and overlying cortex (forebrain regions) of Tg2541 mice and then treated them with PLX3397. Compared to un-inoculated mice, K18-inoculated mice had significantly increased tau-prion levels in the ipsilateral (inoculated) forebrain, as well as in the contralateral forebrain and in the hindbrain (Supplementary Fig. 5), which suggests that tau-prions had propagated from the inoculation site to those brain regions. However, acute PLX treatment was sufficient to significantly reduce tau-prion levels in the ipsilateral forebrain and hindbrain, as well as in the contralateral forebrain. Furthermore, tau-prion levels in the contralateral forebrain of PLX-treated mice were not significantly different from the forebrain of un-inoculated, vehicle-treated mice (Supplementary Fig. 5), which indicates that CSF1R inhibition prevented the spreading of tau-prions from the inoculation site to this brain region.

CSF1R inhibition can affect peripheral immune cells such as blood myeloid cells and tissue macrophages, in addition to microglia[17,35]. To determine if the effects of PLX3397 and PLX5622 on pathogenic tau in the brain are due, at least in part, to depletion of peripheral CSF1R-expressing cells we dosed Tg2541 mice with PLX73086[36], a non-brain penetrant CSF1R inhibitor analog of PLX3397 and PLX5622. Chronic treatment with PLX73086 had no significant effect on microglial markers Iba1 and P2YR12, or on levels of tau-prions or pTau[S396] or pTau[T231] in the forebrain or hindbrain of Tg2541 mice (Supplementary Fig. 6). Therefore, the effects of CSF1R inhibitors in peripheral compartments do not significantly contribute to their

reduction of pathogenic tau in the CNS. We also evaluated the numbers of Iba1$^{+}$/CD206$^{+}$ perivascular macrophages (PVMs) and found that PLX3397 treatment did not significantly deplete this cellular population, although there was a trend ($P$ = 0.0947) towards reduced PVMs in female Tg2541 mice (Supplementary Fig. 7). Lastly, because there is limited data for CSF1R expression in neurons after injury[37], we considered whether PLX3397 or PLX5622 might affect neurons or their expression of tau protein in Tg2541 mice. Acute, chronic, and terminal CSF1R inhibition did not significantly reduce levels of neuronal nuclei (NeuN), detected by IHC, or total tau, detected by ELISA (Supplementary Fig. 8). Therefore, CSF1R inhibitors do not directly affect measures of neuronal viability or tau expression, consistent with a prior report using PLX3397 in cultured primary neurons[17]. Together, these data confirm that drug effects on biological and functional end points are due to inhibition of CSF1R in CNS microglia.

**CSF1R inhibition extends survival in female Tg2541 mice**

We next focused on the terminal treatment paradigm with PLX3397 to evaluate the long-term effects of CSF1R inhibition on lifespan and behavior. Tg2541 mice develop paraparesis from 5−6 months of age which makes feeding difficult, resulting in a loss of body weight and thus, a greatly reduced lifespan compared to wild type mice. We found that terminal PLX treatment significantly extended the median survival of female Tg2541 mice [16.5 days longer median survival; $P$ = 0.0004], but not male Tg2541 mice, compared to vehicle treatment (Fig. 2a,b). The extended survival in PLX-treated female mice was preceded by significantly reduced weight loss, which was not observed in male mice (Fig. 2c). Body weight at 180 days of age, irrespective of treatment, was predictive of lifespan in female mice but not in male mice, with less weight loss being correlated with longer survival (Fig. 2d). Lower forebrain tau-prion levels were also correlated with longer survival in female mice but not in male mice (Fig. 2e), suggesting that Tg2541 mice have a sex-specific physiological response to tauopathy. To confirm the effect of PLX treatment on survival in a different experimental paradigm, we used a midbrain inoculation model. Since Tg2541 mice spontaneously develop substantial tau pathology in the midbrain[27], we predicted that K18 inoculation in the midbrain would accelerate and synchronize the disease course, which would be ideal for studying mouse survival. Indeed, female Tg2541 mice inoculated with K18 tau fibrils died significantly earlier than mice inoculated with diluent, though no difference was observed in male mice (Fig. 2f,g). Consistent with our prior result, PLX treatment significantly extended the median survival of female mice inoculated with K18 tau fibrils [29.5 days longer median survival; $P$ = 0.0095], but not male mice, compared to vehicle treatment (Fig. 2h). Taken together, these data indicate that CSF1R inhibition robustly

extends the lifespan of female Tg2541 mice, even during an accelerated disease course.

**CSF1R inhibition reduces aberrant behavioral phenotypes in Tg2541 mice**

To examine the relationship between drug exposure and markers of disease progression more closely, we collected blood plasma at monthly intervals from mice receiving terminal treatment with PLX3397 or vehicle (Fig. 3a). Consistent with previous reports[17], male Tg2541 mice had higher plasma (25.3%; $P < 0.0001$) and brain (44.9%; $P = 0.0250$) concentrations of PLX than did female mice (Fig. 3b and Supplementary Fig. 9a–c); we also observed this difference in wild type mice (Supplementary Fig. 9d,e). Male and female mice had *ad libitum* access to food, and had similar rates of food consumption relative to body weight, independent of whether it contained PLX or vehicle (Supplementary Fig. 10a,b). However, female mice were consistently more active than male mice (Supplementary Fig. 10c,d). Thus, the reduced PLX exposure in female mice is likely due to a higher metabolic and drug clearance rate compared with male mice. In line with the hypothesis that drug exposure was excessive in male mice, we observed a trend towards reduced body weight in male wild type mice receiving terminal PLX treatment, but not in female wild type mice (Supplementary Fig. 9f). In spite of this sex-specific difference in PLX exposure, we found that higher plasma concentrations of PLX were correlated with greater microglial depletion in both forebrain and hindbrain regions, independent of sex (Fig. 3c). Furthermore, higher PLX exposure was correlated with reduced tau-prion levels in the forebrain regions of both male and female mice (Fig. 3d). Together, these data indicate that PLX has dose-dependent on-target effects in both male and female mice.

Previous studies have demonstrated a common hyperactive phenotype in the early stages of tauopathy in transgenic rodent models[38,39]. While the precise mechanism that leads to this deficit is unclear, this phenotype is causally linked with tau aggregate burden[40]. Based on the reduction of tau deposition we observed with PLX treatment, we sought to also examine its effect on this hyperactive phenotype. Using an automated home-cage monitoring system, we longitudinally tracked the activity levels in Tg2541 mice at different ages, measuring their amounts of rearing, locomotion, and wheel running. We confirmed the previous reports, finding that at early ages the Tg2541 mice displayed a hyperactive phenotype relative to wild type mice (90−150 days old in females, 90−120 days old in males), while at later ages their activity was significantly reduced (Fig. 3e), likely due to the accumulation of pathogenic tau in brain regions associated with motor function. PLX treatment led to a consistent reduction in Tg2541 mouse hyperactivity, but did not change their hypoactivity at later ages (Fig. 3e), indicating the activity

reduction is not due to a general weakening effect. Detailed examination of the individual activity measurements revealed that PLX treatment normalized the amounts of wheel running (Fig. 3f) and active time (Fig. 3g). These data indicate that PLX treatment corrects the aberrant behavior of Tg2541 mice towards that of wild type mice.

**Sex-dependent effects of CSF1R inhibition on a biomarker of CNS injury**

To further interrogate CNS damage caused by tauopathy, or potentially caused by the observed sex-dependent PLX exposure, we also evaluated the plasma levels of neurofilament light chain (NfL). NfL is a validated blood-based biomarker of neuronal injury[41] which correlates with disease progression and tau burden in human tauopathy[42,43]. Female PLX-treated mice had reduced levels of NfL compared to vehicle-treated mice (Fig. 4a,b), consistent with reduced CNS injury due to tauopathy. Conversely, NfL levels were increased in male mice following PLX treatment (Fig. 4c), suggestive of PLX-induced toxicity. Consistent with these findings, PLX treatment resulted in significantly increased NfL levels in male mice that received midbrain inoculation of K18 tau fibrils, but not female mice (Fig. 4d–f). We found no correlation between NfL level and survival in female mice, but in male mice, higher NfL levels were strongly correlated with reduced survival in both PLX and vehicle treatment groups (Fig. 4g,h). Furthermore, the concentrations of NfL in both the forebrain and hindbrain at death were positively correlated with PLX3397 concentration in the brains of male, but not female, Tg2541 mice (Fig. 4i,j). Interestingly, intermittent treatment, resulting in a 50% lower total dosage of PLX, produced a significant decrease in NfL levels in male mice, but had no effect in female mice (Fig. 4k–m). Taken together, these data suggest that in female Tg2541 mice, tauopathy drives CNS injury and its reduction by PLX effectively masks any effect of PLX toxicity, whereas in male mice, excessive exposure causes CNS injury that supersedes any benefit of PLX. Consistent with this premise, we found that PLX treatment increased plasma NfL levels in male wild type mice, as expected, but also in female wild type mice (Fig. 4n–p), albeit at substantially lower levels than tau-induced NfL in Tg2541 mice.

**Peripheral CSF1R inhibition does not cause therapeutic or adverse effects in the CNS**

CSF1R inhibitors have known adverse effects in the periphery including anemia, leukopenia, and hepatotoxicity, which have been observed in human clinical trials[44]. To determine if peripheral PLX toxicity was causing NfL release or reducing drug efficacy, we evaluated mice receiving chronic treatment with PLX73086, the non-brain penetrant CSF1R inhibitor analog of PLX3397 and PLX5622. We observed no effect of PLX73086 treatment on body weight or

plasma NfL levels in either male or female Tg2541 mice (Fig. 5a–d), indicating that peripheral CSF1R inhibition does not impact tauopathy-driven phenotypes. Furthermore, we observed no effect of PLX73086 treatment on body weight or plasma NfL levels in wild type mice (Fig. 5e–h), demonstrating that the drug-induced toxicity indicated by NfL rise is dependent on the drug entering the brain. Histopathological evaluation of liver sections of PLX3397-dosed Tg2541 mice stained with hematoxylin and eosin (H&E), Masson's trichrome, or Picosirius red did not reveal any overt signs of liver injury or fibrosis (Fig. 5j), nor did quantification of the Picosirius red-stained liver sections (Fig. 5k). Alkaline phosphatase (ALP) in the plasma, a different indicator of liver damage, was elevated in Tg2541 mice following PLX3397 treatment; however, the ALP levels were elevated in both male and female mice (Fig. 5l), indicating that the sex-specific toxicity of PLX3397 in male mice likely occurs in the brain rather than in the periphery. Taken together, these data further confirm that the drug exposure of brain-penetrant CSF1R inhibitors was appropriate for female Tg2541 mice to reduce tauopathy and significantly extend survival; however, the drug exposure was too high for male Tg2541 mice, and the resulting neurotoxicity outweighed its therapeutic benefit.

**CSF1R inhibition shifts gene expression patterns in Tg2541 mice towards wild type**

To better characterize global molecular changes in the CNS due to CSF1R inhibition, we used the Nanostring platform to analyze a curated panel of gene transcripts related to neuroinflammation, myeloid cell function and neuropathology in bulk brain tissue following chronic treatment of Tg2541 mice with PLX5622. The chronic treatment group was selected for this analysis because the collection time point was synchronized (unlike in the terminal treatment group) and seven months of age is close to the average lifespan of Tg2541 mice. We measured mRNA transcripts of 1,841 genes, many of them shown to be regulated by tau or Aβ pathology in previous genome-wide gene expression studies[12,13]. To validate the Nanostring approach, we identified 53 genes with a broad range of expression level changes and measured mRNA transcripts with quantitative reverse-transcription PCR (RT-qPCR) in the same sample used for sequencing. The RT-qPCR results generally matched the trends shown in the Nanostring data (Supplementary Fig. 11), supporting the validity of our transcriptomic data.

Since microglial cells are directly impacted by PLX treatment, we first excluded the microglial-specific genes (see Methods) and examined the general trend of expression patterns among different treatment groups. Pearson's correlation matrix showed high similarity among wild type brains with or without PLX treatment (Fig. 6a), indicating that the gene expression pattern we

measured is not affected by the treatment itself. In contrast, PLX treatment in Tg2541 mice caused a distinct shift in the gene expression pattern away from the vehicle-treated group. Interestingly, the gene expression patterns of PLX-treated Tg2541 mice showed a stronger correlation with wild type mice than with vehicle-treated Tg2541 mice (Fig. 6a dashed boxes and Fig. 6b). To further quantify this shift, we performed partial-least squares (PLS) regression analysis using the gene expression data from vehicle-treated Tg2541 and wild type mice (Fig. 6c filled circles), and projected the data from PLX-treated mice onto the PLS dimensions (Fig. 6c empty circles). This allowed us to represent the transgene-specific gene expression pattern in a relatively low-dimensional space, and to quantify the changes associated with treatment by calculating the population vector distances and angles in this space. We found that PLX treatment significantly normalized gene expression patterns in Tg2541 mice towards those of wild type mice (Fig. 6d,e, only two out of five dimensions are shown, covering >95% of the total variance). The normalization in gene expression was further confirmed by similar trends in neuron-specific genes (Supplementary Fig. 12). Importantly, PLX treatment in wild type mice showed negligible changes in the gene expression patterns. These results indicate that PLX treatment specifically suppresses the abnormal transcriptome associated with transgene overexpression, consistent with its effects ameliorating pathogenic tau deposition.

**Evidence for excitotoxicity with increased drug exposure**

As described above, although we observed consistent reduction in the levels of pathogenic tau in the brains of both male and female Tg2541 mice with PLX treatment, only female mice benefited from extended survival, functional rescue, and reduced NfL levels (Figs. 1–4). We hypothesized that excessive PLX dosing may underlie this sex-specific effect, as male mice consistently had higher drug exposure in the plasma and CNS (Fig. 3 and Supplementary Fig. 9), and also benefitted from a lower, intermittent PLX dosing paradigm (Supplementary Fig. 4). Indeed, in our transcriptomics analysis we identified individual genes whose expression was associated with brain PLX5622 concentration or with sex (Fig. 6f). First, we ruled out the possibility that sex-dependent functional benefits were caused by differential expression of the drug target, CSF1R, or its ligand, CSF1 (Supplementary Fig. 13). Using a PLS regression of all non-microglia genes to brain PLX concentration and sex for each sample, we calculated the variable importance score along each of these dimensions. Interestingly, many immediate early genes (IEGs) showed high importance scores (Fig. 6g), suggesting that IEGs might be a module that is altered by CNS drug exposure. To further test this possibility, we examined all IEGs (56 genes overlapped in our dataset) and found that their expression patterns fit closely

with the brain PLX concentration (Fig. 6h). Importantly, when we excluded the IEGs and examined the PLX-induced transcriptome shift along the wild type-to-Tg2541 dimension, the correlation of gene expression changes and brain PLX concentration was no longer significant (Fig. 6i), indicating that the IEGs contribute substantially to the PLX treatment effects. Notably, relative to wild type vehicle-treated mice, only male PLX5622-treated Tg2541 mice had significantly upregulated expression of IEGs (Fig. 6j), which we also validated using qPCR of the five most highly expressed IEGs (Supplementary Fig. 14). Furthermore, we observed the same drug-dependent IEG up-regulation in male mice in a completely independent study using PLX3397 (Supplementary Fig. 14), thereby confirming that this is a robust sex-specific effect of CSF1R inhibition. As increased IEG expression can be indicative of neuronal hyperactivity, these data provide a plausible mechanism by which excessive PLX dosing may have led to excitotoxicity, thereby masking its therapeutic effect in male mice.

**CSF1R inhibition ameliorates pathological activation of astrocytes**

As suggested by the reduction of tau deposition, we hypothesized that astrocyte-driven neuroinflammation would also be reduced by PLX treatment. Therefore, we examined transcriptome shifts in astrocyte-specific genes upon PLX treatment. Similar to the neuronal-specific genes, we observed a normalization of astrocyte-specific gene expression patterns towards wild type in both forebrain and hindbrain regions (Fig. 7a,b). Using previously described astrocytic gene signatures of disease[45], we found that PLX treatment led to a dose-dependent reduction in the expression of the A1 astrocytic gene cluster associated with neurotoxic effects (Fig. 7c,d). In addition, we measured astrogliosis over time using longitudinal bioluminescence imaging (BLI) methods based on a previously established transgenic reporter system of glial fibrillary acidic protein (GFAP)-driven luciferase[46], which we validated by IHC and mRNA analyses (Supplementary Fig. 15). To perform reliable BLI in Tg2541 mice, we intercrossed each transgenic line to an albino background and refined the method, using a synthetic luciferin substrate to increase signal from deep hindbrain regions (see Methods and Supplementary Fig. 16). This technique allowed us to non-invasively measure astrogliosis in live mice longitudinally over the course of PLX treatment. In vehicle-treated Tg2541 mice, the BLI signal gradually increased with age (Supplementary Fig. 17), in accordance with the accumulation of tau pathology and gliosis reported in Tg2541 mice[23,47]. Consistent with our hypothesis and with measurement of GFAP using other methods (Supplementary Fig. 15), CSF1R inhibition suppressed the BLI signal in both the forebrain and the hindbrain (Fig. 7e−g). Together, these data suggest that astrocytic inflammation, in particular the neurotoxic astrocytes, driven by

383 microgliosis was attenuated by CSF1R inhibition, thus leading to a general neuroprotective
384 effect.

385 **CSF1R inhibition preferentially eliminates a highly activated microglia subpopulation**

386 Given reported roles of microglia in driving astrocytic inflammation and neurotoxicity in disease,
387 we next interrogated whether resilient microglial phenotypes could be responsible for the sex-
388 specific neurofunctional effects. Thus, we examined the morphological and transcriptional
389 changes in microglia following CSF1R inhibition. In tauopathy, microglia acquire an activated
390 morphology in brain regions where neurons contain tau aggregates, a phenomenon seen in
391 many focal neuropathologies[48]. Interestingly, the elimination of microglia in the Tg2541 mouse
392 brain following PLX3397 treatment was not uniform nor complete, but was the most effective in
393 the vicinity of tau aggregates (Fig. 8a,b). The microglial density near tau-laden neurons was
394 reduced by more than 60%, but in distal regions (>200 microns) the microglial density was not
395 significantly changed (Fig. 8c), indicating that microglia in the vicinity of the tau aggregates may
396 have increased sensitivity towards CSF1R inhibition. We then compared the morphologies of
397 PLX-resistant (residual microglia in PLX-treated mice) and PLX-sensitive microglia (in vehicle-
398 treated mice). Notably, we found that PLX resistance was associated with more abundant and
399 intricate microglial cell processes, close to the levels seen in wild type mice (Fig. 8d−g). The
400 number of microglial process branches ($P$ = 0.0075), process lengths ($P$ = 0.028), and territory
401 sizes ($P$ = 0.011) in the forebrain were also significantly different between male and female
402 PLX-treated mice, with female mice showing more abundant and intricate microglial processes
403 by all three metrics (Fig. 8d−g). These data suggest that microglia associated with tau pathology
404 may be in an “activated” state, with a reduced number of processes. This view is consistent with
405 previous reports that activated microglia adopt a “disease-associated microglial” (DAM)
406 phenotype, with some of the signature genes associated with inflammatory responses that are
407 detrimental to adjacent neural cells[49,50]. Interestingly, our data suggests that DAM in tauopathy
408 are more vulnerable to PLX treatment, and that surviving microglia might be neuroprotective,
409 particularly in female mice.

410 In support of this view, transcriptome analyses showed that many microglial-specific genes were
411 upregulated in Tg2541 mice (Fig. 9a), among which the most notable were signature DAM
412 genes such as *Tyrobp*, *Clec7a*, *Trem2* and *CD68*. By correlation analysis among different
413 samples using a generalized Louvain algorithm[51], we found that the microglia-specific genes in
414 our dataset were clustered into three groups (Fig. 9b and Supplementary Fig. 18). The red-

cluster genes showed the highest degree of modulation by transgene overexpression, while the blue-cluster genes showed a moderate degree of modulation, and the green-cluster genes showed almost no difference between Tg2541 and wild type mice (Fig. 9c). Transgene-modulated genes clustered into red and blue groups, consistent with a recent finding that tau pathology activates both immune-activation and immune-suppression gene expression modules[10].

We next compared the gene expression patterns in vehicle- and PLX5622-treated brains. We examined all previously reported DAM signature genes[50] and found a partial match with the activation markers in each of our identified gene clusters (Fig. 9d). Regardless of the designation of homeostatic or activation genes reported in previous studies, the red-cluster genes showed a stereotypical pattern of transgene activation and sensitivity to PLX treatment, while green- and blue-cluster genes did not appear to be modulated by these factors. Given that PLX predominantly eliminated microglia in the vicinity of the tau deposits (Fig. 8c), these data suggest that red-cluster genes are preferentially expressed by tau-associated microglia. Interestingly, when we examined PLX-induced expression changes in male and female mice separately, we found that while the expression of red cluster genes were substantially diminished by PLX independent of sex, green cluster genes were markedly increased in treated male mice (Fig. 9c). The increase in green cluster gene expression is remarkable considering the >50% reduction in microglial cell number. To account for microglial cell reduction, we calculated the gene expression of resilient microglia by normalization to six microglia-specific housekeeping genes. The normalized data showed a trend towards increased gene expression in male mice, yet most of the male-specific PLX-induced genes belonged to the green cluster (Fig. 9f), many of which are known to be pro-inflammatory. Indeed, subsequent Ingenuity Pathway Analysis revealed a higher activation of inflammation-related pathways in PLX-treated male mice compared to female mice (Fig. 9g). These inflammation-related pathways included tau-activated NF-κB[52] and excitotoxicity[53] pathways, but not amyloid-induced inflammasome genes[54] (Supplementary Fig. 19). Pathways related to phagocytosis or microglia growth, on the other hand, did not show such consistent sex-specific change (Fig. 9g). Taken together, our data show morphological and transcriptional changes in microglia associated with tau deposition, consistent with a pattern of pathological activation. CSF1R inhibition appears to preferentially eliminate these microglia in female mice, leaving the brain with a more quiescent and less inflammatory microglial population. Male mice, on the other hand, showed a drug-induced inflammatory microglia phenotype, which might contribute to neuronal excitotoxicity and

diminished therapeutic effect.

## DISCUSSION

Our study reveals several major findings from a comprehensive evaluation of CSF1R inhibitors in preclinical models of tauopathy. Importantly, we present the first line of evidence that CSF1R inhibition reduces pathology that leads to functional improvements associated with longer lifespan and reduced behavioral deficits in tauopathy mice (Figs. 2 and 3). Overall, our data showing a reduction of pathogenic tau is consistent with prior studies using a different drug scaffold targeting CSF1R (JNJ-527; edicotinib) in Tg2541 mice[18], or using PLX3397 in a different mouse model of tauopathy (TgPS19)[17]. However, in our study, neuroprotection occurred despite incomplete microglia depletion (~60%); upon deeper analysis, we identified distinct microglial-specific gene clusters suggesting subsets of microglia responsive to tauopathy or resilient to CSF1R inhibition (Fig. 9). This finding is in line with the wealth of data demonstrating that microglia exist as unique subsets in different brain regions, sexes, ages or disease states[2-4]. From this perspective, our data suggest that it may be possible to target specific subsets of activated microglia in tauopathy, without affecting other beneficial microglia populations. Taken together, we argue that CSF1R inhibition causing complete microglia ablation is unnecessary for therapeutic benefits, and may possibly be detrimental in humans given that microglia are important for brain homeostasis and defending against other insults. Several prior studies have suggested that therapeutic outcomes may only be achieved with complete ablation of microglia, although these studies used different mouse models or dosing regimens[17,19]. Nevertheless, these disparate findings in prior literature are now more interpretable alongside our study, which sheds light on the intricate relationships between CSF1R inhibitor dosing, microglial depletion and therapeutic outcomes.

The precise mechanism of CSF1R inhibitors causing reduced tau pathology is still unclear, but our data indicates that activated microglia are the primary target resulting in reduced numbers of cells producing pro-inflammatory cytokines[7-9] and other disease-associated microglial factors (Fig. 9) that stoke tau pathogenesis in neurons, such as apolipoprotein E[17,55] and complement proteins[56]. In addition, it seems plausible that CSF1R inhibitors may also block microglia-mediated activation of A1 astrocytes[45], which in turn secrete factors that also drive tau pathogenesis; blocking this cellular feed-forward pathway using a different drug targeting microglia led to neuroprotection in a synucleinopathy model of Parkinson's disease[57].

Consistent with this view, PLX-treated mice exhibited a restored astrocyte phenotype, suggesting that therapeutic benefits in our study may also be due, in part, to quelling neurotoxic A1 astrocytes (Fig. 7). Pharmacological CSF1R inhibition has been reported to also deplete PVMs[58]. Although we did not detect a significant reduction in the numbers of cortical blood vessel-associated PVMs in our studies (Supplementary Fig. 7), their roles in tauopathy remain to be determined. While there is cross-talk between peripheral immune cells and microglia[1], we show that a non-brain penetrant analog, PLX73086, did not affect CNS microglia, tau pathology or NfL levels (Fig. 5 and Supplementary Fig. 6), and it is thus unlikely that CSF1R inhibition in the periphery contributes to the phenotypic rescue observed in our study. Lastly, it is possible that chronic PLX treatment caused depletion of some oligodendrocyte progenitor cells (OPCs) in our study, but we expect that PLX did not affect mature oligodendrocytes or myelination[59]. The relationship between OPC biology and tau pathology in neurons is largely unknown, and thus it remains unclear how CSF1R inhibition in OPCs contributes, if at all, to the mechanism of action. Nevertheless, this topic warrants further investigation.

Tau pathology in Tg2541 mice is associated with moderate microgliosis and an up-regulation of transcriptomic signatures of microglial activation[10,49]. Our transcriptome analysis showed activation of two major clusters of microglial-specific genes in Tg2541 mice. These two clusters had a high degree of overlap with the immune activation and suppression modules recently described in tauopathy mice and FTLD patients[10], indicating a specific reactive transcriptional program of microglia towards tau pathology. Consistent with this view, genes in the activated clusters also matched transcriptome modules described in activated microglia in neurodegeneration models (such as *Itgax* and *Clec7a*), but not in tumor or acute inflammation models[49]. We found an additional cluster of microglial genes that had similar expression in Tg2541 and wild type mice. Intriguingly, this cluster was not affected by PLX treatment in female mice, while in male mice this cluster exhibited marked activation (Fig. 9). Considering that PLX eliminates more than half of the total microglia population, a parsimonious explanation for this sustained gene cluster is that they are preferentially expressed by an inert microglial subpopulation that does not respond to tauopathy or lower dose CSF1R inhibition[60]. Consistent with this notion, we found that PLX treatment preferentially eliminates activated microglia in the vicinity of tau deposits, and thus most surviving microglia are not in direct contact with tau-laden neurons (Fig. 8). This is in contrast to Aβ mice, in which the surviving microglia are usually associated with Aβ plaques following PLX treatment[22,61]. We found that surviving microglia in female mice were non-inflammatory, and had longer and more elaborate processes compared

to vehicle-treated microglia, showing functional and morphological features more similar to those of wild type microglia (Fig. 8). In sum, our data describe a microglial genetic signature that remains stable in Tg2541 mice with or without PLX treatment, likely representing a “dormant” microglial subpopulation that are less dependent on CSF1R for survival, or are less sensitive to CSF1R inhibition at the doses administered in our study.

Sex-specific differences exist in mouse microglial function, gene expression, and response to tauopathy, and the differences increase with age[62-64]. Our data identify a sex-dependent effect on therapeutic exposure and efficacy of CSF1R inhibition in Tg2541 mice. A difference in the plasma levels of PLX3397 during *ad libitum* oral dosing in male and female mice has been noted previously[17]; however, only male mice were evaluated further. We examined both male and female Tg2541 mice and found that, despite similar food intake, plasma and brain levels of PLX3397 were higher in male mice compared to female mice (Fig. 3 and Supplementary Fig. 9). However, at this level of drug exposure, only female mice received a functional benefit from CSF1R inhibition, an unexpected and clinically relevant outcome that would have been overlooked had our analysis been focused on a single sex. In male Tg2541 mice, despite a robust reduction of microglia and pathogenic tau, PLX treatment did not slow weight loss or extend survival, and plasma NfL levels were significantly increased, indicative of neuronal damage[41]. Neurodegeneration in Tg2541 mice has been shown to be largely limited to spinal cord motor neurons[23,65], and we found that NeuN and total tau immunoreactivity in the brain were largely unchanged by CSF1R inhibition (Supplementary Fig. 8). Thus, the functional deficits we measured are likely caused by neuronal dysfunction rather than neuronal death, but can be rescued by CSF1R inhibition. It has been suggested before that microglia from male animals may exhibit an increased responsiveness to CSF1R depletion compared to microglia from female animals[66]. Our results indicate that despite robust on-target effects for microglial depletion, male mice developed a PLX-induced inflammatory microglial phenotype. Furthermore, we observed a concentration-dependent activation of IEGs in PLX treated Tg2541 mice, suggesting that excessive PLX dosing in male mice may lead to excitotoxicity (Fig. 6), thus masking the beneficial effect of tau reduction. Microglia in male mice adopted a transcriptome and morphological phenotype that have been previously linked to excitotoxicity[53,67]. Curiously, IEGs were not significantly upregulated in male wild type mice, indicating that their activation may not be due to high concentration of PLX alone, but may also be dependent on tau deposits. Previous studies have linked tau accumulation and aberrant neural activity *in vivo*[68]. On the other hand, microglia are known to mediate neuroprotection

against excitotoxicity[67,69] and elimination of microglia can exacerbate seizures and related neuronal degeneration[70]. Therefore, the concurrent tau removal and drug-induced inflammation driven by surviving microglia may increase the risk for hyperactivity, resulting in excitotoxicity in male mice with high PLX concentrations. Other sex-specific differences may also contribute to microglial sensitivity to CSF1R inhibition by a currently unknown mechanism. Future translational studies of pharmacological CSF1R inhibitors will need to carefully evaluate the role of sex in both safety and therapeutic outcomes.

CSF1R inhibitors were shown to be protective in mouse models of other neurodegenerative diseases, such as AD and Down syndrome[22,71,72]. However, under different treatment conditions, CSF1R inhibition did not affect Aβ plaque burden, but did rescue some functional deficits[61,73]. Therefore, microglia play a dynamic role in the brain's response to Aβ pathogenesis, and their attenuation may impart distinct benefits at different stages of disease. Our results suggest that, in primary human tauopathies, a subset of microglia play a net negative role before, during, and after disease onset and that their removal may be a viable therapeutic strategy. It remains to be determined if similar benefits should be expected for tauopathy in AD given the preceding comorbid Aβ pathology, but this may be elucidated in rodent models co-expressing human tau and Aβ. Nevertheless, because CSF1R inhibition has not been reported to be detrimental in Aβ mice, CSF1R inhibitors could ameliorate AD-related tauopathy even if caused by different disease mechanisms. Ongoing human clinical trials of CSF1R inhibitors in AD (e.g. NCT04121208) may provide additional mechanistic insights.

Primary human tauopathies constitute a class of neurodegenerative diseases caused by tau misfolding and aggregation and include progressive supranuclear palsy (PSP), corticobasal degeneration (CBD) and Pick's disease, among others. When combined with AD, in which tau aggregation follows Aβ deposition, tauopathies afflict a significant proportion of the human population, and thus novel approaches to directly or indirectly block tau pathogenesis or its downstream effects are urgently needed. Our study highlights several aspects of pharmacological CSF1R inhibition that bolster its therapeutic potential for human tauopathies. First, we observed greater efficacy of early (acute) CSF1R inhibition to restrict tau-prion levels in forebrain regions (Fig. 1e), likely due to reduced disease severity there relative to hindbrain regions. At later stages (chronic and terminal), CSF1R inhibition with PLX3397 did reduce tau-prion levels in the hindbrain, albeit a modest reduction relative to the effects in the forebrain (Fig. 1f,g). These findings suggest that early and long-term CSF1R inhibition (though not necessarily continuous) would most effectively mitigate human tauopathy. Second, we

579 demonstrated that interventional dosing of Tg2541 mice, initiated at a stage when robust tau
580 deposition had already occurred[23,27], led to a significant reduction in pathogenic tau
581 (Supplementary Fig. 4). Therefore, our data support some potential clinical benefit of CSF1R
582 inhibitors for treatment, in addition to prevention, of tauopathy. This is important because
583 prophylactic prevention of non-autosomal dominant neurodegenerative diseases may be difficult
584 due to a lack of definitive prognostic biomarkers paired with the fact that aggregation of the
585 causative proteins can occur years or decades prior to symptom onset[30]. Third, we found that
586 intermittent dosing of Tg2541 mice at three-week intervals produced a significant reduction in
587 pathogenic tau (Supplementary Fig. 4). Despite relatively minimal off-target effects from
588 continuous, long-term dosing of CSF1R inhibitors in mice[22], non-human primates[74], and
589 humans[21], intermittent dosing would be clinically preferable if a similar therapeutic outcome was
590 achieved, given the important functions for microglia and related peripheral cells in innate
591 immunity. Because neurodegenerative tauopathies are slow, protracted diseases and microglia
592 are long-lived[75], it is conceivable that breaks in dosing may occur on the order of months or
593 years and be informed by medical imaging probes for microglia activation[76]. Imaging will be
594 highly valuable for guiding intermittent dosing because microglial repopulation in a pathological
595 setting (e.g., disease or normal aging) may not necessarily result in a return to baseline
596 transcriptional profiles. Fourth, we found CSF1R inhibition to extend the survival of female
597 Tg2541 mice (Fig. 2), indicating that the reduction in pathogenic tau in this model system
598 translates to an improved clinically relevant outcome. We postulate that if CSF1R inhibitor
599 dosing was optimized for male Tg2541 mice, any adverse effects in the CNS or periphery would
600 likely be diminished and their survival extended. Fifth, we showed that complete microglial
601 depletion is not necessary, or even desirable, for a therapeutic benefit. As discussed above, the
602 microglia that survive CSF1R inhibition represent a unique microglial sub-population that likely
603 serves important functions in brain homeostasis. Future preclinical studies may pinpoint the
604 precise level, timing, and frequency of CSF1R inhibition such that the detrimental effects of
605 microglial activation are minimized while an appropriate number of homeostatic microglia
606 remain for brain surveillance. Lastly, CSF1R inhibitors applied in conjunction with tau
607 immunotherapy may prove to be a successful combination therapy; because microglia are not
608 needed for antibody effector function[77], removing tauopathy-activated microglia would slow tau
609 pathogenesis and may also increase the efficacy of tau immunotherapy. Taken together, our
610 data strongly support the therapeutic modulation of microglial activation by CSF1R inhibitors as
611 a promising approach to treating human tauopathies.

## METHODS

### Animals

The Tg2541 transgenic mouse line expresses the human 0N4R tau isoform under the Thy1.2 genetic promoter. Tg2541 mice were originally generated on a mixed C57BL/6J × CBA/Ca background[23] and were then bred onto a congenic C57BL/6J background using marker-assisted backcrossing for eight generations before intercrossing to generate homozygous mice. Albino Tg2541 mice were generated by intercrossing Tg2541 with C57BL/6J mice expressing a spontaneous mutation in the tyrosinase gene (homozygous for $Tyr^{c\text{-}2J}$) causing albinism (Jackson Laboratory; 000058). To generate mice for *in vivo* bioluminescence imaging, we employed Tg(*Gfap*-luc) mice, which express firefly luciferase under the control of the murine *Gfap* promoter (gift from Caliper Life Sciences). These reporter mice were originally on the FVB background, but we backcrossed them to a congenic B6 background, and then crossed them to the B6-albino background. To create bigenic mice, albino Tg2541 mice were crossed with albino Tg(*Gfap*-luc) animals to produce double hemizygotes; next, double hemizygotes were crossed and the progeny were screened for the presence of both transgenes expressed at homozygosity. Animals were maintained in a facility accredited by the Association for Assessment and Accreditation of Laboratory Animal Care International in accordance with the *Guide for the Care and Use of Laboratory Animals*. All procedures for animal use were approved by the University of California, San Francisco's Institutional Animal Care and Use Committee.

### PLX compound formulation in mouse chow

PLX3397 was provided by Plexxikon Inc. and was formulated in AIN-76A standard chow by Research Diets Inc. at 275 mg/kg as previously described[78]. PLX5622 was provided by Plexxikon Inc. and was formulated in AIN-76A standard chow by Research Diets Inc. at 1200 mg/kg as previously described[61]. PLX73086 was provided by Plexxikon Inc. and was formulated in AIN-76A standard chow by Research Diets Inc. at 200 mg/kg as recommended by Plexxikon Inc.

### Immunohistochemistry and slide scanning

Formalin-fixed samples were embedded into paraffin (FFPE) using standard procedures and

642 microtome-cut into 8 µm sagittal brain sections or coronal spinal cord sections and mounted
643 onto slides. To reduce tissue autofluorescence, paraffin slides were photobleached for 48 hours.
644 Slides were deparaffinized in a 61°C oven for 15 minutes and rehydrated through alcohols.
645 Antigen retrieval was performed by autoclaving for 10 minutes at 121°C in 0.01 M citrate buffer.
646 Sections were blocked in 10% normal goat serum (NGS) (Vector Labs) for 1 hour at room
647 temperature. All primary antibodies were used at 1:250 dilution and included rabbit monoclonal
648 anti-Iba1 (Abcam, ab178847), rabbit polyclonal anti-P2YR12 (Atlas, HPA014518), mouse
649 monoclonal anti-NeuN (Millipore, MAB377), chicken anti-GFAP (Abcam, ab4674), and mouse
650 monoclonal anti-pS202/T205 tau (AT8; Thermo Fisher, MN1020). Primary antibodies were
651 diluted in 10% NGS in PBS and allowed to incubate on the slides overnight at room
652 temperature. Primary antibody detection was performed using goat secondary antibodies with
653 conjugated AlexaFluor 488, AlexaFluor 555, or AlexaFluor 647 (Life Technologies) at 1:500
654 dilution. Slides were cover-slipped using PermaFluor mounting medium (Thermo). Whole-
655 section tiled images were acquired with an Axioscan.Z1 slide scanner (Zeiss) at 20×
656 magnification, and quantification was performed with Zen 2.3 software (Zeiss).

657 **Cellular bioassay to measure tau-prion activity**

658 A HEK293T cell line expressing the repeat domain of 4R human tau (aa 243–375) containing
659 the P301L and V337M mutations and C-terminally fused to YFP was previously generated as
660 described[29]. A stable monoclonal line was maintained in DMEM, supplemented with 10% FBS
661 and 1% penicillin/streptomycin. To perform the bioassay, 3,000 cells (containing 0.1 µg/ml
662 Hoechst 33342) were plated in 70 µl per well into 384-well plates (Greiner) and incubated for 2
663 hours before treatment with samples. Clarified brain lysate at a final concentration of 1.25 µg/mL
664 total protein was first incubated with Lipofectamine 2000 (0.2% final concentration) and
665 OptiMEM (9.8% final concentration) for 90 minutes, and then added to the plated cells in
666 quadruplicate. Plates were incubated at 37°C for 1–3 days, and then the live cells were imaged
667 using an INCell Analyzer 6000 Cell Imaging System (GE Healthcare) and custom algorithms
668 were used to detect fluorescent YFP-positive puncta (aggregates).

669 **Mechanical tissue homogenization**

670 Postmortem brains and spinal cords were thawed and weighed to determine the mass in grams.
671 Brains were bisected into forebrain and hindbrain pieces using a single cut with a scalpel blade
672 between the striatum and hypothalamus. Tissue was homogenized in nine volumes of cold
673 DPBS containing Halt Protease Inhibitor Cocktail (1x, Thermo Fisher Scientific) using a

Precellys 24-bead beater (Bertin Instruments) with metal bead lysing matrix (MP Biomedical). Where necessary, brain lysates were clarified by centrifugation at 10,000 × *g* for 10 min at 4°C. All tissue and samples were stored at −80°C until further use.

**Formic acid extraction of insoluble proteins in brain tissue for ELISA**

Fifty microliters of formic acid were added to 25 µL of 10% brain homogenate and placed in an ultracentrifuge tube. The samples were vortexed, sonicated for 20 minutes at 37°C in a water-bath sonicator, and then centrifuged at 100,000 x g for 1 hour. Fifty microliters of supernatant were recovered to a low-binding tube and neutralized with 950 µL of neutralization buffer (1 M Tris base and 500 mM dibasic sodium phosphate). Samples were aliquoted into low-binding tubes and flash frozen in liquid nitrogen. The following ELISA kits from Thermo Fisher Scientific were used according to the manufacturer's protocols: total tau (KHB0041), p-tau S396 (KHB7031), and p-tau T231 (KHB8051). Each sample was analyzed in duplicate. Raw ELISA values were adjusted to total brain protein (grams) in the clarified 10% brain homogenate as determined by bicinchoninic acid (BCA) assay (Pierce/Thermo Fisher Scientific).

**Quantification of total protein in brain homogenate**

Total protein content in the PBS-soluble (clarified 10% brain homogenate) and detergent-soluble fractions was quantified using the Pierce BCA Protein Assay Kit (Thermo Fisher Scientific) following the manufacturer's protocol.

**Generation of tau K18*P301L fibrils**

Production, purification and fibrillization of recombinant tau K18*P301L fibrils were performed as previously described[79].

**Stereotaxic injections in Tg2541 mice**

Forebrain inoculation: Ten-week-old Tg2541 mice received unilateral inoculations of 10 µl of 1.5 mg/ml tau K18 P301L fibrils using stereotaxic methods. Injections followed a two-step process: the needle was first advanced to the hippocampus (Bregma -2.5mm, Lateral 2.0mm; Depth -2.3 mm from the skull surface) to deliver 5 µl over three minutes, then the Hamilton syringe pump was paused for five minutes to allow for diffusion prior to retracting the needle to the overlying cortex (Depth -1.3 mm) where the remaining 5 µl was injected. After fibril injection, the needle remained in place for five minutes to allow for diffusion of fibrils before retraction, patching the skull and suturing the scalp. Midbrain inoculation: Ten-week old Tg2541 mice received bi-lateral

inoculations of 10 µl of 1.5 mg/ml tau K18 P301L fibrils using stereotaxic methods. Five microliters was injected at each site in the midbrain (Bregma, -4.3 mm; Lateral, 1.0 mm, Depth, -2.5 mm) and (Bregma, -4.3 mm; Lateral, -1.0 mm, Depth, -2.5 mm).

**Automated home cage monitoring of behavior**

Total activity measurements of freely moving mice were made every 30 days after PLX dosing in Promethion cages (Sable Systems International). At each time point, mice were first randomized and placed individually in Promethion cages for 4 to 6 days. Real-time cage activity recording was continuous during the entire session using a combination of a running wheel with sensors to measure speed and distance traveled, three balances to measure body weight, food and water consumption, and a matrix of infrared light beams to measure XYZ movements with 0.25 cm resolution. Analysis of these metrics was used to detect behaviors such as sleep, rearing and general locomotion. For each mouse, data used for analyses were average readings per light or dark cycle. Data from the first circadian cycle were excluded due to variable behavior during habituation. To calculate the activity scores, wheel use, locomotion and rearing were first normalized to a 0−1 scale by the maximum value in the whole dataset, and then the geometric mean of the normalized values for each session was calculated.

**Quantification of PLX compound levels in brain tissue and plasma**

Brain homogenates (20% w/v) were prepared in PBS by one 30-second cycle of bead beating at 5500 rpm with a Precellys 24-bead beater (Bertin Instruments) or plasma samples were prepared by dilution to 25% with PBS. Compounds were recovered by mixing equal parts of brain homogenate with a 50/50 (v/v) solution of acetonitrile (ACN) and methanol containing 1 mM niflumic acid. Precipitated proteins were removed by vacuum filtration (Captiva ND, Agilent). Analysis was performed using a liquid chromatography-tandem mass spectrometry system consisting of an API4500 triple quadra-pole instrument (AB Sciex, Foster City, CA) interfaced with a CBM-20A controller, LC20AD 230 pumps, and a SIL-5000 auto-sampler (Shimadzu Scientific, Columbia, MD). Samples were injected onto a BDS Hypersil C8 column maintained at room temperature. The amount of ACN in the gradient was increased from 75–95% ACN over two minutes, held for one minute, and then re-equilibrated to 75% ACN over 1.4 minutes. Data acquisition used multiple reaction monitoring in the positive ion mode. Specific methods were developed for each compound (PLX3397 and PLX5622), enabling the determination of absolute concentrations.

## Blood plasma neurofilament light (NfL) protein measurement using SIMOA

At monthly time points, 150 µl blood was collected in EDTA-coated tubes. The plasma was centrifuged at 1,000 x g for ten minutes to clarify the samples, and was then diluted with sample diluent buffer included in the kit by 25-fold and 100-fold, respectively, prior to the measurement. Plasma NfL concentration was measured and analyzed using the NfL kit (Quanterix) with the SIMOA HD-1 analyzer (Quanterix). Briefly, samples, magnetic beads coated with capture antibody, and biotinylated detector antibodies were combined. Thereafter, the capture beads were resuspended with streptavidin-β-galactosidase (SBG) and resorufin β-D-galactopyranoside (RGP) and transferred to the SIMOA disk. Each bead fit into a microwell in the disk and if NfL was captured then the SBG hydrolysed the RGP substrate which generated a fluorescent signal, and then the concentration was measured against a standard curve derived from known concentrations of recombinant NfL included in the kit. The lower limit of quantification of the assay for plasma was 17.15 pg/mL.

## Masson's trichrome and Picosirius red staining

FFPE liver sections (eight µm) were deparaffinized through xylenes and graded alcohols and then rehydrated in distilled water. The Masson's trichrome staining kit (Abcam #ab150686) was used according to the manufacturer's protocol. The Picro Sirius Red Stain Kit (Abcam #ab150681) was used to stain tissue sections for 60 min at room temperature. The slides were rinsed in two changes of acetic acid, three changes of ethanol, and then mounted using PermaFluor mounting medium (Thermo). Whole-section tiled images were acquired with an Axioscan.Z1 slide scanner (Zeiss) at 20× magnification, and quantification was performed with Zen 2.3 software (Zeiss).

## Alkaline phosphatase (ALP) ELISA of plasma samples

Mouse plasma samples were diluted 1:100 in the provided dilution buffer and measured using the ALP ELISA kit (Biovision #E4572-100) according to the manufacturer's protocol.

## RNA extraction and Nanostring RNA expression measurements

RNAlater-preserved samples were homogenized in PBS and total RNA was extracted from samples using the Quick-RNA Miniprep Kit (Zymo Research). RNA extracts were evaluated for concentration and purity using a Nanodrop 8000 instrument (Thermo Fisher Scientific) and diluted to a concentration of 20 ng/µl. Hybridizations were performed for the mouse

Neuroinflammation, Myeloid cell, and Neuropathology panels according to the nCounter XT Assay user manual (Nanostring). The hybridizations were incubated at 65°C for 16 hours, and then were added to the nCounter SPRINT Cartridge for data collection using the nCounter SPRINT Profiler. Counts were analyzed using the nSolver Analysis Software.

**RNA expression analysis**

In total, there were 10 mice in the Tg2541 vehicle group, 10 mice in the Tg2541 PLX5622 group, 6 mice in the wild type vehicle group, and 6 mice in the wild type PLX5622 group. Each mouse had separate forebrain and hindbrain samples and three panels of Nanostring sequencing were performed on each sample. Data from the three panels were pooled together to form the final dataset. When pooling data, if a gene appeared in more than one panel then the average read value was used in subsequent analysis, unless one panel failed to detect the gene.

To assign cell-type specificity of each gene, we used the transcriptome dataset reported in a previous study[80], inspired by previously reported approaches in bulk tissue samples[49]. We set a specificity threshold in which a gene qualifies to be cell-type specific if its expression in a cell type is greater than five times the sum in all other cell types. Using this standard, our dataset had 242 microglia-specific genes, 47 astrocyte-specific genes and 70 neuron-specific genes. All cell-type specific gene analyses were repeated with a three-time threshold and all results were consistent (data not shown).

We used partial least-square (PLS) regression (MATLAB) to extract the gene expression pattern aligned with Tg2541-wild type axis, using individual gene reads from each mouse as predictors and genotype as responses. Only vehicle groups were used in constructing the PLS regression. Forebrain and hindbrain were calculated separately. Five output dimensions were chosen for all PLS analyses, as they covered 99.99% of the total variance in all cases. The scores in the first two dimensions were plotted. To project PLX3397-treated groups to the PLS dimensions, we used the following formula:

$$Score_{projection} = (Loading_{predictor} \backslash (raw - mean_{predictor})')'$$

To calculate population vector distance, we use the “mhal” command in MATLAB. All five dimensions were used for each mouse. The wild type vehicle group was used as a target.

To calculate the vector angle, each mouse’s gene expression pattern was regarded as a five-

dimension vector in the PLS space, and the angle between each mouse and the average vector of the wild type vehicle group was calculated with the following formula:

$$A = cos^{-1}((u \cdot v)/(|u||v|))$$

To calculate the PLS regression along the PLX concentration and sex-correlated dimensions, we constructed regressions using all non-microglial genes or only immediate early genes[81] to measured brain PLX concentrations and sex of each sample. We then calculated variable importance in projection to isolate the genes important for the regression. To calculate the projected PLX concentrations, we used the products of gene expression levels and coefficients estimated from PLS regression.

To calculate clusters in the microglial-specific genes, we calculated pairwise Pearson's correlation coefficients across 32 samples among each gene. The resulting similarity matrix was then processed with a generalized Louvain community detection algorithm[51].

To estimate the gene expression levels of the resilient microglia, we used 6 genes (Tmem119, P2ry12, Fcrls, Olfml3, Itgam v1, and Itgam v2) as microglial-specific house-keeping genes[82] and used their levels relative to the vehicle-treated group to scale the expression levels of other microglial genes. We used these estimated expression levels as input for the Ingenuity Pathway Analysis (QIAGEN).

**Gene expression analysis by RT-qPCR**

Mouse brains were collected at endpoints and flash frozen in DNA/RNA shield reagent. Tissue was homogenized as described above and total RNA was purified using a commercial isolation kit (Zymo Research). RNA concentration and the RNA integrity number (RIN) were determined using a Bioanalyzer 2100 instrument and an Agilent RNA 6000 Pico Kit (Agilent 5067-1513). Only samples with a RIN score ≥7.0 were used for gene expression analysis. To confirm transcriptome profiling results, 2.5 ng of sample mRNA was applied to triplicate RT-qPCR reactions consisting of 1x TaqPath 1-Step Multiplex Master Mix (ThermoFisher Scientific A28526), Taqman primer/probe sets and a normalizing human MAPT Taqman assay. Reactions were run on a QuantStudio 6 and 7 Pro instrument and amplification yielding cycle threshold ($C_T$) values were corrected with Mustang Purple passive reference dye for each target gene. Gene expression of PLX-treated mice relative to vehicle-treated mice was determined by the comparative $C_T$ method and values were expressed as fold-change.

Comparative $C_T$ equation:

827 $2^{-\Delta\Delta C_T}$=[($C_T$ gene of interest – $C_T$ hMAPT internal control)]PLX-treated mice − [($C_T$ gene of
828 interest – $C_T$ hMAPT internal control)]vehicle-treated mice

829 **In vivo bioluminescence imaging**

830 Bioluminescence imaging was performed on the brains and spinal cords of albino bigenic
831 Tg(2541:*Gfap*-luc) homozygous mice after receiving an intraperitoneal injection of 25 mg/kg
832 cyclic luciferin-1 (CycLuc1) sodium salt solution (Aobious; AOB6377) prepared in PBS, pH 7.4.
833 After CycLuc1 injection, mice were placed in an anesthetization chamber and exposed to an
834 isoflurane/oxygen gas mix for ten minutes. During this time, the heads of the mice were shaved
835 to enhance the bioluminescence signal. After anesthetization, mice were placed in an IVIS
836 Lumina III small animal imaging system (PerkinElmer) and were kept under constant
837 anesthesia. Mice were imaged for 60 s duration at three time points (14, 16 and 18 minutes)
838 following CycLuc1 injection as determined in one-hour time-lapse calibration studies. After
839 image acquisition, the mice were allowed to recover in their home cages. Brain and spinal cord
840 bioluminescence values were calculated from images displaying surface radiance using
841 standardized regions of interest and were then converted to total photon flux (photons per
842 second) using Living Image software version 4.4 (PerkinElmer).

843 **Confocal imaging of thick tissue sections**

844 Vibratome-sectioned brain slices (40 µm thick) were immunolabeled with Iba1, AT8, and/or
845 CD206 (Biorad, MCA2235) antibodies using standard protocols for free-floating sections in
846 multi-well plates. Sections were mounted using PermaFluor and #1.5 coverglass. Using a Leica
847 SP8 confocal microscope equipped with HyD detectors and an AOBS, samples were first
848 visualized using Navigator function to acquire an overview image of each slice using a 20×
849 water-immersion lens (0.95 NA). From the mosaic image, smaller tiled-ROIs were marked in the
850 forebrain and hindbrain to acquire high-resolution, sequential-scanned image stacks using a
851 63× water-immersion lens (1.2 NA). Eight-bit image z-stacks (1 µm steps) were collected at
852 512×512-pixel resolution. Images were processed using custom MATLAB code.

853 **Microglial morphology analysis**

854 Microglia morphology was analyzed using a custom script in MATLAB. Briefly, raw confocal
855 image stacks were smoothed and then maximally projected. Isolated microglia cells were
856 manually selected for analysis. The selected microglia region was binarized with an intensity
857 threshold, and then the cell body was detected by fitting a largest circle in the binary mask. After

858 excluding the cell body region, the remaining microglia processes were skeletonized and branch
859 number, branch length and bounding box were measured using “regionprops” and “bwmorph”
860 commands.

861 **Statistical analysis**

862 Statistical analyses were performed using GraphPad Prism 8. Comparisons between two
863 groups were performed by two-tailed unpaired t test or by Mann-Whitney nonparametric test.
864 For comparisons of more than two groups, one-, two-, or three-way ANOVA was performed with
865 Holm-Šidák post hoc analysis. Following ANOVA, residuals were evaluated for normal
866 distribution using the Anderson-Darling test and the data were evaluated for equal variance
867 using the Brown-Forsythe test. If both assumptions were violated ($P < 0.05$), the data was
868 reanalyzed using Welch’s ANOVA with Dunnett T3 post hoc analysis. For repeated-measures
869 ANOVA, sphericity was not assumed and the Geisser-Greenhouse correction was applied. If
870 any data points were missing, a mixed-effects model (Restricted maximum likelihood; REML)
871 was used instead. Pearson’s correlation tests were performed as one-tailed tests as, in each
872 case, we had a directional hypothesis of either positive or negative correlation. Sample sizes
873 are shown in graphs with each data point representing an individual mouse, or are reported in
874 the figure legends. Experimental replication and exact statistical tests used are detailed in the
875 figure legends.

876

877 **ACKNOWLEDGEMENTS**

878 We thank Plexxikon, Inc for providing the PLX3977, PLX5622 and PLX73086 compounds, and
879 Andrey Reymar and Brian West for consulting on drug dosing and chow formulation. We thank
880 Julian Castaneda, Karina Walker and Lyn Batia (and their staff) at the UCSF Hunter’s Point
881 animal facility for coordinating transgenic mouse development, breeding, and drug efficacy
882 studies. We thank Masahiro Inoue (Daiichi Sankyo, Inc.) for insightful discussions on
883 pharmacokinetics and pharmacodynamics in our study. We thank Stanley Prusiner and David
884 Ramsay at the UCSF Institute for Neurodegenerative Diseases (IND) for access to equipment
885 and technical resources critical for the completion of this study. We thank the following UCSF
886 IND staff for technical assistance: Abby Oehler, Rigoberto Roman-Albarran, Julia Becker, Marta
887 Gavidia and Manuel Elepano. The study was funded by grants from the National Institutes of
888 Health (NIH): (# RF1 AG061874 and P01 AG002132), as well as by the Rainwater Charitable

Foundation, the Sherman Fairchild Foundation, the Henry M. Jackson Foundation, and Daiichi Sankyo, Inc. P.Y. was funded by Shanghai Municipal Science and Technology Major Project and Shanghai Natural Science Foundation (22ZR1415000). Competing interests: The Institute for Neurodegenerative Diseases (UCSF) had a research collaboration with Daiichi Sankyo, Inc. (Tokyo, Japan).

## AUTHOR CONTRIBUTIONS

C.C. conceived the study and designed experiments. N.J., E.C., T.P.L., W.Y., A.B., B.M.R., M.C.S., H.M., K.G., A.A., and C.C. performed experiments and prepared data. N.J., P.Y., and C.C. analyzed and interpreted data. N.J., P.Y., and C.C. wrote the paper. C.C. supervised the study.

## DATA AVAILABILITY

The authors declare that all other data supporting the findings of this study are available within the paper and its supplementary files.

## CODE AVAILABILITY

The transcriptome data (Nanostring) that support the findings of this study, specifically in Figures 6-9, are available from Github with the following link: https://gitfront.io/r/user-8849465/665dd65fd9d9e78650ed02b9f30236d99240de39/UCSF-PLX-nanostring/

## REFERENCES

1. Dionisio-Santos, D.A., Olschowka, J.A. & O'Banion, M.K. Exploiting microglial and peripheral immune cell crosstalk to treat Alzheimer's disease. *J Neuroinflammation* **16**, 74 (2019).

2. Masuda, T., *et al.* Spatial and temporal heterogeneity of mouse and human microglia at single-cell resolution. *Nature* **566**, 388-392 (2019).
3. Kodama, L. & Gan, L. Do Microglial Sex Differences Contribute to Sex Differences in Neurodegenerative Diseases? *Trends Mol Med* **25**, 741-749 (2019).
4. Stratoulias, V., Venero, J.L., Tremblay, M.E. & Joseph, B. Microglial subtypes: diversity within the microglial community. *EMBO J* **38**, e101997 (2019).
5. Schwabe, T., Srinivasan, K. & Rhinn, H. Shifting paradigms: The central role of microglia in Alzheimer's disease. *Neurobiol Dis* **143**, 104962 (2020).
6. Shi, Y. & Holtzman, D.M. Interplay between innate immunity and Alzheimer disease: APOE and TREM2 in the spotlight. *Nat Rev Immunol* **18**, 759-772 (2018).
7. Maphis, N., *et al.* Reactive microglia drive tau pathology and contribute to the spreading of pathological tau in the brain. *Brain* **138**, 1738-1755 (2015).
8. Stancu, I.C., *et al.* Aggregated Tau activates NLRP3-ASC inflammasome exacerbating exogenously seeded and non-exogenously seeded Tau pathology in vivo. *Acta Neuropathol* **137**, 599-617 (2019).
9. Ising, C., *et al.* NLRP3 inflammasome activation drives tau pathology. *Nature* **575**, 669-673 (2019).
10. Rexach, J.E., *et al.* Tau Pathology Drives Dementia Risk-Associated Gene Networks toward Chronic Inflammatory States and Immunosuppression. *Cell Rep* **33**, 108398 (2020).
11. Allen, M., *et al.* Divergent brain gene expression patterns associate with distinct cell-specific tau neuropathology traits in progressive supranuclear palsy. *Acta Neuropathol* **136**, 709-727 (2018).
12. Wang, H., *et al.* Genome-wide RNAseq study of the molecular mechanisms underlying microglia activation in response to pathological tau perturbation in the rTg4510 tau transgenic animal model. *Mol Neurodegener* **13**, 65 (2018).
13. Matarin, M., *et al.* A genome-wide gene-expression analysis and database in transgenic mice during development of amyloid or tau pathology. *Cell Rep* **10**, 633-644 (2015).
14. Stanley, E.R. & Chitu, V. CSF-1 receptor signaling in myeloid cells. *Cold Spring Harb Perspect Biol* **6**(2014).
15. Cannarile, M.A., *et al.* Colony-stimulating factor 1 receptor (CSF1R) inhibitors in cancer therapy. *J Immunother Cancer* **5**, 53 (2017).
16. Asai, H., *et al.* Depletion of microglia and inhibition of exosome synthesis halt tau propagation. *Nat Neurosci* **18**, 1584-1593 (2015).
17. Shi, Y., *et al.* Microglia drive APOE-dependent neurodegeneration in a tauopathy mouse model. *J Exp Med* **216**, 2546-2561 (2019).
18. Mancuso, R., *et al.* CSF1R inhibitor JNJ-40346527 attenuates microglial proliferation and neurodegeneration in P301S mice. *Brain* **142**, 3243-3264 (2019).
19. Bennett, R.E., *et al.* Partial reduction of microglia does not affect tau pathology in aged mice. *J Neuroinflammation* **15**, 311 (2018).
20. Condello, C., DeGrado, W.F. & Prusiner, S.B. Prion biology: implications for Alzheimer's disease therapeutics. *Lancet Neurol* **19**, 802-803 (2020).
21. Tap, W.D., *et al.* Structure-Guided Blockade of CSF1R Kinase in Tenosynovial Giant-Cell Tumor. *N Engl J Med* **373**, 428-437 (2015).
22. Spangenberg, E., *et al.* Sustained microglial depletion with CSF1R inhibitor impairs parenchymal plaque development in an Alzheimer's disease model. *Nat Commun* **10**, 3758 (2019).
23. Allen, B., *et al.* Abundant tau filaments and nonapoptotic neurodegeneration in transgenic mice expressing human P301S tau protein. *J Neurosci* **22**, 9340-9351 (2002).
24. Bugiani, O., *et al.* Frontotemporal dementia and corticobasal degeneration in a family with a P301S mutation in tau. *J Neuropathol Exp Neurol* **58**, 667-677 (1999).

25. Goedert, M., Jakes, R. & Crowther, R.A. Effects of frontotemporal dementia FTDP-17 mutations on heparin-induced assembly of tau filaments. *FEBS Lett* **450**, 306-311 (1999).
26. Sperfeld, A.D.*, et al.* FTDP-17: an early-onset phenotype with parkinsonism and epileptic seizures caused by a novel mutation. *Ann Neurol* **46**, 708-715 (1999).
27. Johnson, N.R.*, et al.* Evidence for sortilin modulating regional accumulation of human tau prions in transgenic mice. *Proc Natl Acad Sci U S A* **114**, E11029-E11036 (2017).
28. Kovacs, G.G.*, et al.* Distribution patterns of tau pathology in progressive supranuclear palsy. *Acta Neuropathol* **140**, 99-119 (2020).
29. Sanders, D.W.*, et al.* Distinct tau prion strains propagate in cells and mice and define different tauopathies. *Neuron* **82**, 1271-1288 (2014).
30. Aoyagi, A.*, et al.* Abeta and tau prion-like activities decline with longevity in the Alzheimer's disease human brain. *Sci Transl Med* **11**(2019).
31. Elmore, M.R., Lee, R.J., West, B.L. & Green, K.N. Characterizing newly repopulated microglia in the adult mouse: impacts on animal behavior, cell morphology, and neuroinflammation. *PLoS One* **10**, e0122912 (2015).
32. Iba, M.*, et al.* Synthetic tau fibrils mediate transmission of neurofibrillary tangles in a transgenic mouse model of Alzheimer's-like tauopathy. *J Neurosci* **33**, 1024-1037 (2013).
33. Seeley, W.W., Crawford, R.K., Zhou, J., Miller, B.L. & Greicius, M.D. Neurodegenerative diseases target large-scale human brain networks. *Neuron* **62**, 42-52 (2009).
34. Gustke, N., Trinczek, B., Biernat, J., Mandelkow, E.M. & Mandelkow, E. Domains of tau protein and interactions with microtubules. *Biochemistry* **33**, 9511-9522 (1994).
35. Lei, F.*, et al.* CSF1R inhibition by a small-molecule inhibitor is not microglia specific; affecting hematopoiesis and the function of macrophages. *Proc Natl Acad Sci U S A* **117**, 23336-23338 (2020).
36. Bellver-Landete, V.*, et al.* Microglia are an essential component of the neuroprotective scar that forms after spinal cord injury. *Nat Commun* **10**, 518 (2019).
37. Luo, J.*, et al.* Colony-stimulating factor 1 receptor (CSF1R) signaling in injured neurons facilitates protection and survival. *J Exp Med* **210**, 157-172 (2013).
38. Jul, P.*, et al.* Hyperactivity with Agitative-Like Behavior in a Mouse Tauopathy Model. *J Alzheimers Dis* **49**, 783-795 (2016).
39. Dumont, M.*, et al.* Behavioral deficit, oxidative stress, and mitochondrial dysfunction precede tau pathology in P301S transgenic mice. *FASEB J* **25**, 4063-4072 (2011).
40. Wang, X.*, et al.* Early intervention of tau pathology prevents behavioral changes in the rTg4510 mouse model of tauopathy. *PLoS One* **13**, e0195486 (2018).
41. Bacioglu, M.*, et al.* Neurofilament Light Chain in Blood and CSF as Marker of Disease Progression in Mouse Models and in Neurodegenerative Diseases. *Neuron* **91**, 56-66 (2016).
42. Ashton, N.J.*, et al.* Increased plasma neurofilament light chain concentration correlates with severity of post-mortem neurofibrillary tangle pathology and neurodegeneration. *Acta Neuropathol Commun* **7**, 5 (2019).
43. Rojas, J.C.*, et al.* CSF neurofilament light chain and phosphorylated tau 181 predict disease progression in PSP. *Neurology* **90**, e273-e281 (2018).
44. Benner, B.*, et al.* Pexidartinib, a Novel Small Molecule CSF-1R Inhibitor in Use for Tenosynovial Giant Cell Tumor: A Systematic Review of Pre-Clinical and Clinical Development. *Drug Des Devel Ther* **14**, 1693-1704 (2020).
45. Liddelow, S.A.*, et al.* Neurotoxic reactive astrocytes are induced by activated microglia. *Nature* **541**, 481-487 (2017).
46. Watts, J.C.*, et al.* Bioluminescence imaging of Abeta deposition in bigenic mouse models of Alzheimer's disease. *Proc Natl Acad Sci U S A* **108**, 2528-2533 (2011).
47. Bellucci, A.*, et al.* Induction of inflammatory mediators and microglial activation in mice transgenic for mutant human P301S tau protein. *Am J Pathol* **165**, 1643-1652 (2004).

48. Ishizawa, K. & Dickson, D.W. Microglial activation parallels system degeneration in progressive supranuclear palsy and corticobasal degeneration. *J Neuropathol Exp Neurol* **60**, 647-657 (2001).
49. Friedman, B.A.*, et al.* Diverse Brain Myeloid Expression Profiles Reveal Distinct Microglial Activation States and Aspects of Alzheimer's Disease Not Evident in Mouse Models. *Cell Rep* **22**, 832-847 (2018).
50. Keren-Shaul, H.*, et al.* A Unique Microglia Type Associated with Restricting Development of Alzheimer's Disease. *Cell* **169**, 1276-1290 e1217 (2017).
51. Mucha, P.J., Richardson, T., Macon, K., Porter, M.A. & Onnela, J.P. Community structure in time-dependent, multiscale, and multiplex networks. *Science* **328**, 876-878 (2010).
52. Wang, C.*, et al.* Microglial NF-kappaB drives tau spreading and toxicity in a mouse model of tauopathy. *Nat Commun* **13**, 1969 (2022).
53. Hong, J.*, et al.* Microglial Toll-like receptor 2 contributes to kainic acid-induced glial activation and hippocampal neuronal cell death. *J Biol Chem* **285**, 39447-39457 (2010).
54. Heneka, M.T.*, et al.* NLRP3 is activated in Alzheimer's disease and contributes to pathology in APP/PS1 mice. *Nature* **493**, 674-678 (2013).
55. Krasemann, S.*, et al.* The TREM2-APOE Pathway Drives the Transcriptional Phenotype of Dysfunctional Microglia in Neurodegenerative Diseases. *Immunity* **47**, 566-581 e569 (2017).
56. Dejanovic, B.*, et al.* Changes in the Synaptic Proteome in Tauopathy and Rescue of Tau-Induced Synapse Loss by C1q Antibodies. *Neuron* **100**, 1322-1336 e1327 (2018).
57. Yun, S.P.*, et al.* Block of A1 astrocyte conversion by microglia is neuroprotective in models of Parkinson's disease. *Nat Med* **24**, 931-938 (2018).
58. Kerkhofs, D.*, et al.* Pharmacological depletion of microglia and perivascular macrophages prevents Vascular Cognitive Impairment in Ang II-induced hypertension. *Theranostics* **10**, 9512-9527 (2020).
59. Liu, Y.*, et al.* Concentration-dependent effects of CSF1R inhibitors on oligodendrocyte progenitor cells ex vivo and in vivo. *Exp Neurol* **318**, 32-41 (2019).
60. Zhan, L.*, et al.* A MAC2-positive progenitor-like microglial population is resistant to CSF1R inhibition in adult mouse brain. *Elife* **9**(2020).
61. Spangenberg, E.E.*, et al.* Eliminating microglia in Alzheimer's mice prevents neuronal loss without modulating amyloid-beta pathology. *Brain* **139**, 1265-1281 (2016).
62. Kodama, L.*, et al.* Microglial microRNAs mediate sex-specific responses to tau pathology. *Nat Neurosci* **23**, 167-171 (2020).
63. Guneykaya, D.*, et al.* Transcriptional and Translational Differences of Microglia from Male and Female Brains. *Cell Rep* **24**, 2773-2783 e2776 (2018).
64. Kang, S.S.*, et al.* Microglial translational profiling reveals a convergent APOE pathway from aging, amyloid, and tau. *J Exp Med* **215**, 2235-2245 (2018).
65. Hampton, D.W.*, et al.* Cell-mediated neuroprotection in a mouse model of human tauopathy. *J Neurosci* **30**, 9973-9983 (2010).
66. Berve, K., West, B.L., Martini, R. & Groh, J. Sex- and region-biased depletion of microglia/macrophages attenuates CLN1 disease in mice. *J Neuroinflammation* **17**, 323 (2020).
67. Vinet, J.*, et al.* Neuroprotective function for ramified microglia in hippocampal excitotoxicity. *J Neuroinflammation* **9**, 27 (2012).
68. Busche, M.A.*, et al.* Tau impairs neural circuits, dominating amyloid-beta effects, in Alzheimer models in vivo. *Nat Neurosci* **22**, 57-64 (2019).
69. Badimon, A.*, et al.* Negative feedback control of neuronal activity by microglia. *Nature* **586**, 417-423 (2020).

70. Liu, M., *et al.* Microglia depletion exacerbates acute seizures and hippocampal neuronal degeneration in mouse models of epilepsy. *Am J Physiol Cell Physiol* **319**, C605-C610 (2020).
71. Sosna, J., *et al.* Early long-term administration of the CSF1R inhibitor PLX3397 ablates microglia and reduces accumulation of intraneuronal amyloid, neuritic plaque deposition and pre-fibrillar oligomers in 5XFAD mouse model of Alzheimer's disease. *Mol Neurodegener* **13**, 11 (2018).
72. Pinto, B., *et al.* Rescuing Over-activated Microglia Restores Cognitive Performance in Juvenile Animals of the Dp(16) Mouse Model of Down Syndrome. *Neuron* **108**, 887-904 e812 (2020).
73. Dagher, N.N., *et al.* Colony-stimulating factor 1 receptor inhibition prevents microglial plaque association and improves cognition in 3xTg-AD mice. *J Neuroinflammation* **12**, 139 (2015).
74. Hillmer, A.T., *et al.* Microglial depletion and activation: A [(11)C]PBR28 PET study in nonhuman primates. *EJNMMI Res* **7**, 59 (2017).
75. Reu, P., *et al.* The Lifespan and Turnover of Microglia in the Human Brain. *Cell Rep* **20**, 779-784 (2017).
76. Horti, A.G., *et al.* PET imaging of microglia by targeting macrophage colony-stimulating factor 1 receptor (CSF1R). *Proc Natl Acad Sci U S A* **116**, 1686-1691 (2019).
77. Lee, S.H., *et al.* Antibody-Mediated Targeting of Tau In Vivo Does Not Require Effector Function and Microglial Engagement. *Cell Rep* **16**, 1690-1700 (2016).
78. Elmore, M.R., *et al.* Colony-stimulating factor 1 receptor signaling is necessary for microglia viability, unmasking a microglia progenitor cell in the adult brain. *Neuron* **82**, 380-397 (2014).
79. Barghorn, S., Biernat, J. & Mandelkow, E. Purification of recombinant tau protein and preparation of Alzheimer-paired helical filaments in vitro. *Methods Mol Biol* **299**, 35-51 (2005).
80. Zhang, Y., *et al.* Purification and Characterization of Progenitor and Mature Human Astrocytes Reveals Transcriptional and Functional Differences with Mouse. *Neuron* **89**, 37-53 (2016).
81. Wu, Y.E., Pan, L., Zuo, Y., Li, X. & Hong, W. Detecting Activated Cell Populations Using Single-Cell RNA-Seq. *Neuron* **96**, 313-329 e316 (2017).
82. Chiu, I.M., *et al.* A neurodegeneration-specific gene-expression signature of acutely isolated microglia from an amyotrophic lateral sclerosis mouse model. *Cell Rep* **4**, 385-401 (2013).

## FIGURES

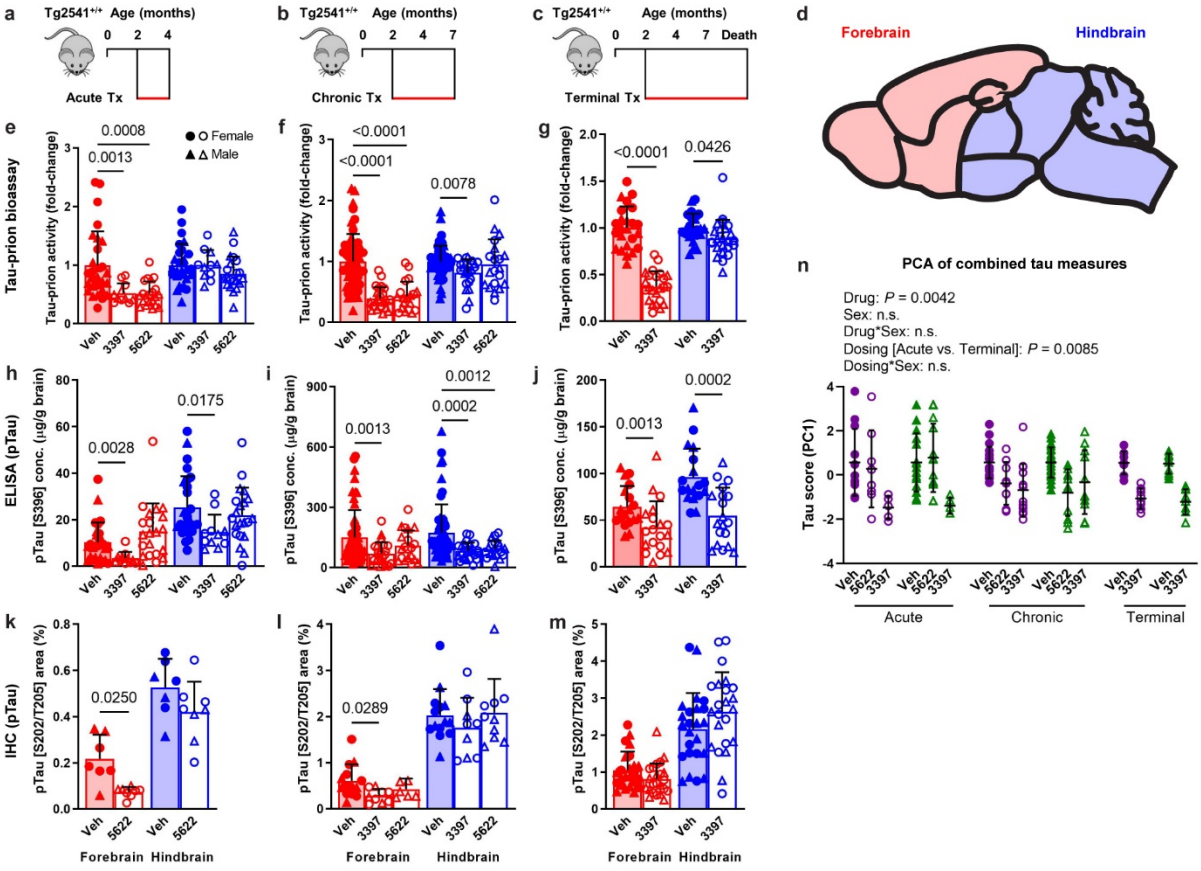


**Fig. 1| CSF1R inhibition by three treatment paradigms reduces pathogenic tau levels in the brains of Tg2541 mice. a–c**, Schematics of acute (**a**), chronic (**b**), or terminal (**c**) PLX treatment of Tg2541 mice from 2–4 mo of age, 2–7 mo of age, or 2 mo of age until death, respectively. **d**, Sagittal view of the mouse brain divided into two regions: the forebrain, containing the cortex, hippocampus, striatum, and olfactory bulb; and the hindbrain, containing the thalamus, hypothalamus, midbrain, cerebellum, and brain stem. **e–g**, Tau-prion levels in forebrain and hindbrain tissue homogenates of Tg2541 mice receiving acute (**e**), chronic (**f**), or terminal (**g**) treatment with vehicle, PLX3397 (275 mg/kg oral), or PLX5622 (1200 mg/kg oral), measured using the HEK293T cell tau-prion bioassay and normalized to the vehicle-treated group. **h–j**, Levels of pTau [S396] measured by ELISA in formic acid extracts of forebrain and hindbrain tissue homogenates of Tg2541 mice receiving acute (**h**), chronic (**i**), or terminal treatment (**j**) with vehicle, PLX3397, or PLX5622, normalized to total protein concentration. **k–m**, Quantification of pTau [S202/T205]-positive area by IHC analysis of forebrain and hindbrain areas of Tg2541 mice receiving acute (**k**), chronic (**l**), or terminal (**m**) treatment with

vehicle, PLX3397, or PLX5622. Welch ANOVA with Dunnett T3 post hoc testing was used in **e**, **f**, **h**, **i**, and **l**. Two-way ANOVA with Holm-Šidák post hoc testing was used in **g**, **j**, **k**, and **m**. *P* values for all statistically significant differences ($P < 0.05$) are shown. **n**, Principal component analysis was performed, using all tau-prion and pTau[S396] data presented in Fig. 1e−j to calculate a 'tau score' that represents the amount of pathogenic tau in both the forebrains and hindbrains of Tg2541 mice. All data was first standardized to the respective vehicle-treated group of the same sex and same dosing paradigm. Then, two principal components (PC1 and PC2) were identified which accounted for 70.7% of the total variance in the data. Multiple linear regression was performed on PC1 of the drug-treated groups to evaluate the main effects sex and dosing paradigm, and the dosing*sex interaction effect. Multiple linear regression was performed on all groups to determine the main effect of drug and the drug*sex interaction effect. *P* values for all statistically significant differences ($P < 0.05$) are shown. n.s. indicates not statistically significant. PC2 was also evaluated, but only the drug main effect was statistically significant. In **e**−**n**, each symbol represents the forebrain or hindbrain of an individual mouse, with female mice shown as closed or open circles and male mice shown as closed or open triangles. Error bars represent the s.d. of the mean.

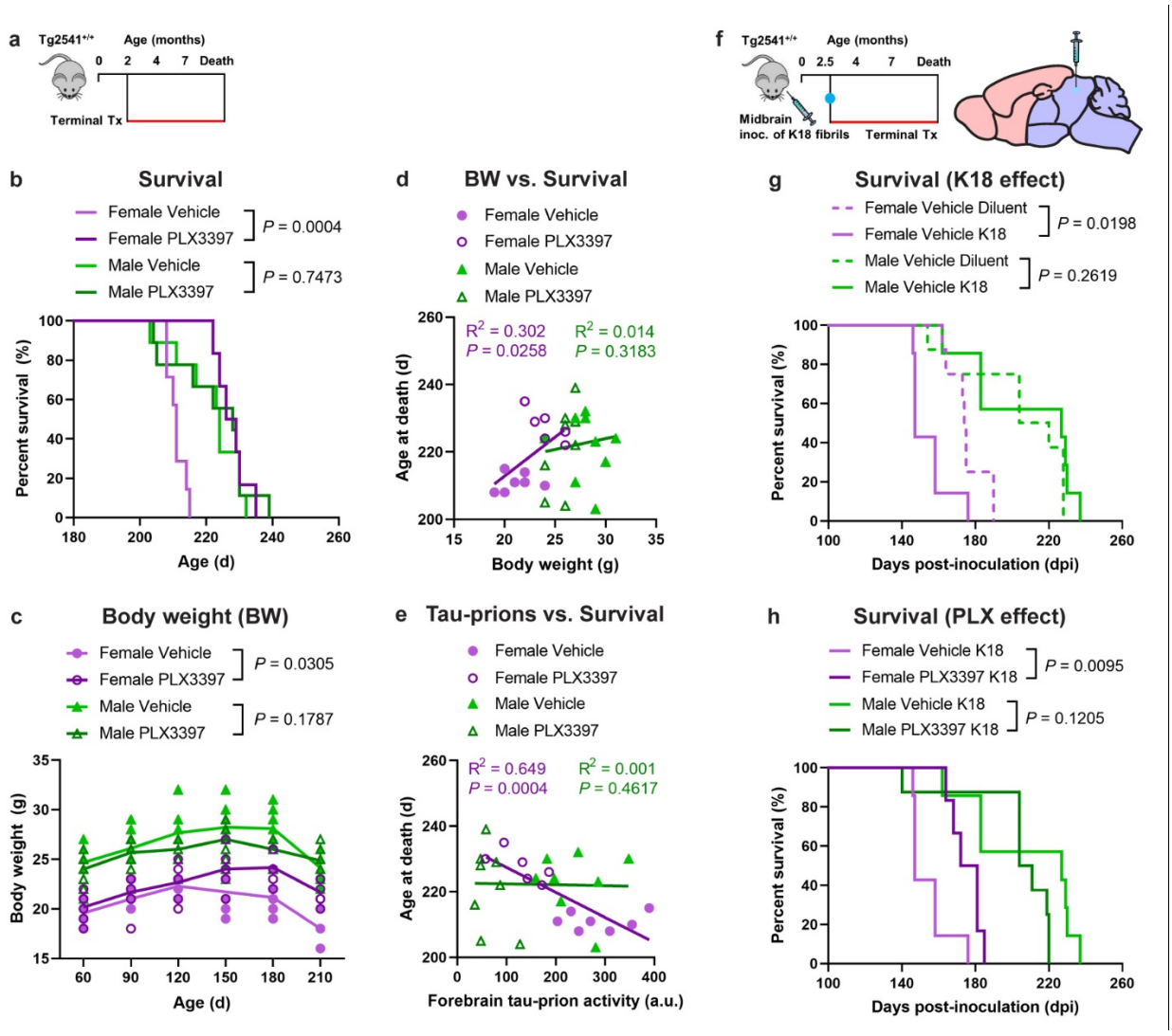


**Fig. 2| CSF1R inhibition extends survival of female Tg2541 mice. a**, Schematic of terminal PLX3397 treatment (275 mg/kg oral) of Tg2541 mice from 2 mo of age until death. **b**, Kaplan-Meier plot showing percent survival of female or male Tg2541 mice treated with vehicle or PLX3397. n=7 mice for Female Vehicle; n=6 mice for Female PLX3397; n=9 mice for Male Vehicle; n=9 mice for Male PLX3397. **c**, Body weights of female or male Tg2541 mice treated with vehicle or PLX3397. Differences in weight between vehicle and PLX3397 treatment in female or male mice were evaluated by mixed-effects analysis (Restricted maximum likelihood). Each symbol represents an individual mouse and lines indicate group means. **d**, **e**, Correlation plots for body weight at 180 d of age (**d**) or forebrain tau-prion activity at death (**e**) and survival for female or male Tg2541 mice treated with vehicle or PLX3397. Each symbol represents an individual mouse and linear regression lines are shown for female or male mice, with vehicle- and PLX3397-treated mice combined. Pearson's correlation analysis was performed and the

results are shown. **f**, Schematic of terminal PLX3397 treatment of Tg2541 mice from 2.5 mo of age until death, following inoculation of K18 tau fibrils into the midbrain (hindbrain region) at 2.5 mo of age. **g**, Kaplan-Meier plot showing percent survival of female or male Tg2541 mice inoculated with K18 tau fibrils or diluent. n=8 mice for Female Vehicle Diluent; n=7 mice for Female Vehicle K18; n=8 mice for Male Vehicle Diluent; n=7 mice for Male Vehicle K18. Differences in survival between diluent and K18 inoculation in male or female mice treated with vehicle were evaluated by Log-rank (Mantel-Cox) test. **h**, Kaplan-Meier plot showing percent survival of female or male Tg2541 mice inoculated with K18 tau fibrils and then receiving terminal treatment of vehicle or PLX3397 (275 mg/kg oral). n=7 mice for Female Vehicle K18; n=6 mice for Female PLX3397 K18; n=7 mice for Male Vehicle K18; n=8 mice for Male PLX3397 K18. In **b**, **g**, and **h**, differences in survival between treatment groups were evaluated by Log-rank (Mantel-Cox) test.

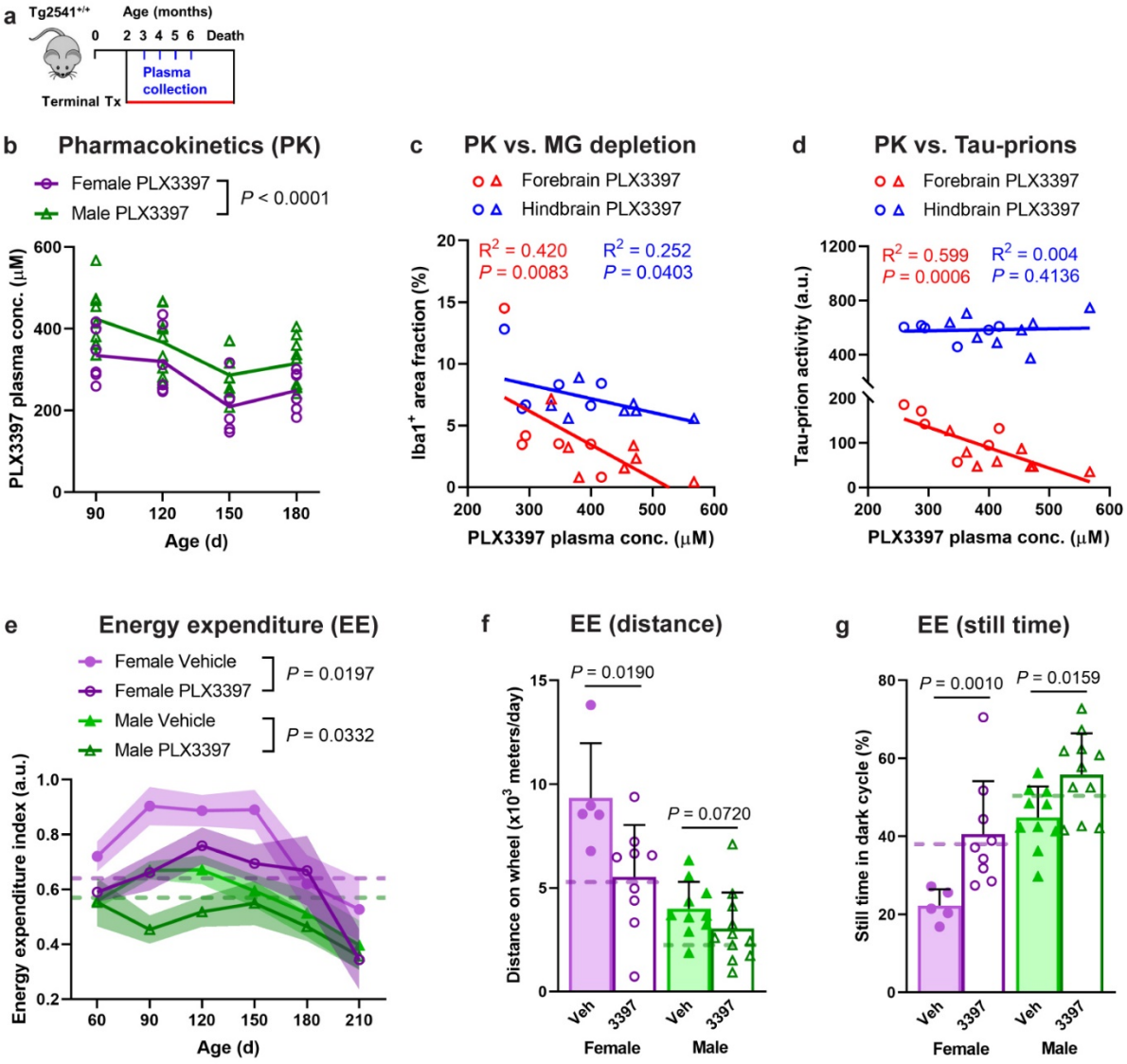


**Fig. 3| PLX3397 has sex-dependent pharmacokinetics and reduces hyperactivity in Tg2541 mice. a**, Schematic of terminal PLX3397 treatment (275 mg/kg oral) of Tg2541 mice from 2 mo of age until death and blood plasma collected at 3, 4, 5, and 6 mo of age. **b**, Plasma concentration of PLX3397 in female or male Tg2541 mice. Each symbol represents an individual mouse and the lines indicate group means. The difference between female and male mice was assessed by two-way repeated measures ANOVA. **c**, **d**, Correlation plots for plasma concentration of PLX3397 at 90 d age and Iba1 area fraction by IHC (**c**) or tau-prion activity (**d**) in the forebrains or hindbrains of Tg2541 mice at death. Female mice are shown as open circles and male mice shown as open triangles. Linear regression was performed with female and male mice combined and best-fit lines are shown. Pearson's correlation analysis was performed and

the results are shown. **e**, Longitudinal energy expenditure indices (see Methods) of female or male Tg2541 mice treated with vehicle or PLX3397. Symbols represent the group means and shaded regions indicate the s.d. of the mean. Group sizes are the same as shown in **f** and **g**. Differences between vehicle and PLX3397 treatment in female or male mice were assessed by three-way repeated measures ANOVA. **f**, **g**, Average distance traveled on the running wheel (**f**) or still time during the dark cycle (**g**) in female or male Tg2541 mice treated with vehicle or PLX3397, and measured between 90-d-old and 150-d-old. Each symbol represents an individual mouse and the dashed lines indicate the same measurements in 90-d-old wild type mice. Differences between vehicle and PLX3397 treatment in female or male mice were assessed by Mann-Whitney test.

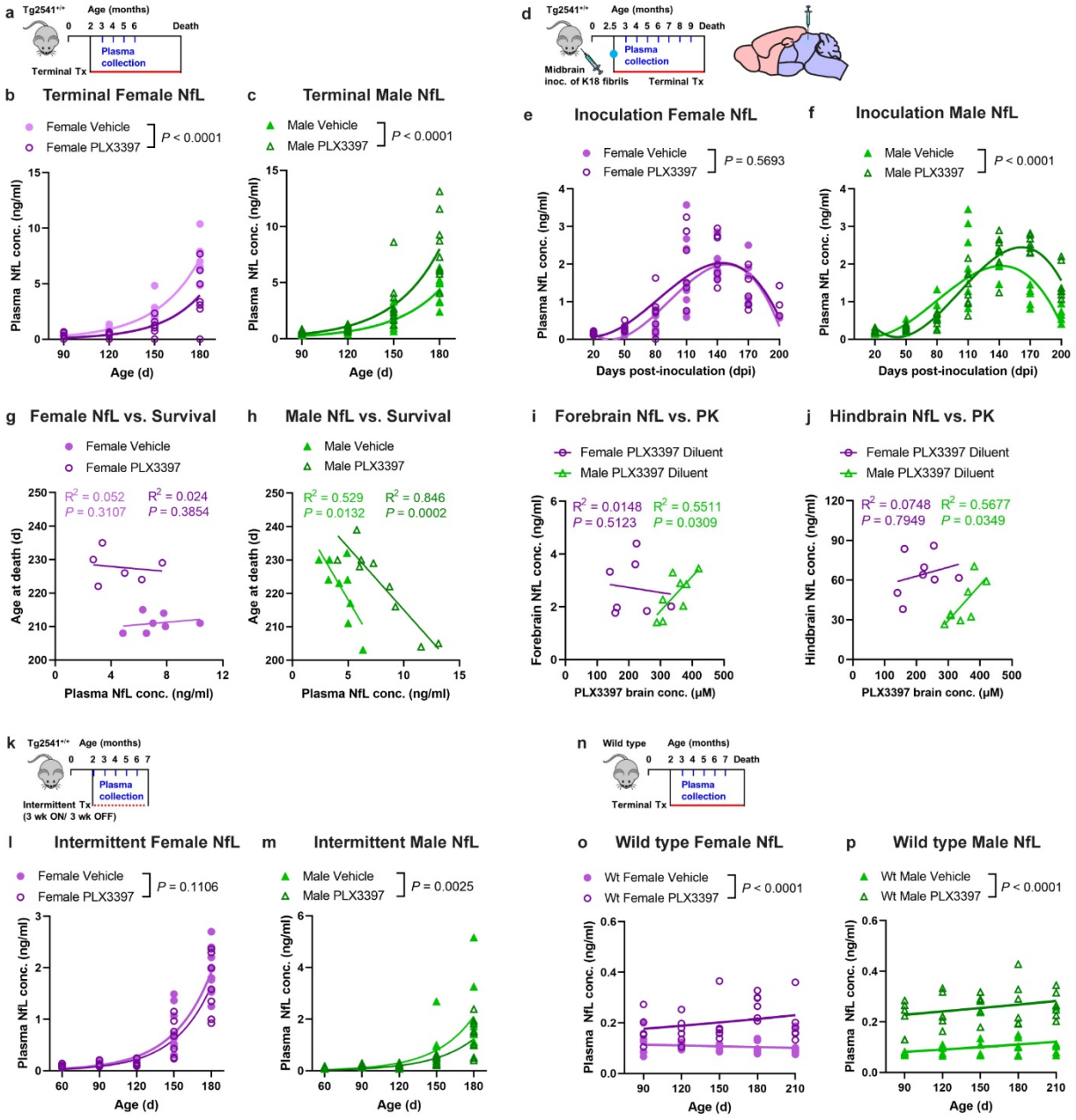


1182

1183 **Fig. 4| Plasma NfL levels are reduced by PLX3397 in female Tg2541 mice and increased**
1184 **in male mice. a**, Schematic of terminal PLX3397 treatment (275 mg/kg oral) of Tg2541 mice
1185 from 2 mo of age until death and blood plasma collected at 3, 4, 5, and 6 mo of age. **b**, **c**,
1186 Plasma concentration of NfL in female (**b**) or male (**c**) Tg2541 mice treated with vehicle or
1187 PLX3397. **d**, Schematic of terminal PLX3397 treatment of Tg2541 mice from 2.5 mo of age until
1188 death, following inoculation of K18 tau fibrils into the midbrain (hindbrain region) at 2.5 mo of
1189 age, and blood plasma collected monthly thereafter until death. **e**, **f**, Plasma concentration of
1190 NfL in female (**e**) or male (**f**) Tg2541 mice inoculated with K18 followed by terminal treatment

with vehicle or PLX3397, plotted over days post-inoculation (dpi). **g**, **h**, Correlation plots for plasma NfL concentration and survival in female (**g**) or male (**h**) Tg2541 mice. Each symbol represents an individual mouse. **i**, **j**, Correlation plots for brain concentration of PLX3397 and NfL concentration in the (**i**) forebrains or (**j**) hindbrains of Tg2541 mice receiving midbrain inoculation with diluent. Each symbol represents the forebrain or hindbrain of an individual mouse. In **g**−**j**, linear regression and Pearson's correlation analysis were performed and the results are shown. **k**, Schematic of intermittent PLX treatment of Tg2541 mice from 2−7 mo of age, with three weeks on treatment followed by three weeks off of treatment, and blood plasma collected at 3, 4, 5, and 6 mo of age. **l**, **m**, Plasma concentration of NfL in female (**l**) or male (**m**) Tg2541 mice receiving intermittent treatment with vehicle or PLX3397. **n**, Schematic of terminal PLX treatment of C57BL/6J wild type mice (Wt) from 2 mo of age until death and blood plasma collected at 3, 4, 5, 6, and 7 mo of age. **o**, **p**, Plasma concentration of NfL in female (**o**) or male (**p**) Wt mice treated with vehicle or PLX3397. In **b**, **c**, **e**, **f**, **l**, **m**, **o**, and **p**, the differences between vehicle or PLX3397 treatment were evaluated by non-linear regression using exponential growth models (**b**, **c**, **l**, **m**, **o**, and **p**) or third-order polynomial models (**e** and **f**) and the best-fit lines and statistical results are shown. Each symbol represents an individual mouse.

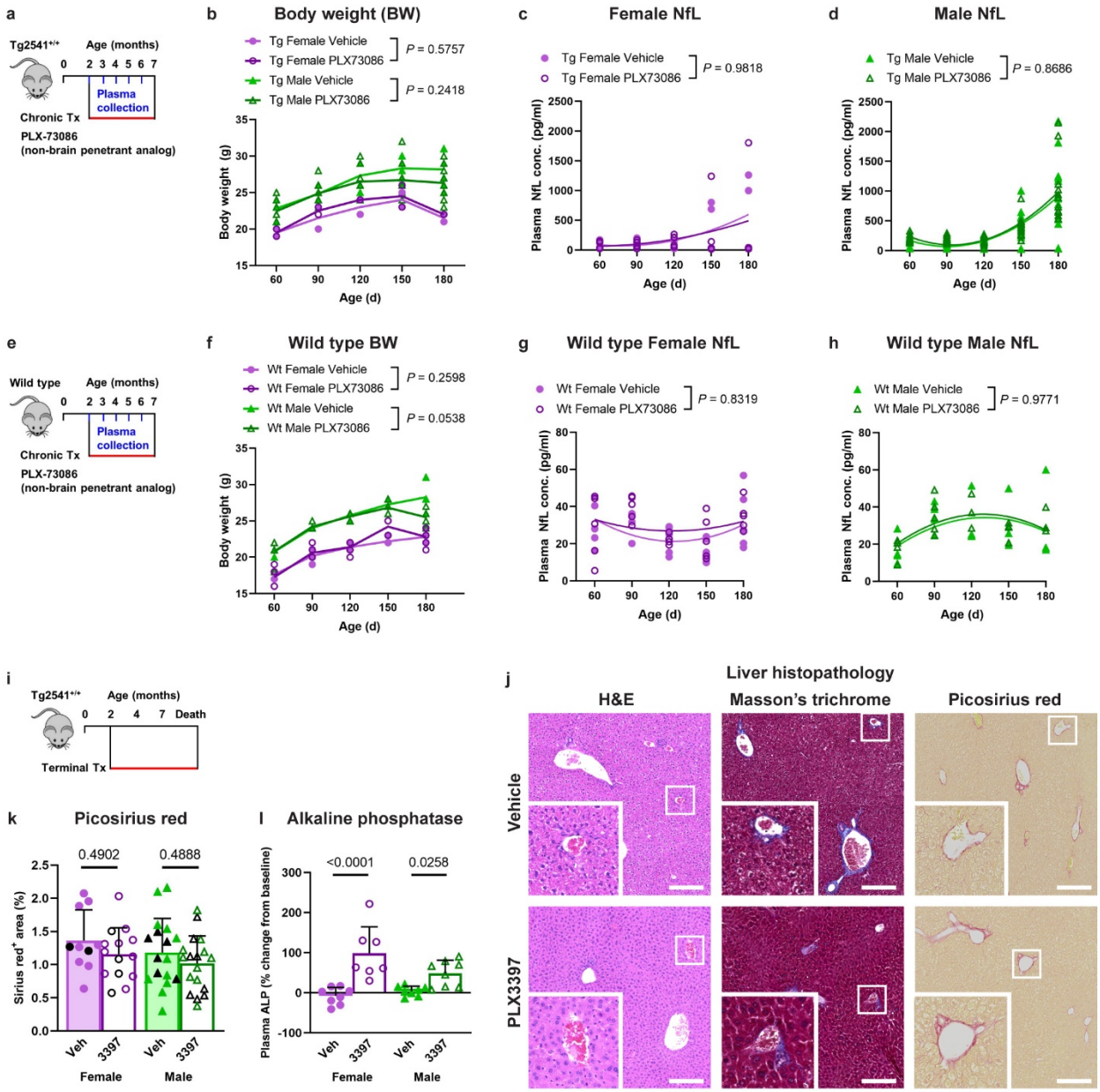


**Fig. 5| Sex-dependent effects of CSF1R are not caused by peripheral toxicity. a**, Schematic of chronic treatment of Tg2541 mice from 2−7 mo of age with PLX73086 (200 mg/kg oral), a non-brain penetrant analog of PLX3397 and PLX5622. **b**, **c**, Plasma concentration of NfL in female (**b**) or male (**c**) Tg2541 mice treated with vehicle or PLX73086. **d**, Body weights of female or male T2541 mice treated with PLX73086. **e**, Schematic of chronic treatment of wild type (Wt) mice from 2−7 mo of age with PLX73086 (200 mg/kg oral). **f**, **g**, Plasma concentration of NfL in female (**f**) or male (**g**) Wt mice treated with vehicle or PLX73086. **h**, Body weights of female or male wild type mice treated with PLX73086. In **b**, **c**, **f**, and **g**, the differences between vehicle or PLX3397 treatment were evaluated by non-linear regression using quadratic models.

Each symbol represents an individual mouse and the best-fit lines and statistical results are shown. In **d** and **h**, differences in weight between vehicle and PLX73086 treatment in male or female mice were evaluated by two-way repeated measures ANOVA and *P* values are shown. Each symbol represents an individual mouse and lines indicate group means. **i**, Schematic of terminal treatment of Tg2541 mice from 2 mo of age until death with PLX3397. **j**, Representative histopathology images of liver sections of Tg2541 mice receiving terminal treatment with vehicle or PLX3397, stained with hematoxylin and eosin (H&E), Masson's trichrome, or Picosirius red. High magnification insets are shown of the regions outlined with a white box. Scale bars, 200 µm. **k**, Sirius red-stained liver sections of Tg2541 mice that received acute or terminal treatment with vehicle or PLX3397 were quantified for percent positive area. The acute and terminal treatment groups were combined for the analysis due to a limited sample size of terminal treatment groups and because the group means were similar for the two treatment paradigms. Mice receiving terminal treatment are shown as black symbols and mice receiving acute treatment are shown as purple or green symbols. **l**, Alkaline phosphatase (ALP) levels were measured at eight months of age in the plasma of Tg2541 mice receiving midbrain inoculation of diluent at 2.5 mo of age and then treated with vehicle or PLX3397 until death. The data are presented as a percent change from ALP levels at two months of age in the same mice. In **k** and **l**, the differences between vehicle and PLX3397 treatment were evaluated by ANOVA with Holm-Šidák post hoc analysis and *P* values are shown. Each symbol represents an individual mouse and error bars indicate the s.d. of the mean.

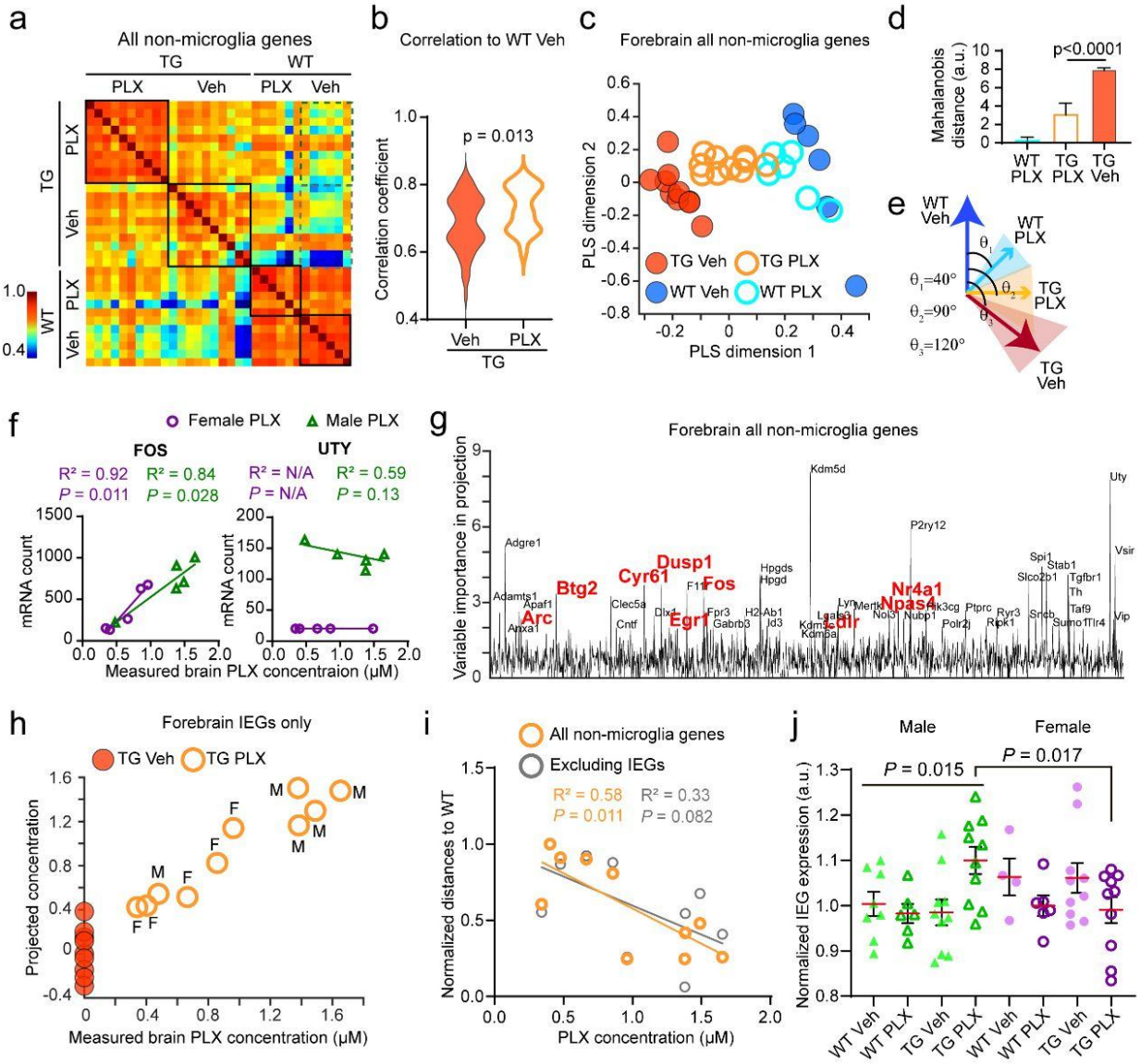


**Fig. 6| PLX treatment normalizes gene expression profile, but dose-dependent excitotoxicity occurs with higher drug exposure. a**, Pearson's correlations among individual mice for non-microglia gene expression patterns (1,599 genes for each mouse). Mice from the same treatment group (black boxes) show a high degree of correlations. Dashed boxes show correlations of Tg2541 mice and wild type vehicle group mice. **b**, Distributions of correlation coefficients in the two groups in dashed boxes in **a**. **c**, Partial least square (PLS) regression scores and projections of non-microglia gene expression patterns in different groups (1,599 genes for each mouse). The first two dimensions are shown covering >95% of the total variance. Vehicle-treated mice (filled dots) were used for regression (five dimensions covering 99.99% of the total variance) and PLX5622-treated (1200 mg/kg oral) mice (empty circles) were projected onto the regression dimensions. **d**, Mahalanobis population vector distances of gene

expression patterns in PLS dimensions relative to the wild type vehicle group. Mann-Whitney test was used for statistical comparison. **e**, Population vector angles of gene expression patterns in PLS dimensions from different treatment groups. **f**, Example plots of measured brain PLX concentration against mRNA counts for a PLX-modulated gene (*FOS*) and a sex-modulated gene (*UTY*). Linear regression and Pearson's correlation analysis were performed and the results are shown. N/A indicates that there was no detectable expression of the UTY gene in female mice. See Supplementary Data File 2 for statistical comparisons between male and female PLX-treated mice of all genes. **g**, Variable importance in projection (VIP) scores in a PLS regression using non-microglial gene expression patterns to brain PLX concentration and sex. Genes with VIP scores above 2 are labeled. Red fonts indicate a subset that belongs to immediate early genes (IEGs). **h**, Scatter plot of measured vs. projected brain PLX concentration, which was based on a PLS regression with IEG expression. **i**, Correlation of brain PLX concentration and the population vector distances between PLX-treated individual mouse transcriptome pattern to WT, with and without the IEGs (1,599 and 1,543 genes for each mouse, respectively). Linear regressions were calculated for each group. **j**, Quantification of normalized expression levels from all IEGs (56 genes for each mouse) in the forebrain. Mann-Whitney tests were used for comparing between groups. In **c**, **f**, and **h**−**j**, each symbol represents an individual mouse.

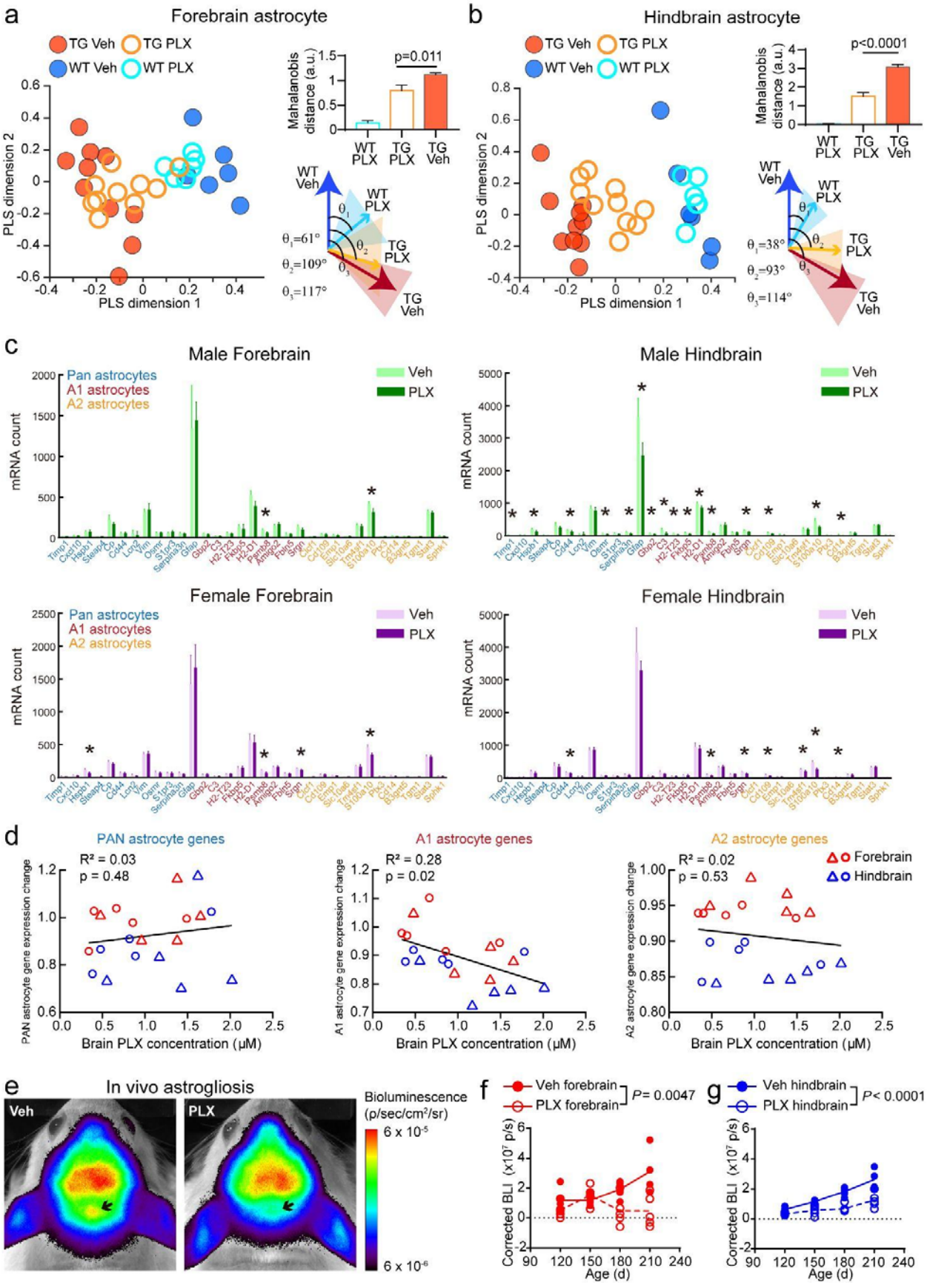

**Fig. 7| CSF1R inhibition ameliorates tau-induced pathological astrocyte activation**. **a**, **b**, Analyses similar to Fig. 6c−e using astrocyte-specific genes (47 genes in each mouse) in (**a**) forebrain and (**b**) hindbrain regions. For other cell types and brain regions, see Supplementary Fig. 12. **c**, Quantifications of featured astrocyte genes in different conditions. Data are represented as mean ± S.D. T-tests were used to compare vehicle and PLX-treated groups for each gene, with 5% false discovery rate correction for multiple comparisons. **d**, Correlation of brain PLX concentration and different groups of astrocyte gene expression. Based on a prior study[45], A1 genes are associated with neurotoxic astrocytes following lipopolysaccharide exposure and A2 genes are associated with neuroprotective function in an artery occlusion model. Linear regressions were calculated for each group. **e**, Representative images of *in vivo* bioluminescence imaging of GFAP activity in Tg2541 mice with vehicle or PLX3397 treatment. Arrows indicate hindbrain regions. **f**, **g**, Quantifications of longitudinal measurements of astrogliosis-driven bioluminescence in the (**f**) forebrains or (**g**) hindbrains of Tg2541 mice with vehicle or PLX3397 treatment. Differences in BLI signal between vehicle and PLX treatment were evaluated by mixed-effects analysis (Restricted maximum likelihood). In **a**, **b**, **d**, **f**, and **g**, each symbol represents an individual mouse.

1284

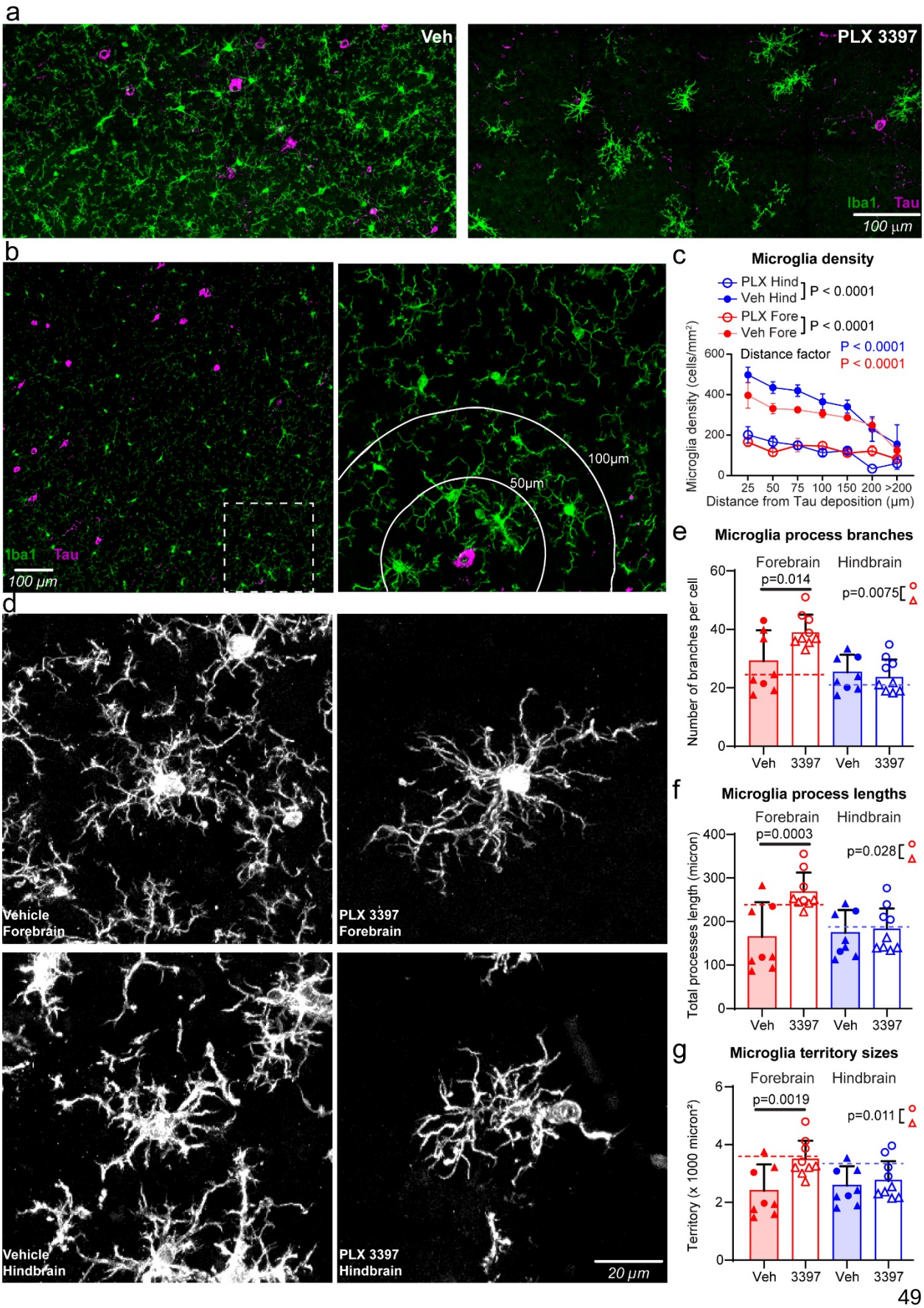

**Fig. 8| PLX3397 treatment preferentially eliminates reactive microglia around tau deposits. a**, Representative confocal images of immunostaining of tau protein (magenta) and microglia (Iba1, green) in the brain of a vehicle-treated (left) or PLX3397-treated (right) 210-d-old Tg2541 mouse. **b**, Representative confocal images, similar to panel **a**, of a vehicle-treated 210-d-old Tg2541 mouse. The right panel shows the zoomed image from the dashed box in the left panel. The white lines in the right panel show distances from the tau deposit at the center. **c**, Quantification of microglial densities at different distances from the nearest tau deposit in Tg2541 mice treated with vehicle or PLX3397 (275 mg/kg oral). Two-way ANOVA was used to compare statistical differences between treatment groups and distance bins. **d**, Representative confocal images of microglial processes labeled by Iba1 immunohistochemistry. **e**−**g**, Quantification of microglial processes branch numbers (**e**), total lengths (**f**) and territory sizes (**g**) in Tg2541 mice treated with vehicle or PLX3397. Each data point shows the average value of the microglia measured in an individual mouse. Error bars represent the s.d. of the mean. Circles indicate female mice and triangles indicate male mice. Dotted lines show the average measurements from microglia in wild type mice. Mann-Whitney tests were used to compare between groups. The forebrain regions of PLX3397-treated male and female mice were also compared directly and the *P* values are shown on each plot.

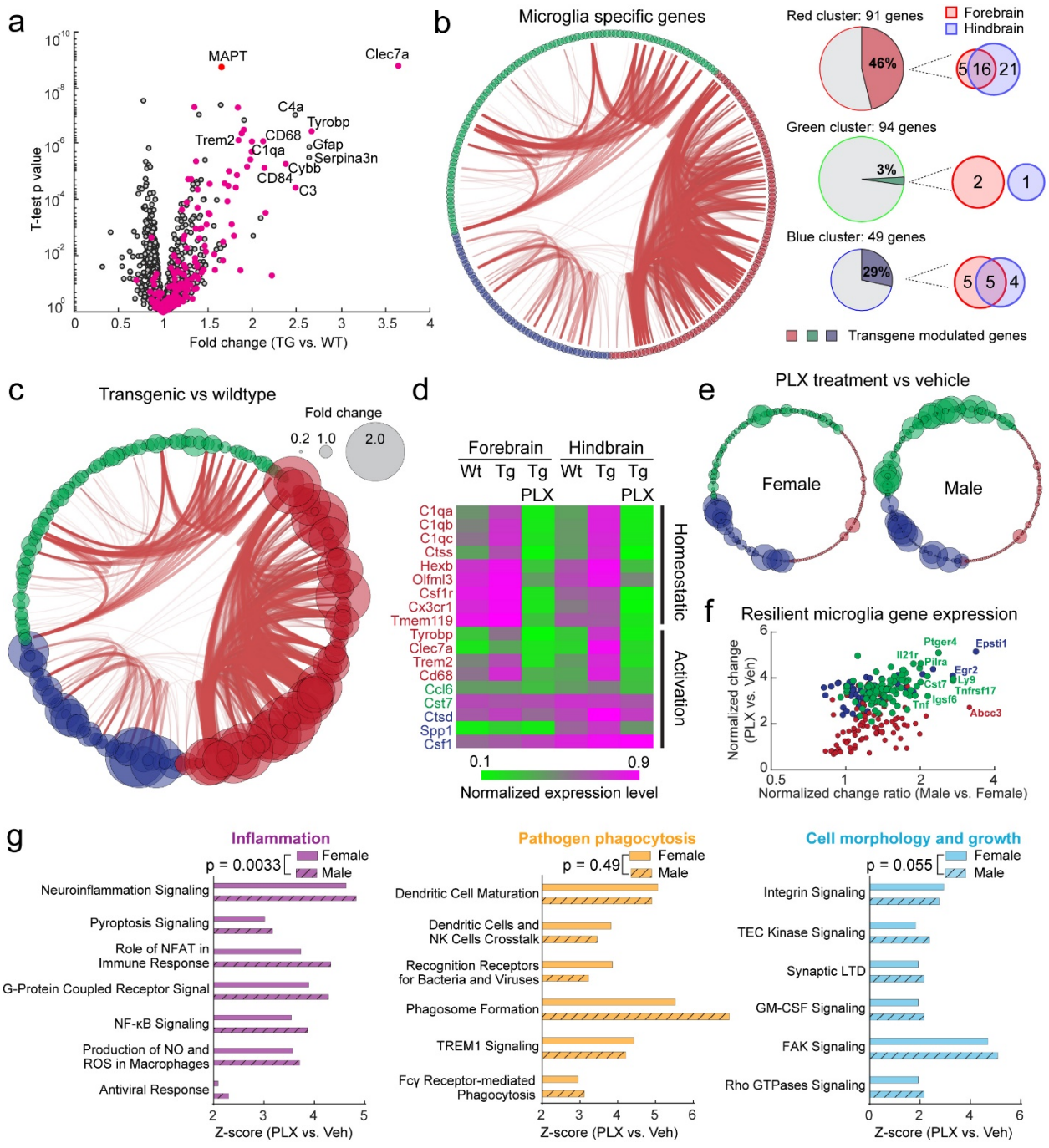


**Fig. 9| Selective ablation of tau-activated microglia gene expression by PLX5622. a**, Volcano plot of gene expression changes between Tg2541 and wild type mice. Many microglial-specific genes (magenta dots) show trends of up-regulation in Tg2541 mice. **b**, Microglial-specific genes (242 genes in our dataset) are clustered into three groups: red, green and blue. Connecting arcs between genes represent the degree of correlation. The pie charts on the right show the percentage of genes in each group that are differentially expressed in Tg2541 and

wild type mice, and the Venn diagrams indicate the brain regions of differential expression. **c**, Schemaball graphs of microglial-specific genes comparing Tg2541 to wild type. Individual circle sizes indicate fold changes. **d**, Heatmap showing expression level changes in DAM genes[50]. Gene names are color coded to show their group assignments. **e**, Schemaball graphs of microglial-specific genes comparing Tg2541 vehicle to PLX5622 treatment (1200 mg/kg oral) in male and female mice. **f**, Estimated gene expression levels in resilient microglia comparing between genders and treatment. Each dot represents a different gene, and is color-coded according to the cluster to which it belongs. **g**, Ingenuity Pathway Analysis of the gene expression patterns in the resilient microglia in male and female mice. Paired t-tests were used in each category to compare sexes.

# SUPPLEMENTARY INFORMATION

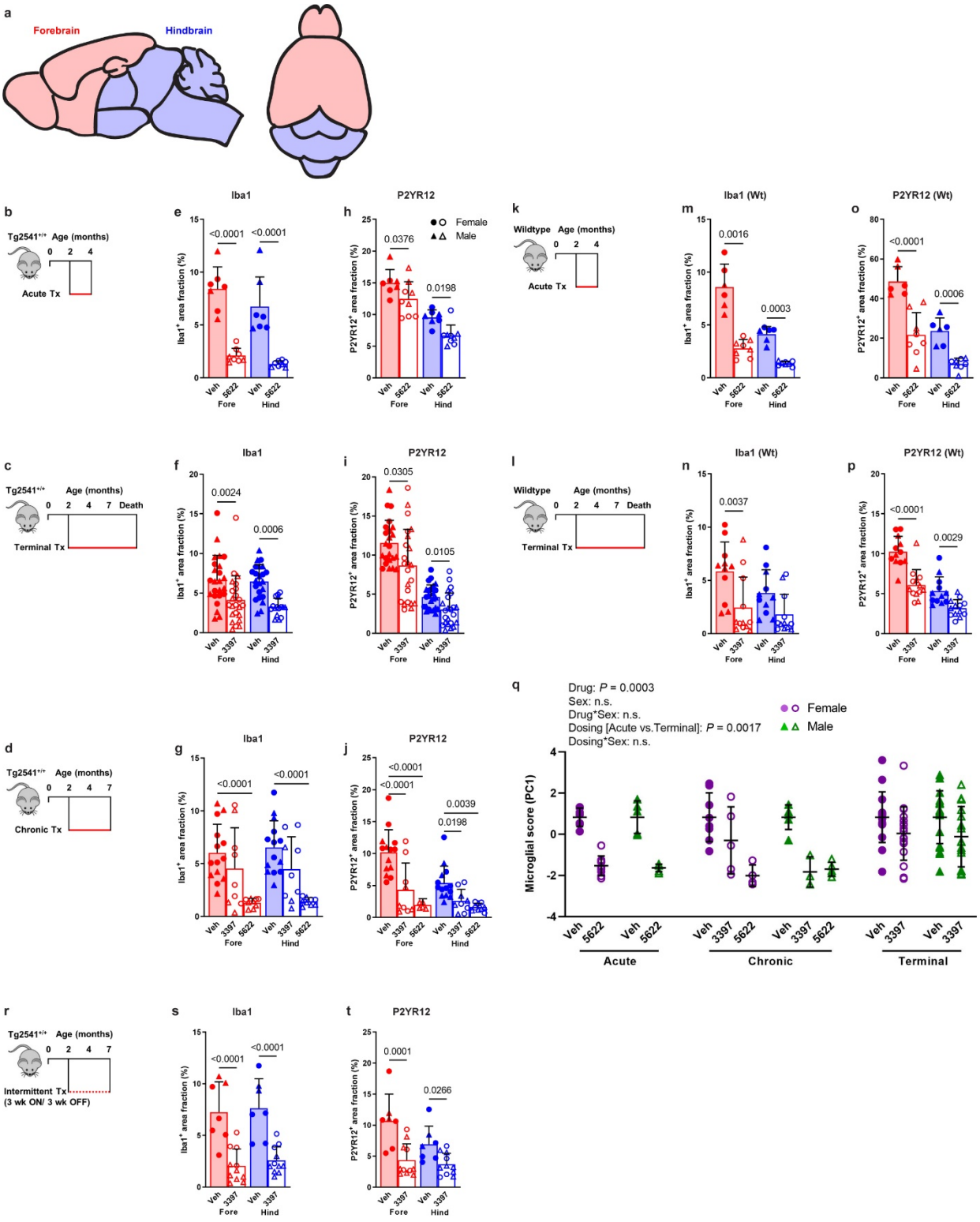


**Supplementary Fig. 1| Microglial depletion by CSF1R inhibitors in Tg2541 and wild type**

**mice. a**, Sagittal and superior diagrams of the mouse brain divided into two regions: the forebrain, containing the cortex, hippocampus, striatum, and olfactory bulb; and the hindbrain, containing the thalamus, hypothalamus, midbrain, cerebellum, and brain stem. **b**–**d**, Schematics of acute (**b**), terminal (**c**), or chronic (**d**) PLX treatment of Tg2541 mice from 2–4 mo of age, 2 mo of age until death, or 2–7 mo of age, respectively. **e**–**g**, Quantification of the Iba1-positive area fraction by IHC in the forebrains or hindbrains of Tg2541 mice receiving acute (**e**), terminal (**f**), or chronic (**g**) treatment with vehicle, PLX3397 (275 mg/kg oral), or PLX5622 (1200 mg/kg oral). **h**–**j**, Quantification of the P2YR12-positive area fraction by IHC in the forebrains or hindbrains of Tg2541 mice receiving acute (**h**), terminal (**i**), or chronic (**j**) treatment with vehicle, PLX3397, or PLX5622. **k**, **l**, Schematics of acute (**k**) or terminal (**l**) PLX treatment of C57BL/6J wild type mice (Wt) from 2–4 mo of age, or 2 mo of age until death, respectively. **m**, **n**, Quantification of the Iba1-positive area fraction by IHC in the forebrain and hindbrain of Wt mice receiving acute (**m**) or terminal (**n**) treatment with vehicle, PLX3397, or PLX5622. **o**, **p**, Quantification of the P2YR12-positive area fraction by IHC in the forebrains or hindbrains of Wt mice receiving acute (**o**) or terminal (**p**) treatment with vehicle, PLX3397, or PLX5622. *P* values for all statistically significant differences ($P < 0.05$) are shown. **q**, Principal component analysis was performed, using all data presented in **e**–**j** and **m**–**p** to calculate a 'microglial score' that represents the amount of Iba1 and P2YR12 staining in both the forebrains and hindbrains of Tg2541 and Wt mice. All data was first standardized to the respective vehicle-treated group of the same sex and same dosing paradigm. Then, two principal components (PC1 and PC2) were identified which accounted for 79.0% of the total variance in the data. Multiple linear regression was performed on PC1 of the drug-treated groups to evaluate the main effects sex and dosing paradigm, and the dosing*sex interaction effect. Multiple linear regression was performed on all groups to determine the main effect of drug and the drug*sex interaction effect. *P* values for all statistically significant differences ($P < 0.05$) are shown. n.s. indicates not statistically significant. PC2 was also evaluated, but only the drug main effect was statistically significant. **r**, Schematic of intermittent PLX treatment of Tg2541 mice from 2–7 mo of age, with three weeks on treatment followed by three weeks off of treatment. **s**, **t**, Quantification of the Iba1-positive (**s**) or P2YR12-positive (**t**) area fractions by IHC in the forebrains or hindbrains of Tg2541 mice receiving intermittent treatment with vehicle or PLX3397. In **e**–**j**, **m**–**p**, **s**, and **t**, each symbol represents the forebrain or hindbrain of an individual mouse, with female mice shown as closed or open circles and male mice shown as closed or open triangles. Error bars represent s.d. of the mean. Two-way ANOVA with Holm-Šidák post hoc testing was used in **e**, **f**, **h**, **i**, **m**–**p**, **s**, and **t**. Welch ANOVA with Dunnett T3 post hoc testing was used in **g** and **j**.

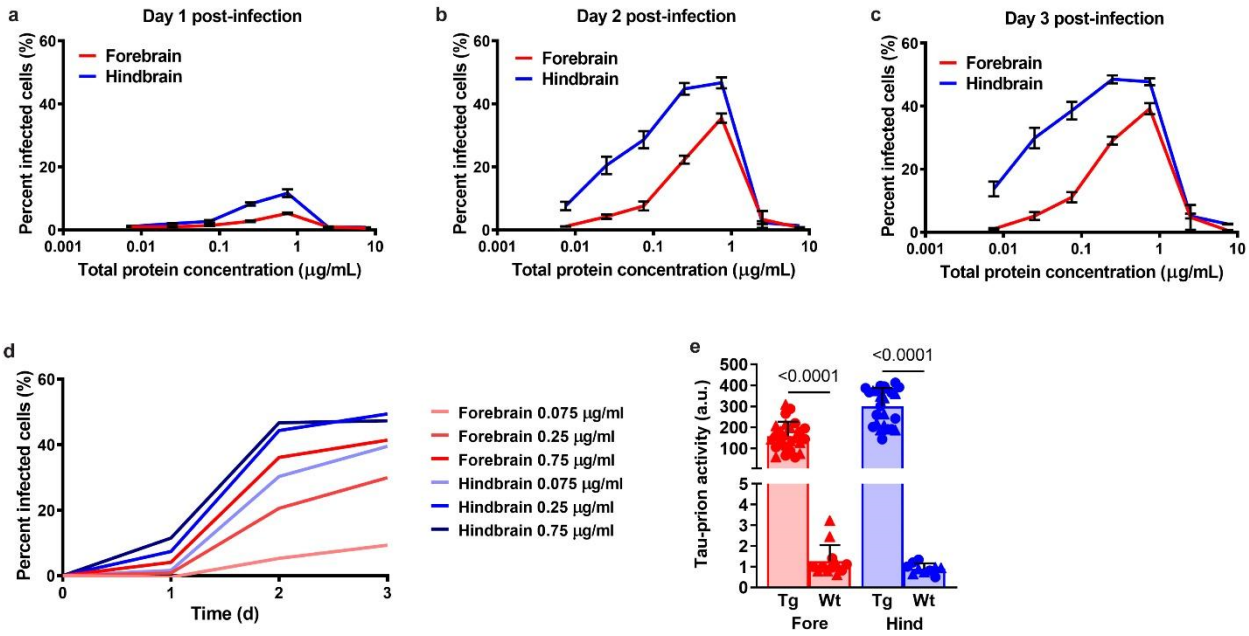


**Supplementary Fig. 2| Optimization of HEK293T cell bioassay for measuring tau-prions in Tg2541 mouse brain homogenates. a−c**, Percent of HEK293T cells expressing YFP-tau-RD*P301L/V337M with tau aggregates at one (**a**), two (**b**), or three (**c**) days post-infection with Tg2541 mouse forebrain or hindbrain homogenates at concentrations ranging from 0.0075−7.5 µg/ml. Error bars represent s.e.m. of three terminal Tg2541 mice. **d**, Percent of cells infected with tau aggregates over time following infection with 0.075, 0.25, or 0.75 µg/ml Tg2541 mouse forebrain or hindbrain homogenates. Lines represent the means of three terminal Tg2541 mice. **e**, Tau-prion levels in 0.25 µg/ml forebrain or hindbrain homogenates of Tg2541 (Tg) or wild type (Wt) mice, measured using the optimized HEK293T cell tau-prion bioassay. Each symbol represents the forebrain or hindbrain of an individual mouse and female mice are shown as closed circles while male mice are shown as closed triangles. Two-way ANOVA with Holm-Šidák post hoc testing was used and *P* values for all statistically significant differences ($P < 0.05$) are shown.

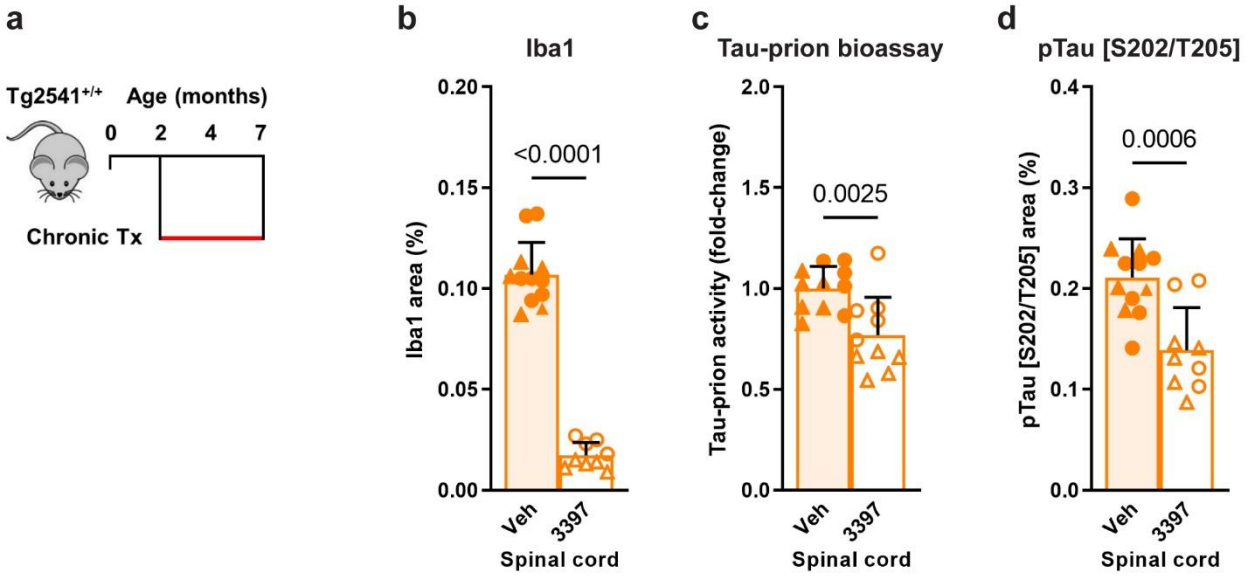


**Supplementary Fig. 3| CSF1R inhibition reduces microglia and pathogenic tau levels in the spinal cords of Tg2541 mice. a**, Schematic of chronic PLX treatment of Tg2541 mice from 2−7 mo of age. **b**, Quantification of the Iba1-positive area fraction by IHC in the spinal cords of Tg2541 mice receiving chronic treatment with vehicle or PLX3397 (275 mg/kg oral). **c**, Tau-prion levels in spinal cord tissue homogenates of Tg2541 mice receiving chronic treatment with vehicle or PLX3397, measured using the HEK293T cell tau-prion bioassay and normalized to the vehicle group. **d**, Quantification of pTau [S202/T205]-positive area by IHC in the spinal cords of Tg2541 mice receiving chronic treatment with vehicle or PLX3397. In **b**−**d**, each symbol represents an individual mouse, with female mice shown as closed or open circles and male mice shown as closed or open triangles. Error bars represent s.d. of the mean. Unpaired t tests were used and *P* values for all statistically significant differences ($P < 0.05$) are shown.

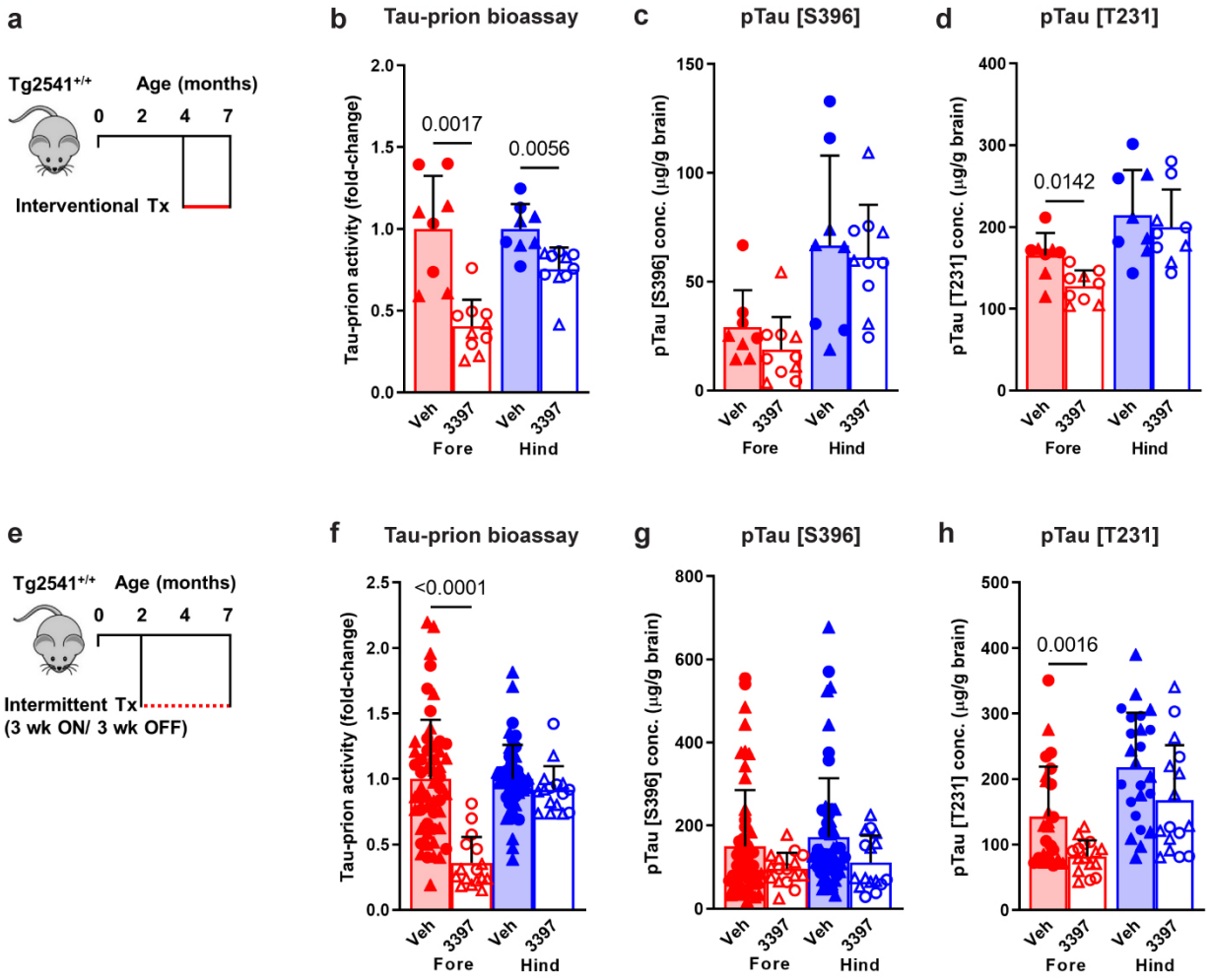


**Supplementary Fig. 4| Interventional or intermittent CSF1R inhibition reduces pathogenic tau levels in the brains of Tg2541 mice. a**, Schematic of interventional PLX treatment of Tg2541 mice from 4−7 mo of age. **b**, Tau-prion levels in forebrain and hindbrain tissue homogenates of Tg2541 mice receiving interventional treatment with vehicle or PLX3397 (275 mg/kg oral), measured using the HEK293T cell tau-prion bioassay and normalized to the vehicle group. **c**, Levels of pTau [S396] measured by ELISA in formic acid extracts of forebrain and hindbrain tissue homogenates of Tg2541 mice receiving interventional treatment with vehicle or PLX3397, normalized to total protein concentration. **d**, Levels of pTau [T231] measured by ELISA in formic acid extracts of forebrain and hindbrain tissue homogenates of Tg2541 mice receiving interventional treatment with vehicle or PLX3397, normalized to total protein concentration. **e**, Schematic of intermittent PLX treatment of Tg2541 mice from 2−7 mo of age, with three weeks on treatment followed by three weeks off of treatment. **f**, Tau-prion levels in forebrain and hindbrain tissue homogenates of Tg2541 mice receiving intermittent treatment

with vehicle or PLX3397, measured using the HEK293T cell tau-prion bioassay and normalized to the vehicle group. **g**, Levels of pTau [S396] measured by ELISA in formic acid extracts of forebrain and hindbrain tissue homogenates of Tg2541 mice receiving intermittent treatment with vehicle or PLX3397, normalized to total protein concentration. **h**, Levels of pTau [T231] measured by ELISA in formic acid extracts of forebrain and hindbrain tissue homogenates of Tg2541 mice receiving intermittent treatment with vehicle or PLX3397, normalized to total protein concentration. In **b**−**d** and **f**−**h**, each symbol represents the forebrain or hindbrain of an individual mouse, with female mice shown as closed or open circles and male mice shown as closed or open triangles. Error bars represent s.d. of the mean. Two-way ANOVA with Holm-Šidák post hoc testing was used and *P* values for all statistically significant differences ($P < 0.05$) are shown.

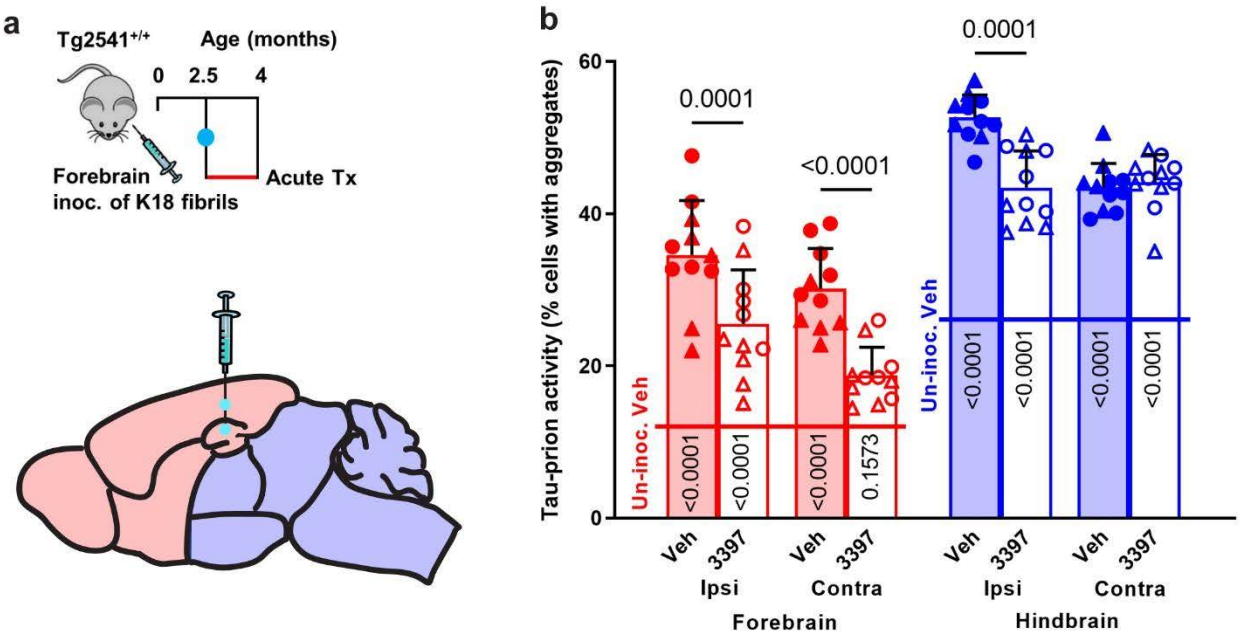


**Supplementary Fig. 5| CSF1R inhibition reduces pathogenic tau spreading following K18 forebrain inoculation. a**, Schematic of acute PLX treatment of Tg2541 mice from 2.5−4 mo of age following inoculation of K18 tau fibrils into the hippocampus and overlying cortex (forebrain regions) at 2.5 mo of age. **b**, Tau-prion levels in the ipsilateral (inoculated side) or contralateral (un-inoculated side) forebrain or hindbrain tissue homogenates of Tg2541 mice receiving acute treatment with vehicle or PLX3397 (275 mg/kg oral) following K18 forebrain inoculation, measured using the HEK293T cell tau-prion bioassay and presented as percent of cells with tau aggregates. Horizontal lines across bars indicate the mean tau-prion level in forebrain (12.54% cells with aggregates) or hindbrain (26.06% cells with aggregates) tissue homogenates of Tg2541 mice that did not undergo K18 inoculation and received acute treatment with vehicle (Un-inoc. Veh). Each symbol represents the ipsilateral or contralateral forebrain or hindbrain of an individual mouse, with female mice shown as closed or open circles and male mice shown as closed or open triangles. Error bars represent s.d. of the mean. Three-way ANOVA with Holm-Šidák post hoc testing was used and *P* values for all statistically significant differences ($P < 0.05$) between Veh and 3397 are shown above the bars. *P* values for all differences between each group and the respective brain region of Un-inoc. Veh mice are shown on the bars.

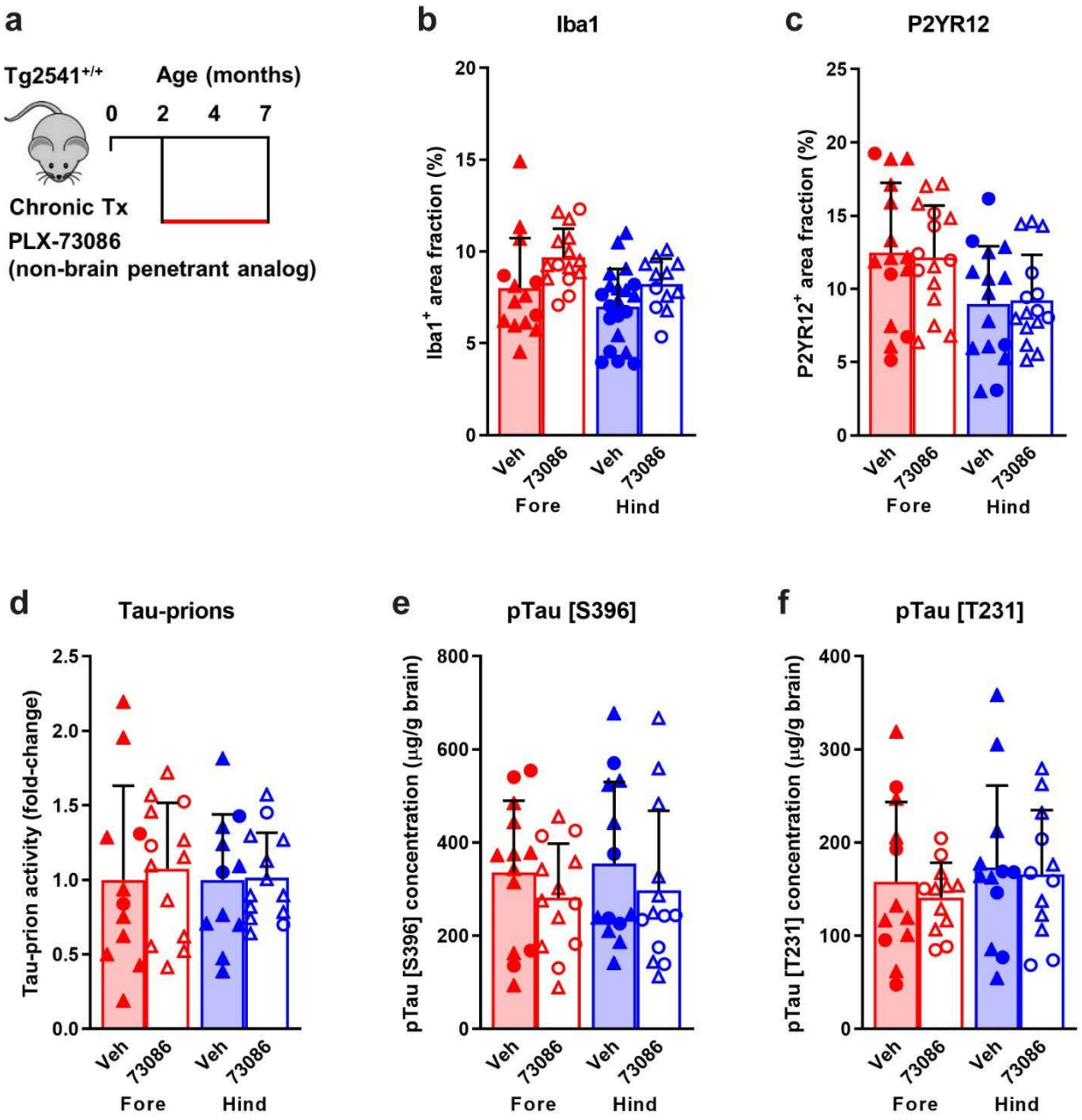


**Supplementary Fig. 6| Non-brain penetrant analog of CSF1R inhibitors does not reduce microglia or pathogenic tau levels in the brains of Tg2541 mice. a**, Schematic of chronic treatment of Tg2541 mice from 2−7 mo of age with PLX73086, a non-brain penetrant analog of PLX3397 and PLX5622. **b**, **c**, Quantification of the Iba1-positive (**b**) or P2YR12-positive (**c**) area fractions by IHC in the forebrains or hindbrains of Tg2541 mice receiving chronic treatment with vehicle or PLX73086 (200 mg/kg oral). **d**, Tau-prion levels in forebrain and hindbrain tissue homogenates of Tg2541 mice receiving chronic treatment with vehicle or PLX73086, measured

using the HEK293T cell tau-prion bioassay and normalized to the vehicle group. **e**, **f**, Levels of pTau [S396] (**e**) or pTau [T231] (**f**) measured by ELISA in formic acid extracts of forebrain and hindbrain tissue homogenates of Tg2541 mice receiving chronic treatment with vehicle or PLX73086, normalized to total protein concentration. In **b**−**f**, each symbol represents the forebrain or hindbrain of an individual mouse, with female mice shown as closed or open circles and male mice shown as closed or open triangles. Error bars represent s.d. of the mean. Two-way ANOVA with Holm-Šidák post hoc testing was used and *P* values for all statistically significant differences ($P < 0.05$) are shown.

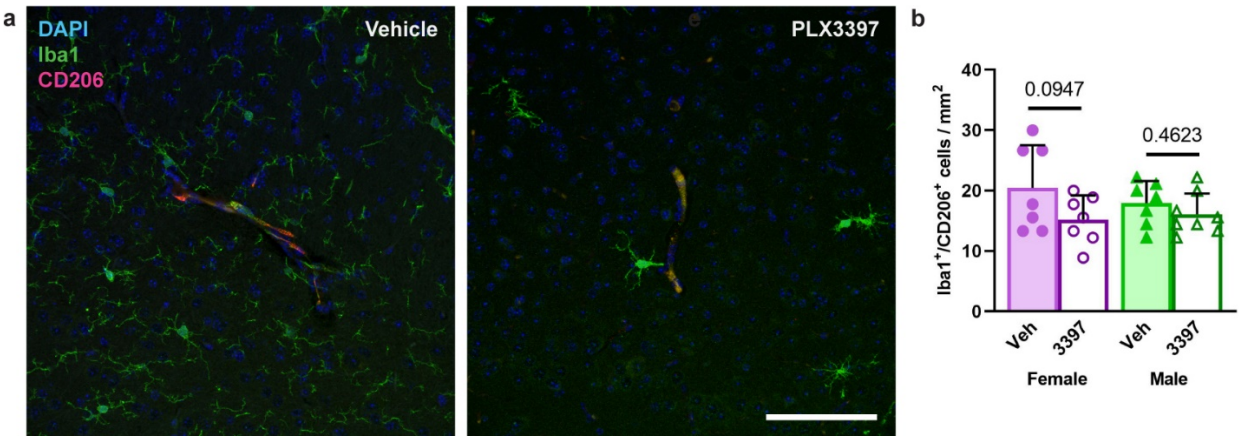


**Supplementary Fig. 7| Pharmacological CSF1R inhibition does not deplete perivascular macrophages. a**, Representative immunofluorescence images of Tg2541 mouse cortical blood vessels labeled for perivascular macrophages (Iba1$^+$/CD206$^+$) and microglia (Iba1$^+$/CD206$^-$). Iba1 labels both PVMs and microglia. Mice were treated with PLX3397 from 2.5 mo of age until death, following inoculation of K18 tau fibrils into the midbrain (hindbrain region) at 2.5 mo of age. Scale bar, 100 µm. **b**, Quantification of Iba1$^+$/CD206$^+$ cell density in images of Tg2541 mouse cortical blood vessels. Each symbol represents the average of six blood vessel images from each individual mouse. Error bars represent s.d. of the mean. Two-way ANOVA was used and the *P* values for Holm-Šidák post hoc testing between treatment groups are shown.

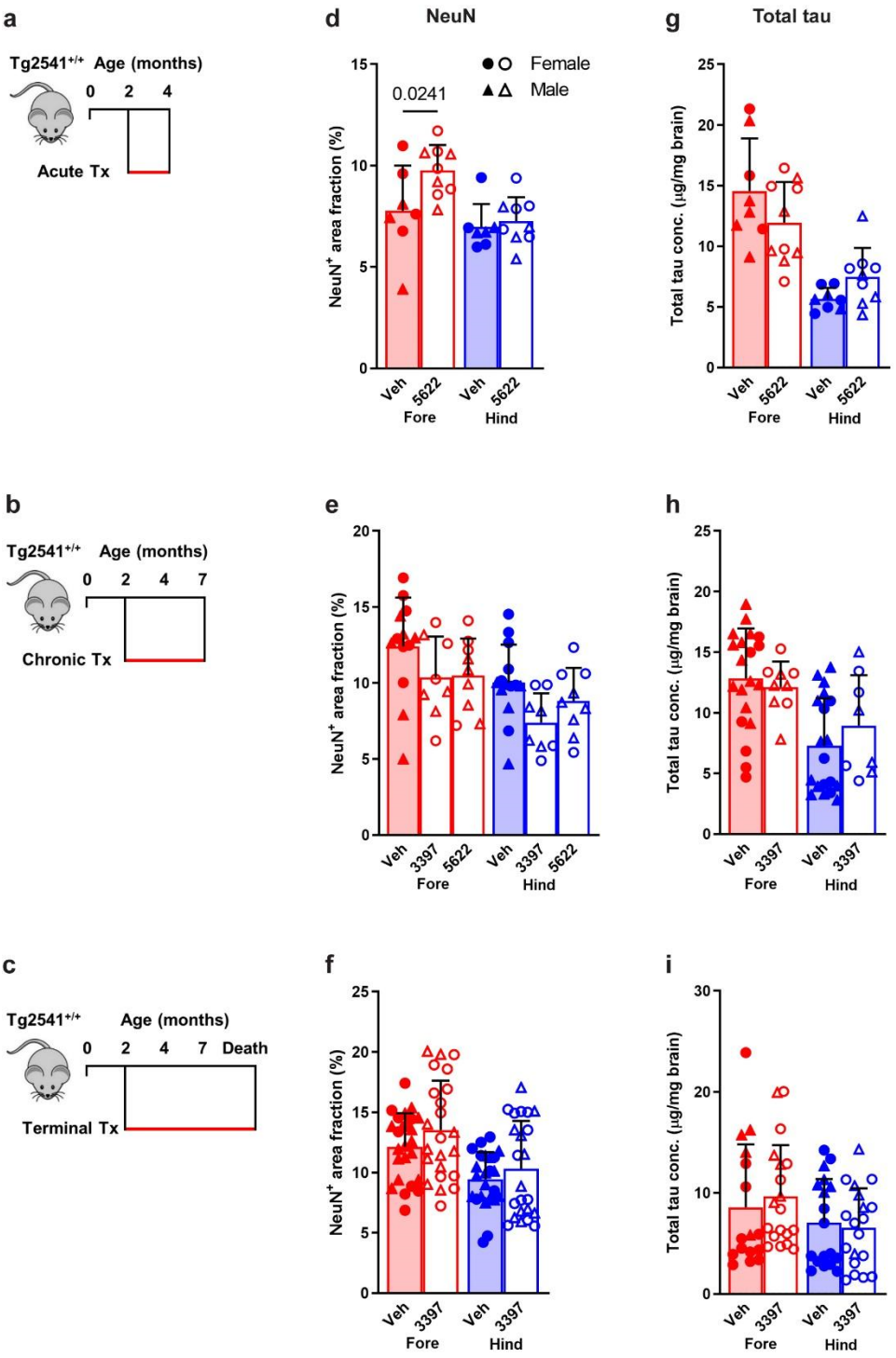


1451

1452 **Supplementary Fig. 8| CSF1R inhibition by three treatment paradigms does not affect**
1453 **neurons or total tau levels. a−c**, Schematics of acute (**a**), chronic (**b**), or terminal (**c**) PLX
1454 treatment of Tg2541 mice from 2−4 mo of age, 2−7 mo of age, or 2 mo of age until death,
1455 respectively. **d−f**, Quantification of neuronal nuclei (NeuN)-positive area fraction by IHC analysis

of forebrain and hindbrain areas of Tg2541 mice receiving acute (**d**), chronic (**e**), or terminal (**f**) treatment with vehicle, PLX3397 (275 mg/kg oral), or PLX5622 (1200 mg/kg oral). **g**−**i**, Levels of total tau measured by ELISA in forebrain and hindbrain tissue homogenates of Tg2541 mice receiving acute (**g**), chronic (**h**), or terminal treatment (**i**) with vehicle, PLX3397, or PLX5622, normalized to total protein concentration. In **d**−**i**, each symbol represents the forebrain or hindbrain of an individual mouse, with female mice shown as closed or open circles and male mice shown as closed or open triangles. Error bars represent s.d. of the mean. Two-way ANOVA with Holm-Šidák post hoc testing was used in **d**, and **f**−**i**. One-way ANOVA with Holm-Šidák post hoc testing was used in **e**. *P* values for all statistically significant differences ($P < 0.05$) are shown.

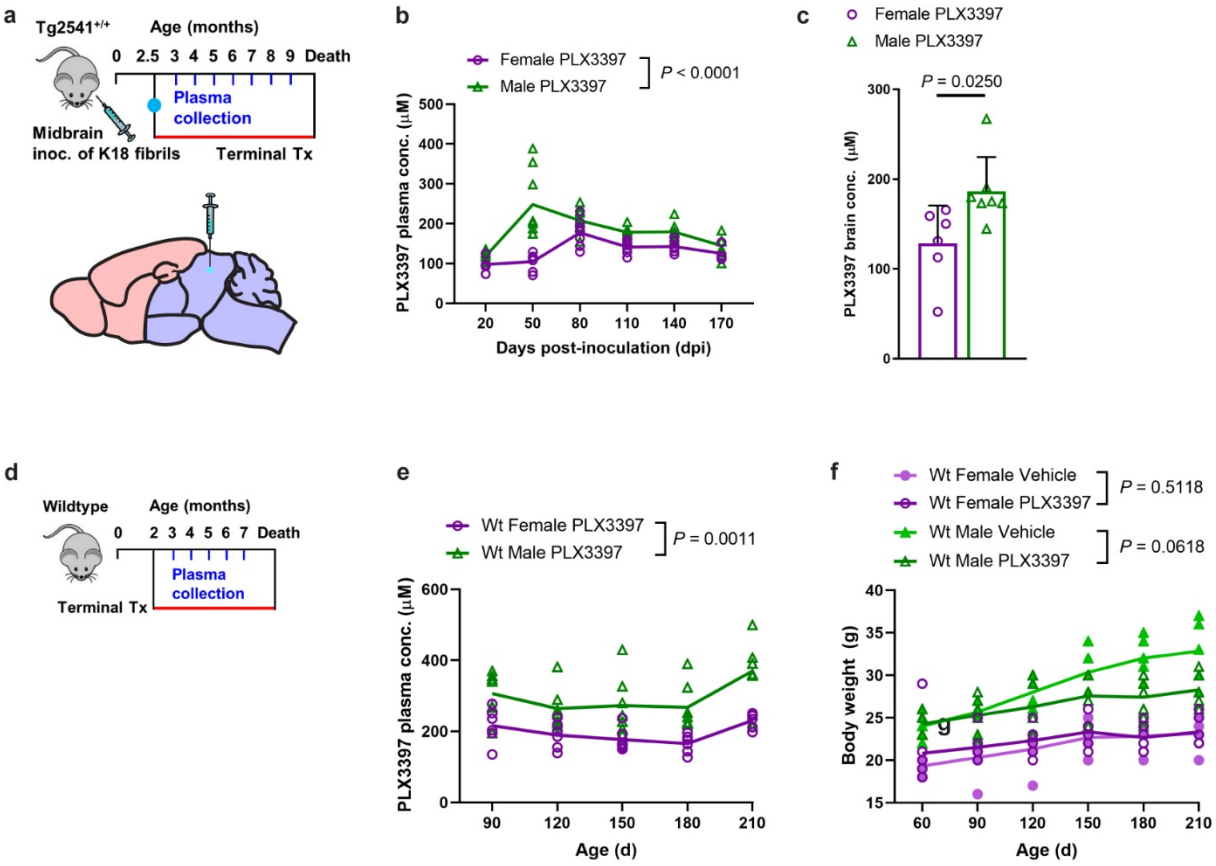


**Supplementary Fig. 9| PLX3397 levels are increased in male Tg2541 and wild type mice.** **a**, Schematic of terminal PLX3397 treatment of Tg2541 mice from 2.5 mo of age until death, following inoculation of K18 tau fibrils into the midbrain (hindbrain region) at 2.5 mo of age. Blood plasma was collected at monthly intervals from 3−9 mo of age. **b**, Plasma concentration of PLX3397 in female or male Tg2541 mice inoculated with K18 followed by terminal treatment with PLX3397, plotted over days post inoculation (dpi). Mixed-effects analysis (Restricted maximum likelihood) was used to compare female and male mice and the *P* value is shown. **c**, Brain concentration of PLX3397 at death in female or male Tg2541 mice inoculated with K18 followed by terminal treatment with PLX3397. Unpaired t test was used to compare female and male mice and the *P* value is shown. Each symbol represents an individual mouse and the error bars represent the s.d. of the mean. **d**, Schematic of terminal PLX treatment of C57BL/6J wild type mice (Wt) from 2 mo of age until death and blood plasma collected at 3, 4, 5, 6, and 7 mo of age. **e**, Plasma concentration of PLX3397 in female or male Wt mice. The difference between female and male mice was assessed by two-way repeated measures ANOVA and the *P* value is

shown. **f**, Body weights of female or male Wt mice treated with vehicle or PLX3397. Differences in weight between vehicle and PLX3397 treatment in male or female mice were evaluated by two-way repeated measures ANOVA and *P* values are shown. In **b**, **e**, and **f**, each symbol represents an individual mouse and the lines represent the group means.

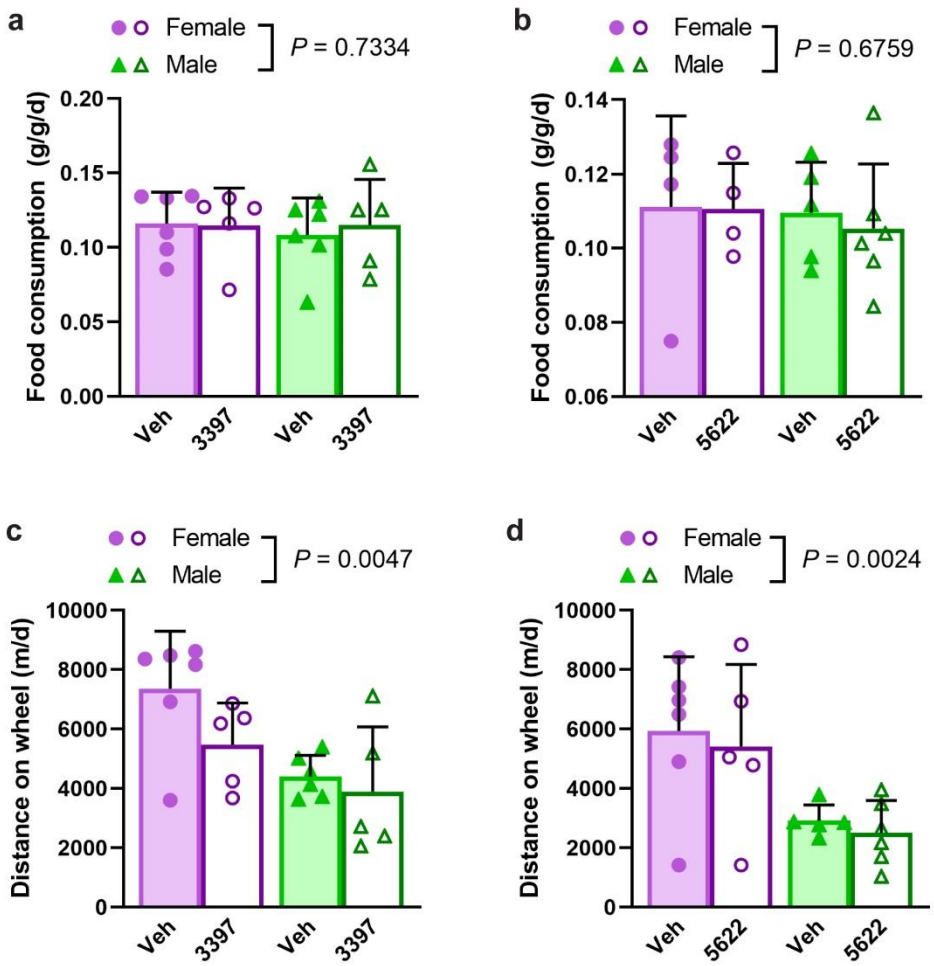


**Supplementary Fig. 10| Food consumption and activity of Tg2541 mice treated with CSF1R inhibitors. a**, **b**, Food consumption measured in Tg2541 mice receiving terminal treatment with vehicle or PLX3397 (275 mg/kg oral) (**a**), or vehicle or PLX5622 (1200 mg/kg oral) (**b**), reported as grams of food per gram of mouse body weight per day (g/g/d). **c**, **d**, Running wheel activity measured in Tg2541 mice receiving terminal treatment with vehicle or PLX3397 (**c**), or vehicle or PLX5622 (**d**), reported as total distance traveled in meters per day (m/d). In **a**–**d**, each symbol represents an individual mouse, with female mice shown as closed or open circles and male mice shown as closed or open triangles. Error bars represent s.d. of the mean. Two-way ANOVA was used to compare female and male mice and *P* values are shown.

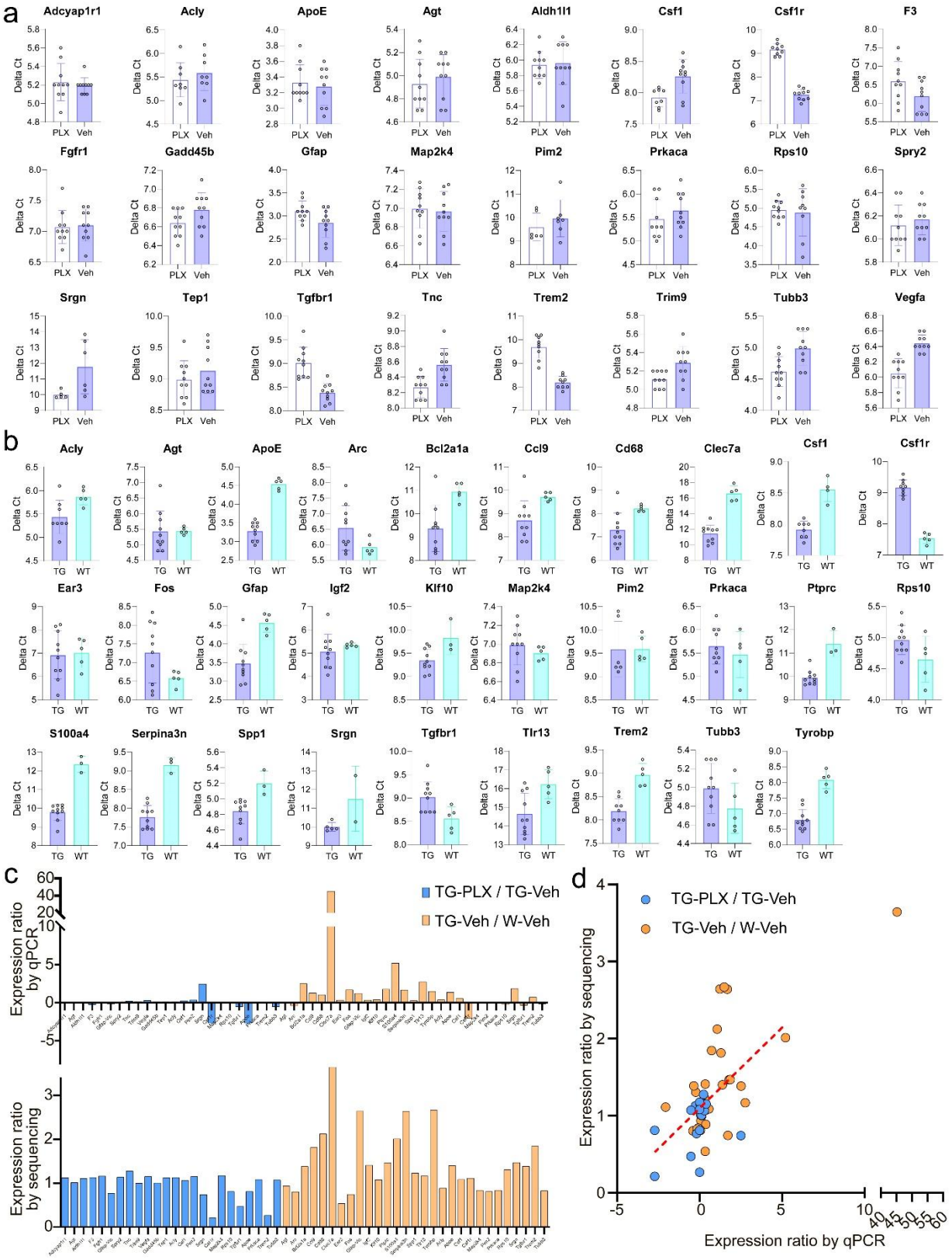


**Supplementary Fig. 11| Validation of Nanostring sequencing results with real-time PCR.**

**a**, Delta Ct values of 24 selected genes in hindbrains of Tg2541 mice treated with PLX5622

(1200 mg/kg) and vehicle. A lower Delta Ct reading indicates higher expression level. **b**, Delta Ct values of 29 selected genes in hindbrains of Tg2541 and wild type mice treated with vehicle. A lower Delta Ct reading indicates higher expression level. **c**, Expression ratios of the 53 genes in (**a**) and (**b**) as measured by qPCR and Nanostring sequencing. **d**, Scatter plot of the data in (**c**). Red dotted line shows a linear trend line.

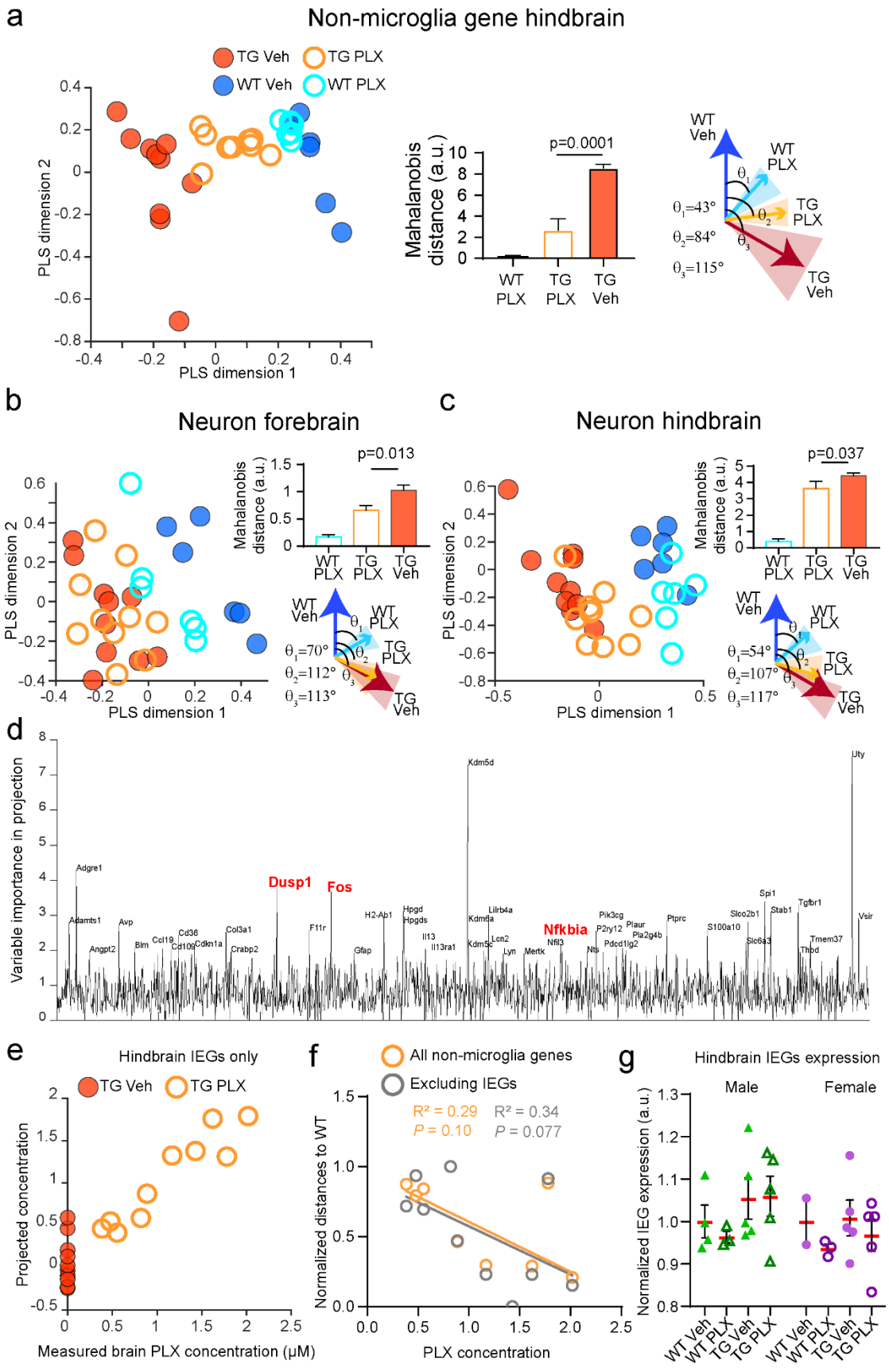

**Supplementary Fig. 12| Gene expression pattern analyses of non-microglial and neuron-specific genes**. **a−c,** Analyses similar to Fig. 6c−e, using (**a**) all non-microglial genes in hindbrain, or neuron-specific genes in (**b**) forebrain and (**c**) hindbrain. **d−g**, Analyses similar to Fig. 6g−j, using data from hindbrains.

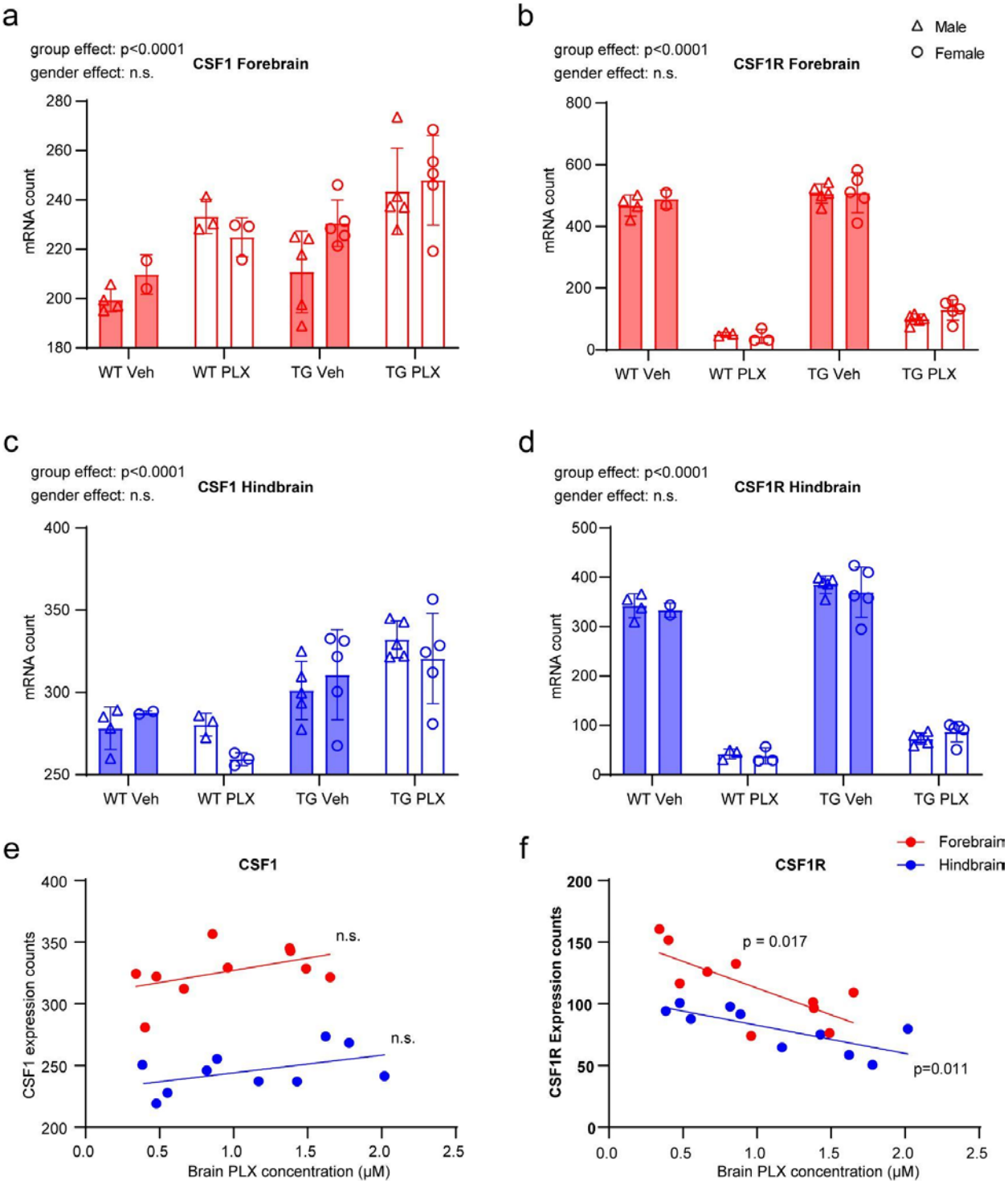


1509

1510 **Supplementary Fig. 13| PLX treatment led to increased CSF1 expression and decreased**
1511 **CSF1R expression**. Quantification of CSF1 expression showed slight increase after PLX
1512 treatment, while CSF1R expression showed marked decrease. Two-way ANOVA was used for

1513 statistical tests. Bottom panels showed scatter plots of brain PLX concentration against CSF1 or
1514 CSF1R expression. Linear regressions were calculated for each group.

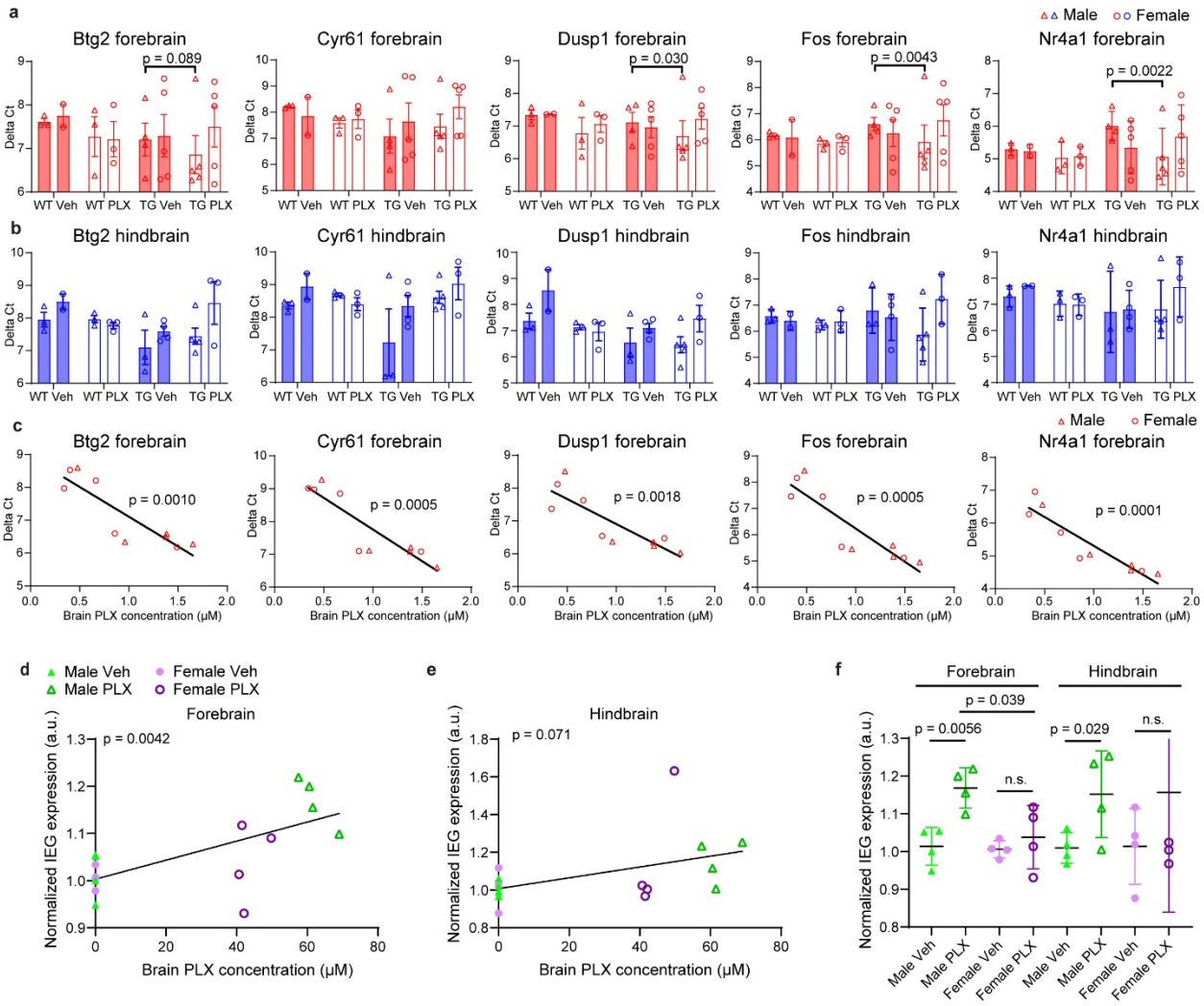


**Supplementary Fig. 14| Validation of IEG up-regulation following PLX treatment. a**, **b**, Real-time PCR quantifications of the mRNA levels of five IEGs in forebrains (**a**) and hindbrains (**b**) from PLX5622- or vehicle-treated Tg2541 or wildtype mice. **c,** Correlation of brain PLX concentration and expression levels from the five immediate early genes in the forebrains from PLX5622-treated Tg2541 mice. **c**, **d**, Correlation of brain PLX concentration and normalized expression levels from all immediate early genes (IEGs, 56 genes for each mouse) in the (**d**) forebrains and (**e**) hindbrains of vehicle- and PLX3397-treated Tg2541 mice. Pearson's correlation analysis was performed and the *P* values are shown. **f**, Quantification of normalized expression levels from all IEGs (56 genes for each mouse) in the forebrain and hindbrain of vehicle- and PLX3397-treated Tg2541 mice. Mann-Whitney tests were used for comparisons between groups. Each symbol represents an individual mouse.

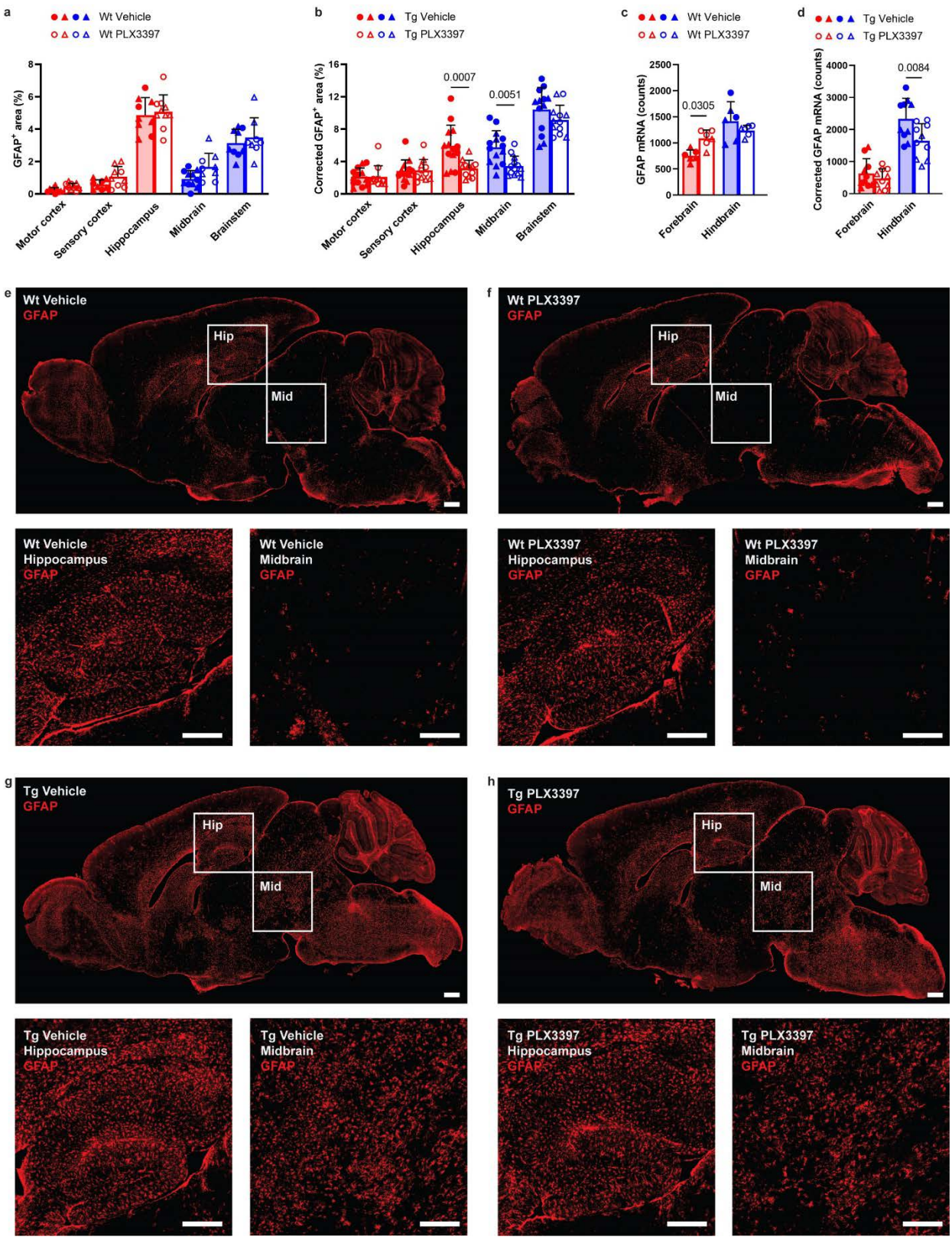


**Supplementary Fig. 15| GFAP expression is reduced by PLX3397 treatment in Tg2541 mice. a**, **b**, GFAP levels measured by IHC in five different brain regions, three forebrain regions

and two hindbrain regions, of (**a**) wild type (Wt) and (**b**) Tg2541 mice treated with PLX3397 (275 mg/kg oral) or vehicle. GFAP levels in Tg2541 mice were corrected for the average levels in each brain region of PLX3397- and vehicle-treated Wt mice. **c**, **d**, *GFAP* mRNA levels measured by Nanostring in the forebrain or hindbrain of (**c**) wild type and (**d**) Tg2541 mice treated with PLX3397 (275 mg/kg oral) or vehicle. *GFAP* mRNA levels in Tg2541 mice were corrected for the average levels in each brain region of PLX3397- and vehicle-treated Wt mice. In **a**−**d**, Two-way ANOVA with Holm-Šidák post hoc testing was used to evaluate the differences between vehicle- and PLX3397-treated groups within each brain region and *P* values of statistically significant differences ($P < 0.05$) are shown. Each symbol represents an individual mouse with female mice shown as closed or open circles and male mice shown as closed or open triangles. **e**−**h**, Representative GFAP IHC images of a brain section from (**e**) a Wt vehicle-treated mouse, (**f**) a Wt PLX3397-treated mouse, (**g**) a Tg2541 vehicle-treated mouse, and (**h**) a Tg2541 PLX3397-treated mouse. High-magnification images of the indicated hippocampus (Hip) and midbrain (Mid) regions are shown below each image. Scale bars, 500 μm.

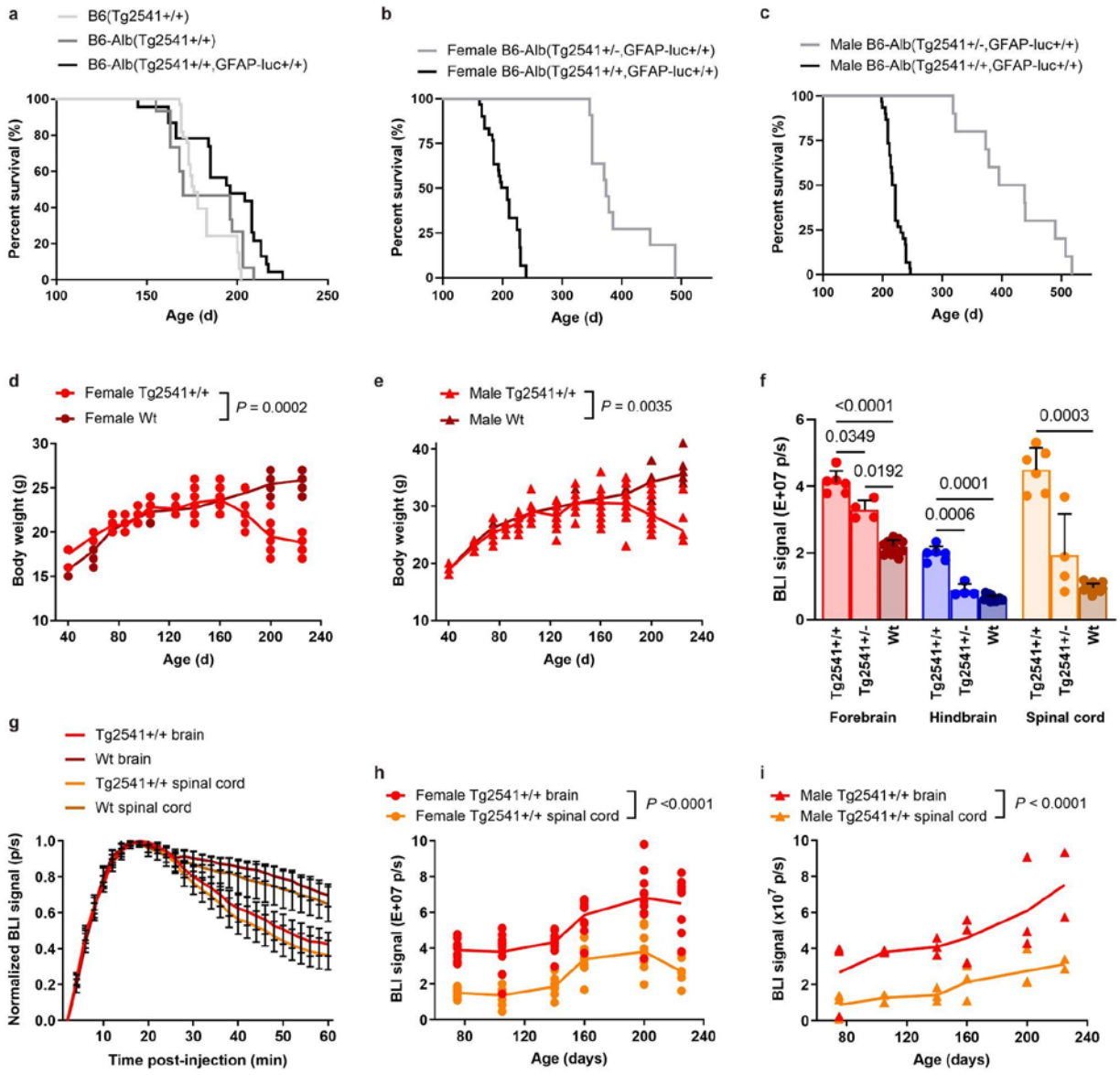


**Supplementary Fig. 16| Generation, optimization, and validation of bigenic Tg2541/GFAP-luciferase mice for in vivo bioluminescent imaging (BLI) of astrocytosis. a**, Kaplan-Meier plot shows that the survival curve (kinetics of disease) is unchanged for Tg2541 homozygous mice bred to B6-albino background and homozygous for the reporter GFAP-luciferase transgene. **b**, **c**, Kaplan-Meier plots for (**b**) female and (**c**) male mice showing that survival curves of homozygous and hemizygous B6-albino bigenic Tg2541 mice is not sex-dependent; homozygous Tg2541 mice have a median survival of 212 days, and hemizygous Tg2541 mice have a median survival of 378 days. **d**, **e**, As a crude surrogate of general health, longitudinal measurements of mouse body weight (grams) shows that in contrast to Wt mice, (**d**) female and (**e**) male Tg2541 mice lose weight as a result of decreased food intake from increasing

paraparesis with disease progression. Because earlier studies gave a standard volume of d-luciferin substrate regardless of changes in individual mouse weight, we optimized the protocol to give a 25mg/kg of CycLuc1 to increase consistency in BLI measurements. **f**, To validate the GFAP-luciferase reporter gene and the synthetic luciferin substrate (CycLuc1) *in vivo*, we performed BLI in Tg2541 homozygous mice (~200 days old) with advanced disease pathology and showed the BLI signal is significantly increased in the forebrain, hindbrain and spinal cord as compared to similar aged Tg2541 hemizygous and Wt mice. Welch ANOVA with Dunnett T3 post hoc testing was used to compare groups and *P* values for all statistically significant differences ($P < 0.05$) are shown. Error bars represent the s.d. of the mean. **g**, Time-lapse imaging (two-minute intervals) of BLI signal from brain and spinal cord in Tg and Wt mice showed that peak BLI signal occurred between 14 and 20 minutes after CycLuc1 injection to the peritoneum. Thus, to decrease variability in our study, we collect images at 14, 16, and 18 minutes post-injection and average all three time points to account for subtle differences in time of injection and individual mouse pharmacokinetic of CycLuc1. **h**, **i**, Longitudinal BLI plots in (**h**) female and (**i**) male mice show kinetics of gliosis in the Tg2541 brain and spinal cord (3 mice per field of view). **j**, Example image of the field of view (magnification) used to capture both the brain and spinal cord in three mice per time point. In **d**, **e**, **h**, and **i**, differences between groups were evaluated by repeated measures ANOVA and *P* values are shown. Each symbol represents an individual mouse and lines indicate group means.

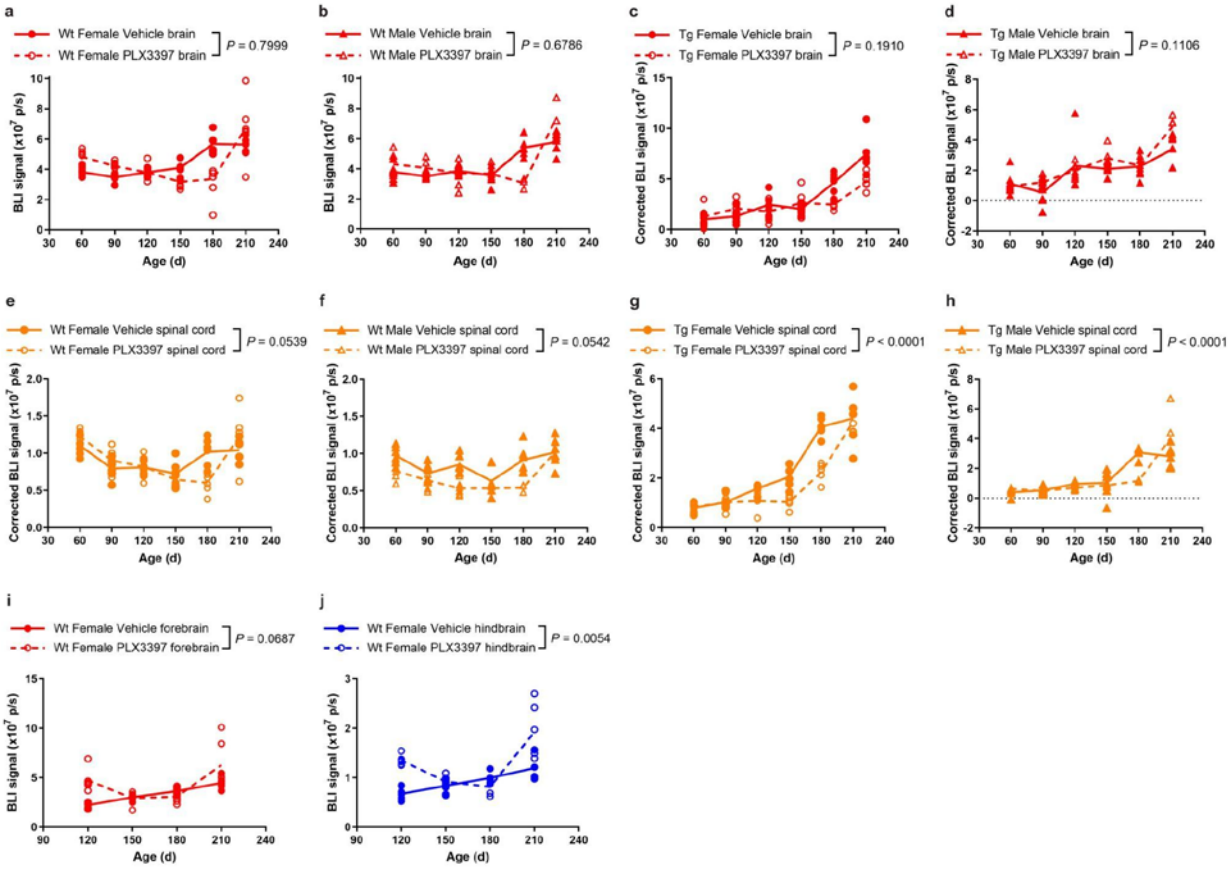


**Supplementary Fig. 17| Brain and spinal cord BLI of PLX3397-treated wild type and Tg2541 mice. a**, **b**, Longitudinal brain BLI plots of (**a**) female and (**b**) male wild type (Wt) mice treated with PLX3397 (275 mg/kg oral) or vehicle. **c**, **d**, Longitudinal brain BLI plots of (**c**) female and (**d**) male Tg2541 mice (Tg) treated with PLX3397 (275 mg/kg oral) or vehicle. The data were corrected for brain BLI levels of PLX3397- and vehicle-treated Wt mice, shown in **a** and **b**. Due to resolution and/or sensitivity of this magnification, we did not observe any differences between PLX3397 and vehicle groups. Higher magnification imaging on single mice from the same cohort was performed as shown in Fig. 7e−g. **e**, **f**, Longitudinal spinal cord BLI plots of (**e**) female and (**f**) male Wt mice treated with PLX3397 (275 mg/kg oral) or vehicle. **g**, **h**, Longitudinal spinal cord BLI plots of (**g**) female and (**h**) male Tg2541 mice (Tg) treated with PLX3397 (275 mg/kg oral) or vehicle. The data were corrected for spinal cord BLI levels of PLX3397- and vehicle-treated Wt mice, shown in **e** and **f**. **i**, **j**, High magnification BLI plots of the (**i**) forebrain and (**j**) hindbrain of female Wt mice treated with PLX3397 (275 mg/kg oral) or vehicle, and used to correct the BLI data of female Tg2541 mice presented in Fig. 7f,g. In **a**−**j**, differences between vehicle and PLX3397 treatment were evaluated by repeated measures ANOVA and *P* values are shown. Each symbol represents an individual mouse and lines

1591 indicate group means.

1592

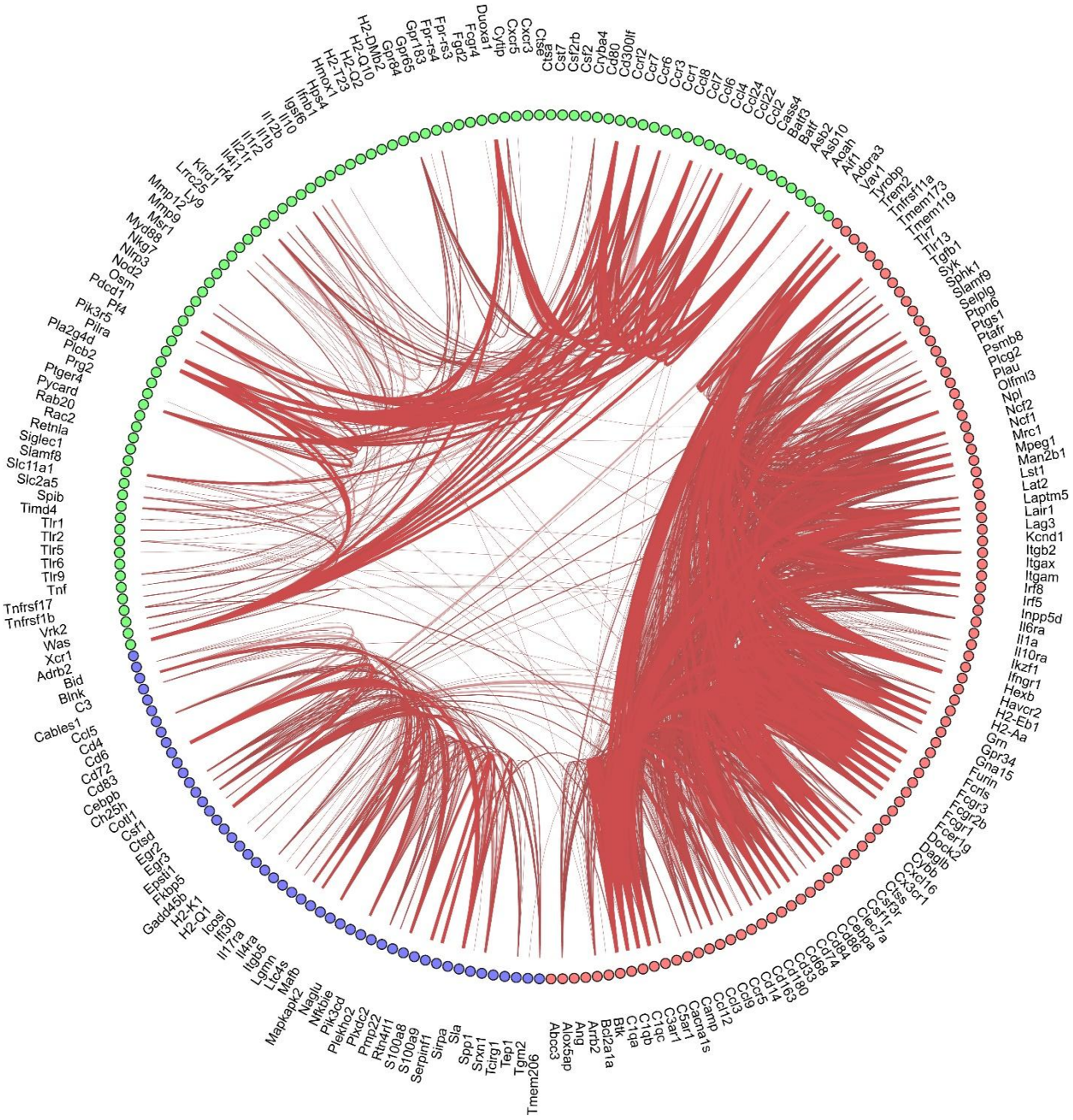


1593

1594 **Supplementary Fig. 18| Clustering of microglia specific genes.** The schemaball graph of

1595 microglial-specific genes as shown in Fig. 9. The name of each gene is shown next to the dot.

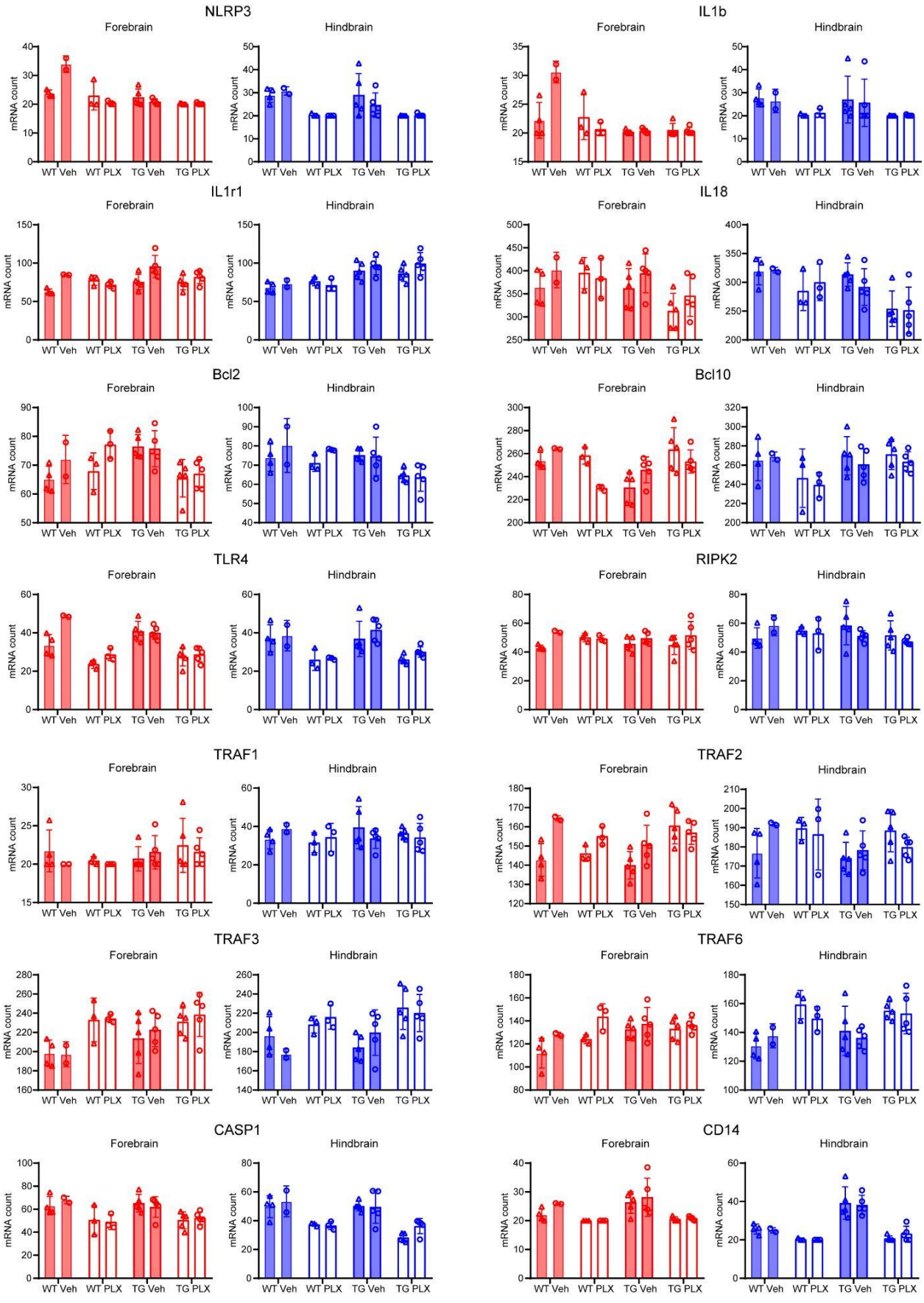

**Supplementary Fig. 19| Tau pathology or PLX treatment did not lead to marked alteration of inflammasome-related genes**. Quantification of 14 inflammasome-related genes in different experimental groups.

**Supplementary Data File 1| Statistical tests of sex-specific drug effects on microglia, tau, and neurons**. **a**, Statistical test results for 3-way ANOVA analyses for each figure panel where female and male mice were combined. Statistical test results include the type III sum-of-squares (SS), the F statistic, and the *P* value for the main effect of sex and for the sex*drug interaction effect. **b**, **c**, Statistical test results for 2-way ANOVA analyses for (**b**) female or (**c**) male mice separately, for each figure panel where female and male mice were combined. Statistical test results include the type III sum-of-squares (SS), the F statistic, and the *P* value for the main effect of drug, and the *P* value for the multiple comparisons post-hoc testing of each drug compared to the vehicle in the forebrain, hindbrain, or spinal cord. 'na' indicates that the data is not available because the drug was not tested in that particular experiment.

**Supplementary Data File 2| Differentially expressed genes in male and female PLX-treated Tg2541 mice.** Forebrain samples from male and female Tg2541 mice were analyzed for gene expression by Nanostring following chronic treatment with PLX5622. The data represent the average expression levels of five male and five female mice, which were then compared by unpaired t-test and the *P* value is shown. Please note that the entire transcriptome dataset which also includes hindbrain data, wild type mice, and vehicle-treated mice are available from Github with the following link: https://gitfront.io/r/user-8849465/665dd65fd9d9e78650ed02b9f30236d99240de39/UCSF-PLX-nanostring/